A study of indirect violation of CPT/CP and CP/T using fully reconstructed CP and flavor eigenstates

Massimo Carpinelli, Francesco Forti, Marcello Giorgi, Fernando Martinez-Vidal[1],
Nicola Neri, Francesco Sandrelli

INFN-Sezione di Pisa and Università di Pisa, Italy

Abstract

We describe a combined study of indirect CPT/CP and CP/T violation using the *BABAR* charmonium CP and flavor hadronic samples. The combined use of these samples offers a way to test simultaneous and consistently the CPT, CP and T invariances of the effective Hamiltonian of the B_d^0 system, in spite of the vanishingly small width difference $\Delta\Gamma$ between the physical states, while providing a robust extraction of this parameter. CPT-odd, CP-odd, T-odd and temporal asymmetries are also constructed to display the different effects.

Two different phase-convention independent formalisms have been investigated. With the (ε, δ) formalism, similar to that used in kaon system phenomenology, an unbinned maximum likelihood fit allows the simultaneous measurement of $\frac{1-|\varepsilon|^2}{1+|\varepsilon|^2}\frac{\mathrm{Re}\delta}{1+|\varepsilon|^2}$, $\frac{\mathrm{Im}\delta}{1+|\varepsilon|^2}$, $\frac{\mathrm{Re}\varepsilon}{1+|\varepsilon|^2}$, $\frac{\mathrm{Im}\varepsilon}{1+|\varepsilon|^2}$, $sign\left(\frac{1-|\varepsilon|^2}{1+|\varepsilon|^2}\right)\Delta\Gamma/\Gamma$ and Δm. In the $(|q/p|, \lambda, z)$ formalism, the corresponding set of parameters is $\frac{\mathrm{Re}\lambda}{|\lambda|}\mathrm{Re}z$, $\mathrm{Im}z$, $|q/p|$, $\frac{\mathrm{Im}\lambda}{|\lambda|}$, $sign(\mathrm{Re}\lambda)\Delta\Gamma/\Gamma$ and Δm. The strategy, feasibility, reach and validation of the proposed analysis are reported. The implementation and validation of the CPT/CP, CP/T models in the *BABAR* event generators are also described.

---

[1] Primary editor.

Contents

1 Introduction

Discrete symmetries play a fundamental role in our description of nature. The CPT theorem [1, 2], which is based on very general principles of relativistic quantum field theories (little more than locality and Lorentz invariance), states that any order of the triple product of the discrete symmetries C, P and T represent an exact symmetry. The theorem predicts that particles and antiparticles have equal masses, lifetimes, charge-to-mass rations and gyromagnetic ratios.

The CPT symmetry has been tested in a variety of experiments [3], remaining to date the only combination of C, P, T that is observed as an exact symmetry in nature. However, precisely because the CPT theorem represents an essential pillar of our present description of nature, it is highly suitable to enhance such tests through detailed studies of EPR correlations in the B meson neutral system, where the extremally small value of the mass difference between the physical states with respect to the B mass (13 orders of magnitude) enhances the sensitivity of the $B^0 \bar{B}^0$ interferometry. As can be found in the literature, the special features of the neutral B meson system can be used to extract not only information on CP [4] but also on CPT [5] violation. We should also keep in mind that superstring theories are not local and therefore do not necessarily fulfil the conditions of the CPT theorem. CPT invariance has also been questioned in the context of quantum gravity [6].

The problem of indirect violation of CP, T and CPT discrete symmetries corresponds to the non-invariance under the corresponding transformations of the effective hamiltonian [7] governing the time evolution of a neutral meson system. Those properties can thus be studied by analyzing the symmetries in the problem of mixing during the time evolution of the meson states, excluding the possible effects from direct decays. Historically, since the discovery of CP violation in 1964 [8], such a study has been performed in the kaon system [9] where the study of *flavour-to-flavour* (B_{flav}) evolution allows the construction of observables which violate CP and T, or CP and CPT. In a similar way as kaon system studies, in the B_d^0 meson system one can perform similar studies [10]. Nevertheless, these T- and CPT-odd observables need the presence of off-diagonal absorptive components in the effective hamiltonian in order to be non-vanishing, even in presence of T and CPT fundamental violation. For the kaon system, this ingredient is guaranteed by the different lifetimes of physical states, K_s^0 and K_L^0. On the contrary, in the case of the B_d^0 system, the width difference $\Delta\Gamma/\Gamma$ between the physical states is expected to be very small, O(10^{-2}) [11].

Therefore the T- and CPT-odd observables proposed for kaons, which are based on *flavor tag* (i.e. preparation of definite flavor states), vanish for a B_d^0 meson system in the limit $\Delta\Gamma = 0$, reducing dramatically its sensitivity and making its interpretation in terms of violation of the fundamental symmetries difficult, in spite of the very large available statistics [10]. However, the study of *CP-to-flavour* (B_{CP}) evolution from the entangled states of B_d^0 mesons allows the construction of observables which are sensitive to indirect CP and T, or CP and CPT violation, independently of the value of $\Delta\Gamma$ [12, 13]. Being the indirect CP violation already established [14], testing simultaneously indirect CP, T and CPT conservation and disentangle whether the CP violation is due to T or CPT violation is a natural step forward, and of great interest [3] as mentioned above. This is the purpose of the analysis proposed here. As a result of the consistent treatment, the analysis provides also a way to extract $\Delta\Gamma$.

The outline of this document is as follows. In section 2 we discuss the theoretical framework required for the analysis, describing the formalisms used for this study. Section 3 describes how the relevant parameters are extracted, and section 4 presents all checks performed to study and validate the fit. Section 5 is devoted to study the CPT, CP and T violation reach and sensitivity. In section 6 we summarize the conclusions of our study.

2 Framework

2.1 Basics

The neutral B meson system is a linear combination of the Schrödinger wave functions for the meson B^0 and its antimeson $\bar{B}^0$, $|\Psi\rangle = a|B^0\rangle + b|\bar{B}^0\rangle$. The time evolution of this combination is governed by the Schrödinger equation, $\frac{\partial \Psi}{\partial t} = -iH\Psi$, where M is the 2×2 non-hermitian (probability is not conserved since the $B^0\bar{B}^0$ system decays) effective hamiltonian,

$$H = M - i\frac{\Gamma}{2} = \begin{pmatrix} M_{11} & M_{12} \\ M_{12}^* & M_{22} \end{pmatrix} - \frac{i}{2}\begin{pmatrix} \Gamma_{11} & \Gamma_{12} \\ \Gamma_{12}^* & \Gamma_{22} \end{pmatrix} \ . \tag{1}$$

M and Γ represent the mass (dispersive) and lifetime (absorptive) parts of the hamiltonian. Unitarity requires that the diagonal elements of M and Γ are real[2].

The flavor eigenstates are connected by

$$CP|B^0\rangle = CP_{12}^*|\bar{B}^0\rangle \tag{2}$$

where

$$CP_{12} = \langle B^0|CP|\bar{B}^0\rangle = e^{-i\alpha} \tag{3}$$

is the unphysical relative phase between $|B^0\rangle$ and $|\bar{B}^0\rangle$. The corresponding CP eigenstates are thus

$$|B_\pm\rangle = \frac{1}{\sqrt{2}}(I \pm CP)|B^0\rangle = \frac{1}{\sqrt{2}}\left[|B^0\rangle \pm CP_{12}^*|\bar{B}^0\rangle\right] \ . \tag{4}$$

Inverting equation (4), one gets

$$|B^0\rangle = \frac{1}{\sqrt{2}}\left[|B_+\rangle + |B_-\rangle\right]$$
$$|\bar{B}^0\rangle = \frac{1}{\sqrt{2}}CP_{12}\left[|B_+\rangle - |B_-\rangle\right] \ . \tag{5}$$

It should be noted here that the off-diagonal elements of H are phase-convention dependent,

$$H_{12} = \langle B^0|H|\bar{B}^0\rangle \rightarrow H_{12}CP_{12} \tag{6}$$

However, combinations $H_{12}CP_{12}^*$ are independent of the phase choice in (2).

---

[2]We use the notation H_{ij}, CP_{ij}, etc. to represent the matrix elements of the corresponding operators in the flavor basis, for instance $H_{12} \equiv \langle B^0|H|\bar{B}^0\rangle$.

2.2 Eigenstates of evolution

The states of evolution are the eigenstates of H, which evolve as

$$
\begin{aligned}
|B_1(t)\rangle &= e^{-i\lambda_1 t}|B_1(0)\rangle \\
|B_2(t)\rangle &= e^{-i\lambda_2 t}|B_2(0)\rangle
\end{aligned}
$$

(7)

where $\lambda_j = M_j - i\frac{\Gamma_j}{2}$ are the eigenvalues, for $j = 1,2$. The following relations are satisfied: $M_j = \mathrm{Re}(\lambda_j)$, $\Gamma_j = -2\mathrm{Im}(\lambda_j)$, $\Delta\lambda = \lambda_1 - \lambda_2 = \Delta m + i\frac{\Delta\Gamma}{2}$, $\Delta m = M_1 - M_2 = \mathrm{Re}(\lambda_1 - \lambda_2)$, $\Delta\Gamma = \Gamma_2 - \Gamma_1 = 2\mathrm{Im}(\lambda_1 - \lambda_2)$, $m = \frac{M_1+M_2}{2}$ and $\Gamma = \frac{\Gamma_1+\Gamma_2}{2}$. Let us note the particular choice of sign in the definition of $\Delta\Gamma$, which coincides with that of the kaon system but is opposite to that adopted by some authors in the B_d^0 system: for Δm positive, we are identifying $|B_1\rangle \equiv |B_H\rangle$ and $|B_2\rangle \equiv |B_L\rangle$, and $\Delta\Gamma$ is therefore positive for kaons.

Let's assume first CPT conservation, which imposes the condition $H_{11} = H_{22}$. Writing the eigenvectors $|B_1\rangle$ and $|B_2\rangle$ in the $B^0\bar{B}^0$ basis, $|B_j\rangle = p_j|B^0\rangle + q_j|\bar{B}^0\rangle$, $j = 1,2$, we obtain

$$
\frac{q_1}{p_1} = \frac{q}{p} = \sqrt{\frac{M_{12}^* - i\Gamma_{12}^*/2}{M_{12} - i\Gamma_{12}/2}} = \frac{M_{12}^* - i\Gamma_{12}^*/2}{F}
$$

(8)

for $j = 1$, and

$$
\frac{q_2}{p_2} = -\frac{q}{p}
$$

(9)

for $j = 2$, where

$$
F = \sqrt{(M_{12} - i\Gamma_{12}/2)(M_{12}^* - i\Gamma_{12}^*/2)} = \frac{1}{2}\left(\Delta m + i\frac{\Delta\Gamma}{2}\right) \ .
$$

(10)

The phase-convention dependence of q/p is well seen in equation (8), since only H_{12}^* terms are involved. The reference phase CP_{12} would make it invariant,

$$
\frac{q}{p}CP_{12} = \frac{1-\varepsilon}{1+\varepsilon}
$$

(11)

where ε is here a phase-convention independent parameter. The eigenstates can then be written as

$$
\begin{aligned}
|B_1\rangle &= \frac{1}{\sqrt{2(1+|\varepsilon|^2)}}\left[(1+\varepsilon)|B^0\rangle + (1-\varepsilon)|CP_{12}^*\bar{B}^0\rangle\right] \\
|B_2\rangle &= \frac{1}{\sqrt{2(1+|\varepsilon|^2)}}\left[(1+\varepsilon)|B^0\rangle - (1-\varepsilon)|CP_{12}^*\bar{B}^0\rangle\right]
\end{aligned}
$$

(12)

where ε is the same parameter as defined in equation (11). Writing the eigenstates $|B_1\rangle$ and $|B_2\rangle$ in the CP basis, $|B_j\rangle = c_j|B_+\rangle + d_j|B_-\rangle$, $j = 1,2$, we obtain

$$|B_1\rangle = \frac{1}{\sqrt{1+|\varepsilon|^2}}[|B_+\rangle + \varepsilon|B_-\rangle]$$

$$|B_2\rangle = \frac{1}{\sqrt{1+|\varepsilon|^2}}[|B_-\rangle + \varepsilon|B_+\rangle] \tag{13}$$

from which it can be seen that ε is the parameter which defines the CP mixing. The independence of ε with the phase choice can be shown explicitly if the coefficients of the linear combination of the eigenvectors are calculated in the CP basis. For $j = 1$,

$$\frac{d_1}{c_1} = \frac{\mathrm{Im}(\Gamma_{12}CP_{12}^*) + 2i\mathrm{Im}(M_{12}CP_{12}^*)}{2\mathrm{Re}(M_{12}CP_{12}^*) - i\mathrm{Re}(\Gamma_{12}CP_{12}^*) + \Delta m + i\Delta\Gamma/2} = \varepsilon \tag{14}$$

where $4\,|\,M_{12}\,|^2 - |\,\Gamma_{12}\,|^2 = (\Delta m)^2 - \frac{1}{4}(\Delta\Gamma)^2$ and $4\mathrm{Re}(M_{12}\Gamma_{12}^*) = -\Delta m\Delta\Gamma$. Similarly, for $j = 2$ we obtain

$$\frac{d_2}{c_2} = \frac{c_1}{d_1} = \frac{1}{\varepsilon} \ . \tag{15}$$

Expression (14) reveals the presence of $H_{12}CP_{12}^*$ terms, which are invariant under rephasing. Let us note that the convention adopted here defining q/p (ε) uses the heavier state, $|\,B_1\rangle$.

Corrections are due to CPT violation, which can be parameterized in terms of the variable $\Delta = H_{11} - H_{22}$. In this case equations (8) and (9) read, respectively

$$\frac{q_1}{p_1} = \sqrt{\frac{(M_{12}^* - i\Gamma_{12}^*/2)(\mathrm{Re}F' + i\mathrm{Im}F' - \Delta/2)}{(M_{12} - i\Gamma_{12}/2)(\mathrm{Re}F' + i\mathrm{Im}F' + \Delta/2)}} \tag{16}$$

and

$$\frac{q_2}{p_2} = -\frac{q_1}{p_1} - \frac{\Delta}{M_{12} - i\Gamma_{12}/2} \tag{17}$$

where

$$F' = \sqrt{F^2 + \Delta^2/4} \ . \tag{18}$$

To leading order in Δ, F' equals to $F = (\Delta m + i\Delta\Gamma/2)/2$, and equations (16) and (17) are simplified as follows:

$$\frac{q_1}{p_1} = \frac{1-\varepsilon_1}{1+\varepsilon_1}CP_{12}^* = \frac{q}{p}\left(1 - \frac{\Delta}{\Delta m + i\Delta\Gamma/2}\right) \tag{19}$$

and

$$\frac{q_2}{p_2} = -\frac{1-\varepsilon_2}{1+\varepsilon_2}CP_{12}^* = -\frac{q}{p}\left(1 + \frac{\Delta}{\Delta m + i\Delta\Gamma/2}\right) \tag{20}$$

6

respectively.

The generalization of equations (14) and (15) to account for CPT violating effects reads

$$\frac{d_1}{c_1} = \frac{\text{Im}(\Gamma_{12}CP_{12}^*) + 2i\text{Im}(M_{12}CP_{12}^*) + \Delta}{2\text{Re}(M_{12}CP_{12}^*) - i\text{Re}(\Gamma_{12}CP_{12}^*) + 2F'} = \varepsilon_1 \tag{21}$$

and

$$\frac{d_2}{c_2} = \frac{2\text{Re}(M_{12}CP_{12}^*) - i\text{Re}(\Gamma_{12}CP_{12}^*) + 2F'}{\text{Im}(\Gamma_{12}CP_{12}^*) + 2i\text{Im}(M_{12}CP_{12}^*) - \Delta} = \frac{1}{\varepsilon_2} \tag{22}$$

respectively.

Alternatively to $\varepsilon_{1,2}$ we may use another pair of parameters ε and δ, which offer a simpler interpretation in terms of symmetries. These parameters are defined as

$$\varepsilon \equiv \frac{\varepsilon_1 + \varepsilon_2}{2} = \frac{\text{Im}(\Gamma_{12}CP_{12}^*) + 2i\text{Im}(M_{12}CP_{12}^*)}{2\text{Re}(M_{12}CP_{12}^*) - i\text{Re}(\Gamma_{12}CP_{12}^*) + 2F'} \tag{23}$$

$$\delta \equiv \varepsilon_1 - \varepsilon_2 = \frac{2\Delta}{2\text{Re}(M_{12}CP_{12}^*) - i\text{Re}(\Gamma_{12}CP_{12}^*) + 2F'} \tag{24}$$

In terms of these parameters, the eigenstates in the flavor basis are:

$$|B_1\rangle = \frac{1}{\sqrt{2(1 + |\varepsilon + \delta/2|^2)}} \left[(1 + \varepsilon + \delta/2)|B^0\rangle + (1 - \varepsilon - \delta/2)|CP_{12}^*\bar{B}^0\rangle \right]$$

$$|B_2\rangle = \frac{1}{\sqrt{2(1 + |\varepsilon - \delta/2|^2)}} \left[(1 + \varepsilon - \delta/2)|B^0\rangle - (1 - \varepsilon + \delta/2)|CP_{12}^*\bar{B}^0\rangle \right] \tag{25}$$

and in the CP basis are:

$$|B_1\rangle = \frac{1}{\sqrt{1 + |\varepsilon + \delta/2|^2}} \left[|B_+\rangle + (\varepsilon + \delta/2)|B_-\rangle \right]$$

$$|B_2\rangle = \frac{1}{\sqrt{1 + |\varepsilon - \delta/2|^2}} \left[|B_-\rangle + (\varepsilon - \delta/2)|B_+\rangle \right] . \tag{26}$$

By inverting (26), we can obtain the master equations for the time evolution for an state that is initially a pure $|B_\pm\rangle$:

$$|B_+(t)\rangle = \frac{e^{-imt}e^{-\Gamma t/2}}{1 - \varepsilon_1\varepsilon_2} \left\{ [h_+(t) - \varepsilon_1\varepsilon_2 h_-(t)]\,|B_+\rangle + [\varepsilon_1(h_+(t) - h_-(t))]\,|B_-\rangle \right\}$$

$$|B_-(t)\rangle = \frac{e^{-imt}e^{-\Gamma t/2}}{1 - \varepsilon_1\varepsilon_2} \left\{ [h_-(t) - \varepsilon_1\varepsilon_2 h_+(t)]\,|B_-\rangle + [\varepsilon_2(h_-(t) - h_+(t))]\,|B_+\rangle \right\} \tag{27}$$

7

where $\varepsilon_1 = \varepsilon + \delta/2$, $\varepsilon_2 = \varepsilon - \delta/2$ and

$$h_\pm(t) = e^{\pm i\Delta\lambda t/2} = e^{\mp i\Delta m t/2}e^{\pm\Delta\Gamma t/4} \quad . \tag{28}$$

Similarly, for a pure $|B^0\rangle$ ($|\bar{B}^0\rangle$) state:

$$\begin{aligned}
|B^0(t)\rangle &= \frac{1}{2}\frac{e^{-imt}e^{-\Gamma t/2}}{1-\varepsilon_1\varepsilon_2}\left\{[(1+\varepsilon_1)(1-\varepsilon_2)h_+(t)+(1-\varepsilon_1)(1+\varepsilon_2)h_-(t)]\,|B^0\rangle + \right.\\
&\qquad \left. [(1-\varepsilon_1)(1-\varepsilon_2)h_+(t)-(1-\varepsilon_1)(1-\varepsilon_2)h_-(t)]CP_{12}^*\,|\bar{B}^0\rangle\right\}\\
|\bar{B}^0(t)\rangle &= \frac{1}{2}\frac{e^{-imt}e^{-\Gamma t/2}}{1-\varepsilon_1\varepsilon_2}\left\{CP_{12}[(1+\varepsilon_1)(1+\varepsilon_2)h_+(t)-(1+\varepsilon_1)(1+\varepsilon_2)h_-(t)]\,|B^0\rangle + \right.\\
&\qquad \left. [(1-\varepsilon_1)(1+\varepsilon_2)h_+(t)+(1+\varepsilon_1)(1-\varepsilon_2)h_-(t)]\,|\bar{B}^0\rangle\right\} \quad . \tag{29}
\end{aligned}$$

2.3 Hierarchy of parameters: the $\Delta\Gamma = 0$ limit

In order to stablish the hierarchy of the CPT, CP and T parameters, it is very useful to evaluate ε and δ in the limit $\Delta\Gamma = 0$. In this limit the anti-hermitian part of the effective hamiltonian is proportional to unity,

$$\begin{pmatrix} \Gamma_{11} & \Gamma_{12} \\ \Gamma_{12}^* & \Gamma_{22} \end{pmatrix} = \Gamma\begin{pmatrix} 1 & 0 \\ 0 & 1 \end{pmatrix} . \tag{30}$$

The hamiltonian can then be diagonalized by a unitary transformation and its physical states will be orthogonal. From (23) and (24), we obtain:

$$\begin{aligned}
\mathrm{Re}(\varepsilon) &= 0\\
\frac{\mathrm{Im}(\varepsilon)}{1+|\varepsilon|^2} &= \frac{\mathrm{Im}(M_{12}CP_{12}^*)}{\Delta m}\\
\frac{\mathrm{Re}(\delta)}{1+|\varepsilon|^2} &= \frac{\Delta}{\Delta m}\\
\mathrm{Im}(\delta) &= 0 \tag{31}
\end{aligned}$$

As can be seen, ε becomes purely imaginary and δ real. We then find $\varepsilon_2 = -\varepsilon_1^*$ and the orthogonality of the states (26) is apparent.

2.4 Restrictions imposed by discrete symmetries

When we pay attention to the restrictions imposed by discrete symmetries on the effective mass matrix, $H = M - \frac{i}{2}\Gamma$, we see that:

- CP conservation imposes $\mathrm{Im}(M_{12}CP_{12}^*) = \mathrm{Im}(\Gamma_{12}CP_{12}^*) = 0$ and $H_{11} = H_{22}$;

- CPT invariance requires $H_{11} = H_{22}$;

- T invariance imposes $\text{Im}(M_{12}CP_{12}^*) = \text{Im}(\Gamma_{12}CP_{12}^*) = 0$.

As a consequence, CPT invariance leads to $\delta = 0$, irrespective of the value of ε. Similarly, T invariance leads to $\varepsilon = 0$, independently of the value of δ. CP conservation requires both $\varepsilon = \delta = 0$. Another consequence is that CPT or T violation requires CP violation, and CP violation implies T or CPT violation (or both).

Therefore we have four real parameters which carry information on the symmetries of the effective mass matrix, according to the following list:

- $\text{Re}\varepsilon \neq 0$ signals CP and T violation, with $\Delta\Gamma \neq 0$;

- $\text{Im}\varepsilon \neq 0$ indicates CP and T violation;

- $\text{Re}\delta \neq 0$ means that CP and CPT violation exist;

- $\text{Im}\delta \neq 0$ shows CP and CPT violation, with $\Delta\Gamma \neq 0$.

Thus we observe that $\text{Re}\varepsilon$ and $\text{Im}\delta$, in spite of being true symmetry violating parameters, will not be helpful to decide the presence of symmetry breaking unless there are also off-diagonal absorptive parts in the effective Hamiltonian. The traditional *flavor-to-flavor* observables constructed for the kaon system turn out to be proportional to these quantities, so that their analogous for the *B*-system will be necessarily small, even in presence of symmetry violation, due to the vanishingly small $\Delta\Gamma$.

2.5 Time dependent decay rates in (ε, δ) formalism

Charge conjugation together with Bose statistics require that the $B^0\overline{B}^0$ state produced from the $\Upsilon(4S)$ decay is given by

$$|i> = \frac{1}{\sqrt{2}}\left(|B^0(\vec{k}), \overline{B}^0(-\vec{k})> - |\overline{B}^0(\vec{k}), B^0(-\vec{k})>\right). \tag{32}$$

As a consequence, one can never simultaneously have two identical mesons. This permits the performance of a *flavor tag*[3]: if at $t = 0$ one of the mesons decays through a channel which is only allowed for one flavor of the neutral *B*, the other meson in the pair must have the opposite flavor at $t = 0$. The correlation (32) between both sides of the entangled state holds at any time after the production, until the moment one *B* decays.

The entangled state can also be expressed in terms of the CP eigenstates as

$$|i> = \frac{1}{\sqrt{2}}\left(|B_-(\vec{k}), B_+(-\vec{k})> - |B_+(\vec{k}), B_-(-\vec{k})>\right) \tag{33}$$

which, as in the case of the flavor case, makes possible to carry out a *CP tag* at any time after the production of the entangled stated.

The time evolution of a *B* meson of the entangled state (32) or (33) observed an interval Δt after the other *B* was *flavor* or *CP tagged* is given by (27) and (29), respectively. In the following the final state

---

[3]In this context by flavor tag we mean 'preparation of a definite flavor state' (reconstructed side), which has to be distinguished of flavor tag in the context of B tagging, i.e. flavor tag of the other *B*.

configuration will be denoted generally as (X, Y). In this notation, appearance of final state X at t_0 (with momentum $\vec{k}$) always precedes that of Y at $t = t_0 + \Delta t$ (with momentum $-\vec{k}$), i.e. $\Delta t > 0$. For example, if X is a CP=$-$ state produced by a CP conserving decay, the correlation of the entangled state ensures that at t_0 the other B was a B_+. Such a state evolves then for a time Δt and its subsequent decay into Y is a projection onto the corresponding flavor state. In the following, the reconstructed CP and flavor final states are denoted as $B_{r\pm}$ and $B_r^0/\bar{B}_r^0$, respectively, while the flavor states used for B flavor tagging will be denoted as $B_t^0/\bar{B}_t^0$. All possible B final states are denoted generally as f.

The probability to find the final state (X, Y) from the initial state (32) or (33) is obtained from (27) and (29), and is given by:

$$| (X, Y) |^2 \equiv | \langle Y | H | \bar{X}(t) \rangle |^2 = \frac{1}{2} \frac{e^{-\Gamma \Sigma t}}{| 1 - \varepsilon_1 \varepsilon_2 |^2} | A_X |^2 | A_Y |^2 \times$$

$$\times \left\{ (\eta_+ + \eta_-) \cosh\left(\frac{\Delta\Gamma\Delta t}{2}\right) + (\eta_+ - \eta_-) \sinh\left(\frac{\Delta\Gamma\Delta t}{2}\right) + \eta_{re} \cos(\Delta m \Delta t) + \eta_{im} \sin(\Delta m \Delta t) \right\} \qquad (34)$$

where $\Sigma t = t_0 + t$ and A_f and $\bar{A}_f$ are the decay amplitudes into an arbitrary final state f,

$$A_f = \langle f | H | B^0 \rangle \quad , \quad \bar{A}_f = \langle f | H | \bar{B}^0 \rangle . \qquad (35)$$

The underlying assumptions in equation (34) are: i) the $\Delta B = \Delta Q$ rule applies ($A_{\bar{B}_t^0} = \bar{A}_{B_t^0} = A_{\bar{B}_r^0} = \bar{A}_{B_r^0} = 0$); ii) there is CP/CPT convervation in the decay, $r_f = | \bar{A}_{\bar{f}}/A_f | = 1$. The values of the coefficients are the following (s_t denotes the flavor of the state Y, $s_t = -1(+1)$ for $\bar{B}_t^0(B_t^0)$):

- CP tag, $X = B_{r-}, Y = B_t^0(\bar{B}_t^0)$:

$$\begin{aligned} \eta_+ &= 1 + | \varepsilon_1 |^2 + s_t 2\mathrm{Re}(\varepsilon_1) \\ \eta_- &= | \varepsilon_1 |^2 \left\{ 1 + | \varepsilon_2 |^2 + s_t 2\mathrm{Re}(\varepsilon_2) \right\} \\ \eta_{re} &= -2 \left\{ \mathrm{Re}(\varepsilon_1 \varepsilon_2) + | \varepsilon_1 |^2 [1 + s_t \mathrm{Re}(\varepsilon_2)] + s_t \mathrm{Re}(\varepsilon_1) \right\} \\ \eta_{im} &= 2 \left\{ \mathrm{Im}(\varepsilon_1 \varepsilon_2) + s_t | \varepsilon_1 |^2 \mathrm{Im}(\varepsilon_2) + s_t \mathrm{Im}(\varepsilon_1) \right\} \end{aligned}$$

$$\qquad (36)$$

- CP tag, $X = B_{r+}, Y = B_t^0(\bar{B}_t^0)$:

$$\begin{aligned} \eta_+ &= | \varepsilon_2 |^2 \left\{ 1 + | \varepsilon_1 |^2 + s_t 2\mathrm{Re}(\varepsilon_1) \right\} \\ \eta_- &= 1 + | \varepsilon_2 |^2 + s_t 2\mathrm{Re}(\varepsilon_2) \\ \eta_{re} &= -2 \left\{ \mathrm{Re}(\varepsilon_1 \varepsilon_2) + | \varepsilon_2 |^2 [1 + s_t \mathrm{Re}(\varepsilon_1)] + s_t \mathrm{Re}(\varepsilon_2) \right\} \\ \eta_{im} &= -2 \left\{ \mathrm{Im}(\varepsilon_1 \varepsilon_2) + s_t | \varepsilon_2 |^2 \mathrm{Im}(\varepsilon_1) + s_t \mathrm{Im}(\varepsilon_2) \right\} \end{aligned}$$

$$\qquad (37)$$

- Flavor tag, $X = B_r^0(\bar{B}_r^0)$, $Y = \bar{B}_t^0(B_t^0)$ (unmixed):

$$
\begin{aligned}
\eta_+ + \eta_- &= \frac{1}{2}\left\{ |\,(1+\varepsilon_1)(1-\varepsilon_2)\,|^2 + |\,(1-\varepsilon_1)(1+\varepsilon_2)\,|^2 \right\} \\
\eta_+ - \eta_- &= \frac{1}{2}s_t\left\{ |\,(1+\varepsilon_1)(1-\varepsilon_2)\,|^2 - |\,(1-\varepsilon_1)(1+\varepsilon_2)\,|^2 \right\} \\
\eta_{re} &= \frac{1}{2}\mathrm{Re}\left\{ (1-\varepsilon_1)(1+\varepsilon_2)(1+\varepsilon_1^*)(1-\varepsilon_2^*) + (1+\varepsilon_1)(1-\varepsilon_2)(1-\varepsilon_1^*)(1+\varepsilon_2^*) \right\} \\
\eta_{im} &= -\frac{1}{2}s_t\mathrm{Im}\left\{ (1-\varepsilon_1)(1+\varepsilon_2)(1+\varepsilon_1^*)(1-\varepsilon_2^*) - (1+\varepsilon_1)(1-\varepsilon_2)(1-\varepsilon_1^*)(1+\varepsilon_2^*) \right\}
\end{aligned}
\tag{38}
$$

- Flavor tag, $X = B_r^0(\bar{B}_r^0)$, $Y = B_t^0(\bar{B}_t^0)$ (mixed):

$$
\begin{aligned}
\eta_+ + \eta_- &= |\,(1+s_t\varepsilon_1)(1+s_t\varepsilon_2)\,|^2 \\
\eta_+ - \eta_- &= 0 \\
\eta_{re} &= -(\eta_+ + \eta_-) \\
\eta_{im} &= 0
\end{aligned}
\tag{39}
$$

In all the above equations we have assumed that the CP and flavor (reconstructed side) states decay first than the opposite B, the one used for B tagging. When the opposite situation happens (X and Y are interchanged), expression (34) still applies by just flipping the sign of the $(\eta_+ - \eta_-)$ and η_{im} coefficients. In presence of CP violation in the decay (B_{CP} events), the corresponding equations are modified to those derived in appendix A. In the case of B_{flav} processes CPT violation in the decay can be introduced multiplying by a global $r_{B_r^0}^2$ factor the coefficients corresponding to $X = \bar{B}_r^0$. Using the lighter state instead of the heavier one to define ε would imply the replacement $\varepsilon_1 \to 1/\varepsilon_1$ and $\varepsilon_2 \to 1/\varepsilon_2$.

Experimentally, the information available for the time sum for the meson evolution Σt in (34) is quite poor compared to Δt. It is therefore appropiate to work with an integrated probability,

$$
f(X,Y;\Delta t) = \int_{\Delta t}^{+\infty} d\Sigma t\, |(X,Y)|^2 \,,
\tag{40}
$$

which gives the final general time dependent intensity.

The hierarchy of the ε and δ complex parameters demonstrated in section 2.3, together with the perturbative characteristic of CPT violation, allow us to calculate equations (34)-(40) to leading order in $\mathrm{Re}(\varepsilon)$ and δ. Assuming CP/CPT conservation in the decay ($r_f = 1$), the time dependent decay rate reads

$$
\begin{aligned}
f(X,Y;\Delta t) = \frac{1}{2}\frac{e^{-\Gamma|\Delta t|}}{\Gamma} |\,A_X\,|^2 |\,A_Y\,|^2 &\left\{ a\cosh\left(\frac{\Delta\Gamma\Delta t}{2}\right)\right. \\
&\left. + b\cos(\Delta m\Delta t) + c\sinh\left(\frac{\Delta\Gamma\Delta t}{2}\right) + d\sin(\Delta m\Delta t) \right\}.
\end{aligned}
\tag{41}
$$

Coefficient	(B_r^0, B_t^0)	$(\bar{B}_r^0, \bar{B}_t^0)$	$(B_r^0, \bar{B}_t^0)$	$(\bar{B}_r^0, B_t^0)$
a	$1+4\frac{\text{Re}\varepsilon}{1+|\varepsilon|^2}$	$1-4\frac{\text{Re}\varepsilon}{1+|\varepsilon|^2}$	1	1
b	$-\left(1+4\frac{\text{Re}\varepsilon}{1+|\varepsilon|^2}\right)$	$-\left(1-4\frac{\text{Re}\varepsilon}{1+|\varepsilon|^2}\right)$	1	1
c	0	0	$-2\frac{\text{Re}\delta}{1+|\varepsilon|^2}$	$2\frac{\text{Re}\delta}{1+|\varepsilon|^2}$
d	0	0	$-2\frac{\text{Im}\delta}{1+|\varepsilon|^2}$	$2\frac{\text{Im}\delta}{1+|\varepsilon|^2}$

Table 1: Coefficients of the various time dependencies in $(B_f^0/\bar{B}_f^0, B_t^0/\bar{B}_t^0)$ events, to leading order in $\text{Re}(\varepsilon)$ and δ, for the (ε, δ) formalism.

Coefficient	$(B_{r\pm}, B_t^0/\bar{B}_t^0)$
a	$1+2s_t\frac{\text{Re}\varepsilon}{1+|\varepsilon|^2} - s_t\eta_{CP}\frac{1-|\varepsilon|^2}{1+|\varepsilon|^2}\frac{\text{Re}\delta}{1+|\varepsilon|^2} - 2\eta_{CP}\frac{\text{Im}\varepsilon}{1+|\varepsilon|^2}\frac{\text{Im}\delta}{1+|\varepsilon|^2}$
b	$-2s_t\frac{\text{Re}\varepsilon}{1+|\varepsilon|^2} + s_t\eta_{CP}\frac{1-|\varepsilon|^2}{1+|\varepsilon|^2}\frac{\text{Re}\delta}{1+|\varepsilon|^2} + 2\eta_{CP}\frac{\text{Im}\varepsilon}{1+|\varepsilon|^2}\frac{\text{Im}\delta}{1+|\varepsilon|^2}$
c	$-\eta_{CP}\frac{1-|\varepsilon|^2}{1+|\varepsilon|^2}\left[1+2s_t\frac{\text{Re}\varepsilon}{1+|\varepsilon|^2}\right] + s_t\frac{\text{Re}\delta}{1+|\varepsilon|^2}$
d	$-2s_t\eta_{CP}\frac{\text{Im}\varepsilon}{1+|\varepsilon|^2}\left[1+2s_t\frac{\text{Re}\varepsilon}{1+|\varepsilon|^2}\right] + s_t\frac{\text{Im}\delta}{1+|\varepsilon|^2}$

Table 2: Coefficients for CP-to-flavor final configurations, to leading order in $\text{Re}(\varepsilon)$ and δ, for the (ε, δ) formalism. s_t is $-1(+1)$ for $\bar{B}_t^0$ (B_t^0) tags, and η_{CP} denotes the CP eigenstate.

where the coefficients a, b, c, d are given in tables 1 and 2 for flavor-to-flavor and CP-to-flavor transitions, respectively.

In *BABAR*, Δt is used as a signed quantity defined as $\Delta t = t - t_0 = t_{REC} - t_{TAG}$ [23]. Compared to the convention described in section 2.5, this is equivalent to say that in the final state (X,Y), X is always the reconstructed side (flavor or CP), Y is the B used for tagging, and the order of appearance is given by the Δt sign. Given that with this convention Δt is positive for flavor-to-CP transitions and flavor-to-flavor(reconstructed), we have to flip the signs of the c and d coefficients:

$$
\begin{aligned}
f(X,Y;\Delta t) &= \frac{1}{N}\frac{e^{-\Gamma|\Delta t|}}{2\Gamma}\left\{a\cosh\left(\frac{\Delta\Gamma\Delta t}{2}\right)\right. \\
&\left. +b\cos(\Delta m\Delta t) - c\sinh\left(\frac{\Delta\Gamma\Delta t}{2}\right) - d\sin(\Delta m\Delta t)\right\},
\end{aligned}
\tag{42}
$$

where N is the normalization factor defined so that

$$
\sum_{Y=B_t^0,\bar{B}_t^0}\int_{-\infty}^{+\infty} f(X,Y;\Delta t)d\Delta t = 1
\tag{43}
$$

for B_{CP} transitions, and

$$
\sum_{X=B_r^0,\bar{B}_r^0}\sum_{Y=B_t^0,\bar{B}_t^0}\int_{-\infty}^{+\infty} f(X,Y;\Delta t)d\Delta t = 1
\tag{44}
$$

for B_{flav} transitions. It should be noted that the normalization (44) does not take into account the fact that T violation introduces B^0-$\bar{B}^0$ differences in the time integrated rates (i.e. $\chi_d^{B^0} \neq \chi_d^{\bar{B}^0}$). The motivation to use a global $B^0\bar{B}^0$ normalization is the constraint from time integrated rates that it implies, improving significantly the precision on Δm [24], while there is no evidence of biases on any of the physics parameters (as shown in section 5).

Figure 1 ilustrates the shape of the time dependent decay rates for flavor-to-flavor transitions (unmixed and mixed) for different values of $\Delta\Gamma/\Gamma$ (0,0.2), $\frac{\mathrm{Re}\varepsilon}{1+|\varepsilon|^2}$(0,0.05) and $\frac{\mathrm{Im}\delta}{1+|\varepsilon|^2}$(0,0.1), asuming Δm=0.472 ps^{-1} and $\frac{1-|\varepsilon|^2}{1+|\varepsilon|^2}\frac{\mathrm{Re}\delta}{1+|\varepsilon|^2}$=0. The distributions for flavor-to-CP transitions can be seen in figure 2, for different values of $\Delta\Gamma/\Gamma$ (0,0.2), $\frac{1-|\varepsilon|^2}{1+|\varepsilon|^2}\frac{\mathrm{Re}\delta}{1+|\varepsilon|^2}$(0,0.2) and $\frac{\mathrm{Re}\varepsilon}{1+|\varepsilon|^2}$(0,0.05), asuming Δm=0.472 ps^{-1}, $\frac{\mathrm{Im}\varepsilon}{1+|\varepsilon|^2} = 0.35$ and $\frac{\mathrm{Im}\delta}{1+|\varepsilon|^2} = 0$.

The $\frac{1-|\varepsilon|^2}{1+|\varepsilon|^2}$ factor entering in the coefficients of the intensities can be expressed in terms of $\frac{\mathrm{Re}\varepsilon}{1+|\varepsilon|^2}$ and $\frac{\mathrm{Im}\varepsilon}{1+|\varepsilon|^2}$. In order to find the algebraic relation, we need first to extract $|\varepsilon|$ from $\frac{\mathrm{Re}\varepsilon}{1+|\varepsilon|^2}$ and $\frac{\mathrm{Im}\varepsilon}{1+|\varepsilon|^2}$, and then calculate $\frac{1-|\varepsilon|^2}{1+|\varepsilon|^2}$.

$|\varepsilon|$ can be related to $x = \frac{\mathrm{Re}\varepsilon}{1+|\varepsilon|^2}$ and $y = \frac{\mathrm{Im}\varepsilon}{1+|\varepsilon|^2}$ via a second order equation in $|\varepsilon|$:

$$|\varepsilon|^2 = \frac{1}{2}\left[-\rho \pm \sqrt{\rho^2 - 4}\right] \tag{45}$$

where

$$\rho = 2 - \frac{1}{x^2 + y^2} . \tag{46}$$

Both solutions are possible, providing opposite sign solutions for $\frac{1-|\varepsilon|^2}{1+|\varepsilon|^2}$. Solving equation (45) with x^2 and y^2 in terms of $|\varepsilon|$,

$$\frac{1}{x^2 + y^2} = \frac{(1+|\varepsilon|^2)^2}{|\varepsilon|^2} , \tag{47}$$

we get that the positive solution of (45) is $1/|\varepsilon|^2$, and the negative one $|\varepsilon|^2$. This ambiguity is a consequence of the choice of ε as the coefficient of the $|B_-\rangle$ state for the physical state $|B_1\rangle$, equation (13). State $|B_1\rangle$ could also be defined, with exactly the same physical meaning, with a coefficient $1/\varepsilon$ in front of $|B_+\rangle$. For consistency with the choice of ε in (13) we take the negative solution. The value of $|\varepsilon|^2$ is constrained to be in the physical region, which corresponds to $\rho^2 - 4 \geq 0$.

It is worth noting that the CPT/CP, CP/T parameters are insensitive to the previous sign ambiguity. From a detailed inspection of equation (42) and table 2, it is concluded that a change of sign in $\frac{1-|\varepsilon|^2}{1+|\varepsilon|^2}$ implies a change of sign in $\frac{\mathrm{Re}\delta}{1+|\varepsilon|^2}$ and $\Delta\Gamma$. However, the product $\frac{1-|\varepsilon|^2}{1+|\varepsilon|^2}\frac{\mathrm{Re}\delta}{1+|\varepsilon|^2}$, to which CPT asymmetries are proportional (as discussed in section 2.8), remains unchanged, and the change in the sign of $\frac{1-|\varepsilon|^2}{1+|\varepsilon|^2}$ would only manisfest in $\Delta\Gamma$. In this case the parameter to which the analysis will be sensitive is therefore $\Delta\Gamma \times sign(\frac{1-|\varepsilon|^2}{1+|\varepsilon|^2})$.

Therefore, our choice of seven independent real physics parameters that model CPT/CP, CP/T and mixing according to equation (42) is
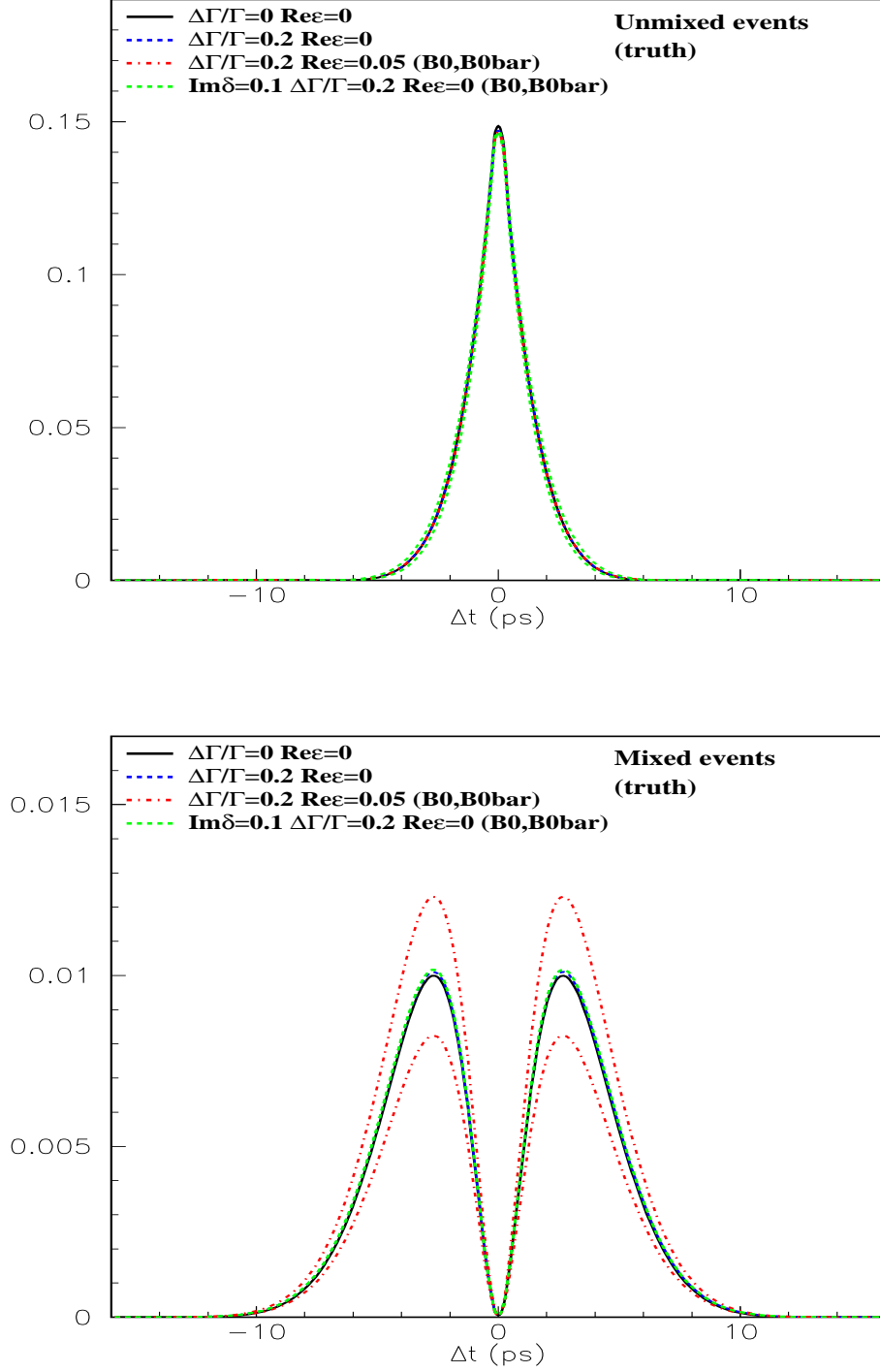
Figure 1: Theoretical decay time distributions for $(B_r^0/\overline{B}_r^0, B_t^0/\overline{B}_t^0)$ transitions for (top) unmixed and (bottom) mixed events. The different curves correspond to different values of $\Delta\Gamma/\Gamma$, $\frac{\mathrm{Re}\varepsilon}{1+|\varepsilon|^2}$ and $\frac{\mathrm{Im}\delta}{1+|\varepsilon|^2}$. Δm is assumed to be 0.472 ps^{-1} and $\delta=0$. No mistag and time resolution have been included.
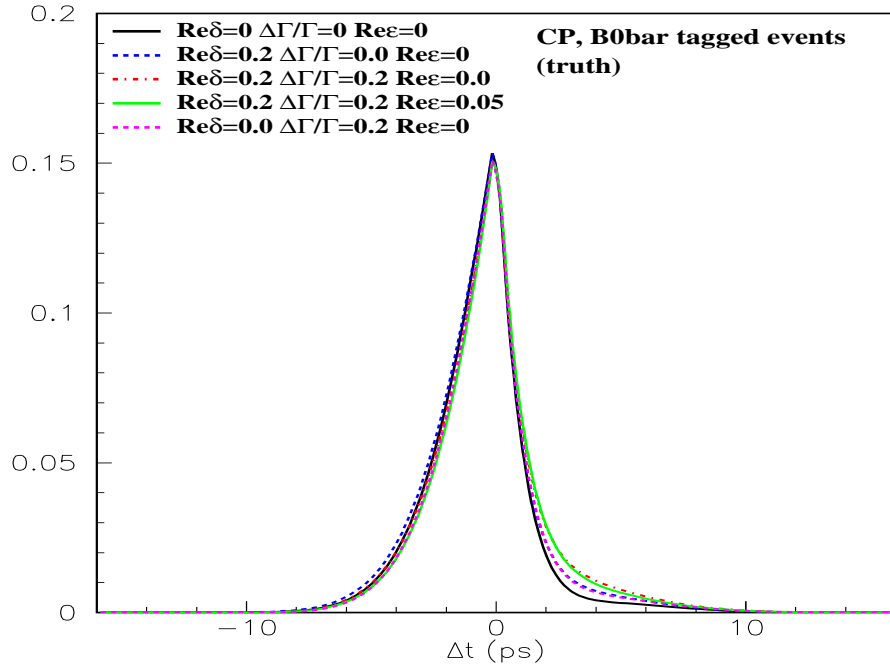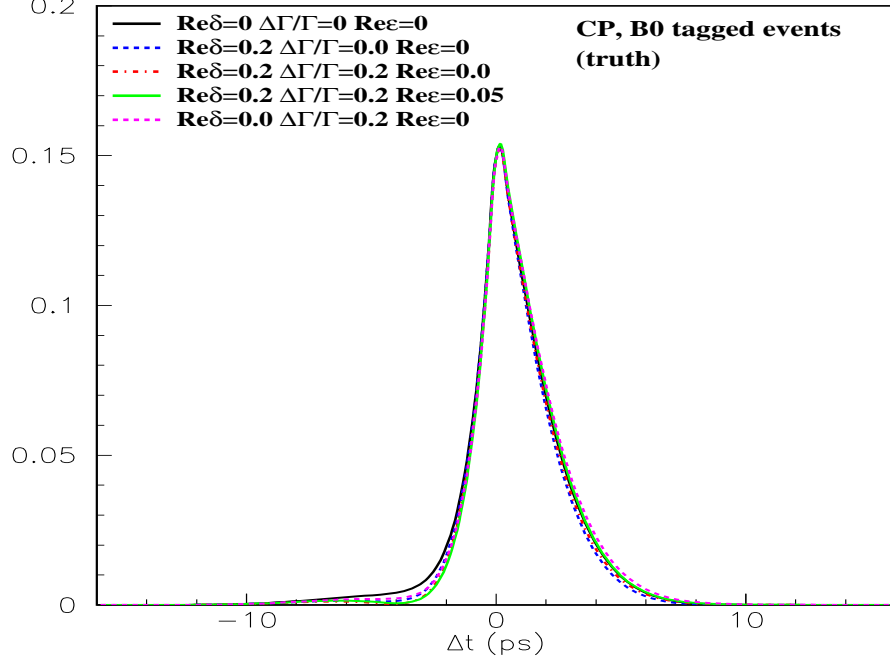
Figure 2: Theoretical decay time distributions for $(B_{r\pm}, B_t^0/\overline{B}_t^0)$ transitions, for (top) B^0 and (bottom) $\overline{B}^0$ tagged events (CP=$-$). The different curves correspond to different values of $\frac{1-|\varepsilon|^2}{1+|\varepsilon|^2}\frac{\mathrm{Re}\delta}{1+|\varepsilon|^2}$, $\Delta\Gamma/\Gamma$ and $\frac{\mathrm{Re}\varepsilon}{1+|\varepsilon|^2}$. Δm is assumed to be 0.472 ps^{-1}, and $\frac{\mathrm{Im}\delta}{1+|\varepsilon|^2}=0$. No mistag and time resolution have been included.

$$\frac{1-|\varepsilon|^2}{1+|\varepsilon|^2}\frac{\text{Re}\delta}{1+|\varepsilon|^2} \quad , \quad \frac{\text{Im}\delta}{1+|\varepsilon|^2} \quad , \frac{\text{Im}\varepsilon}{1+|\varepsilon|^2} \quad , \quad \frac{\text{Re}\varepsilon}{1+|\varepsilon|^2} \quad , \quad \Delta\Gamma/\Gamma \times sign\left(\frac{1-|\varepsilon|^2}{1+|\varepsilon|^2}\right) \quad , \quad \Delta m \quad , \quad \tau$$

2.6 Time dependent decay rates in $(|q/p|,\lambda,z)$ formalism

As outlined in section 2.2, flavor and CP mixing can also be described using the parameters q_i, p_i, $i = 1,2$, instead of ε, δ [13]. The coherent definition of parameters and the calculation of the general time dependent decay rates can be found in [18]. CP/T violating effects are determined here by the set of parameters $\{|q/p|,\lambda_f\}$, and CP/CPT violation is parameterized by z. λ_f is the well-known phase-convention independent parameter defined as

$$\lambda_f \;\; = \;\; \frac{q}{p}\frac{\bar{A}_f}{A_f}\,. \tag{48}$$

λ_f and z are complex valued parameters, while $|q/p|$ is real.

The master equations for the time evolution for an state that is initially a pure $|B^0\rangle$ ($|\bar{B}^0\rangle$) state are written as [18]:

$$|B^0(t)\rangle \;\; = \;\; \frac{1}{2}e^{-imt}e^{-\Gamma t/2}\left\{[g_+(t)+zg_-(t)]\,|B^0\rangle + \sqrt{1-z^2}\frac{q}{p}g_-(t)\,|\bar{B}^0\rangle\right\}$$

$$|\bar{B}^0(t)\rangle \;\; = \;\; \frac{1}{2}e^{-imt}e^{-\Gamma t/2}\left\{[g_+(t)-zg_-(t)]\,|\bar{B}^0\rangle + \sqrt{1-z^2}\frac{p}{q}g_-(t)\,|B^0\rangle\right\} \tag{49}$$

where

$$g_\pm(t) \;\; = \;\; h_+(t)\pm h_-(t)\,. \tag{50}$$

The functions $h_\pm(t)$ are the same as defined in equation (28). The coefficients a, b, c and d of the general time dependent decay rate intensity (42) calculated from (49) are given in tables 3 and 4, for B_{flav} and B_{CP} transitions, respectively. Using the lighter state instead of the heavier to define q/p would imply the replacement $q/p \to -q/p$, or $\lambda_f \to -\lambda_f$. Taking leading order in the CPT parameter z, the coefficients a, b, c and d can be written in a similar way to that used in the (ε,δ), as shown in tables 5 and 6, for B_{flav} and B_{CP} transitions.

Coefficient	(B_r^0,B_t^0)	$(\bar{B}_r^0,\bar{B}_t^0)$	$(B_r^0,\bar{B}_t^0)$	$(\bar{B}_r^0,B_t^0)$
a	$|1-z^2||q/p|^{-2}$	$|1-z^2||q/p|^2$	$1+|z|^2$	$1+|z|^2$
b	$-|1-z^2||q/p|^{-2}$	$-|1-z^2||q/p|^2$	$1-|z|^2$	$1-|z|^2$
c	0	0	$-2\text{Re}z$	$2\text{Re}z$
d	0	0	$-2\text{Im}z$	$2\text{Im}z$

Table 3: Coefficients of the various time dependencies in $(B_r^0/\bar{B}_r^0, B_t^0/\bar{B}_t^0)$ events, for the $(|q/p|,\lambda,z)$ formalism.

If we assume that the mechanisms that contribute to the decay have the same weak phase for $\eta_{CP} = -1$ and $\eta_{CP} = +1$ modes, we can introduce a common phase-convention independent parameter λ,

Coefficient	$(B_{r\pm}, \bar{B}_t^0)$	$(B_{r\pm}, B_t^0)$
a	$\frac{1}{2}\left[1 + \mid z + \sqrt{1-z^2}\lambda_f \mid^2\right]$	$\frac{1}{2}\mid q/p \mid^{-2}\left[\mid \lambda_f \mid^2 + \mid \sqrt{1-z^2} - z\lambda_f \mid^2\right]$
b	$\frac{1}{2}\left[1 - \mid z + \sqrt{1-z^2}\lambda_f \mid^2\right]$	$\frac{1}{2}\mid q/p \mid^{-2}\left[\mid \lambda_f \mid^2 - \mid \sqrt{1-z^2} - z\lambda_f \mid^2\right]$
c	$-\mathrm{Re}\left(z + \sqrt{1-z^2}\lambda_f\right)$	$-\mid q/p \mid^{-2}\left[-\mathrm{Re}\left(\lambda_f^*\sqrt{1-z^2}\right) - \mid \lambda_f \mid^2 \mathrm{Re}z\right]$
d	$-\mathrm{Im}\left(z + \sqrt{1-z^2}\lambda_f\right)$	$\mid q/p \mid^{-2}\left[\mid \lambda_f \mid^2 \mathrm{Im}z - \mathrm{Im}\left(\lambda_f^*\sqrt{1-z^2}\right)\right]$

Table 4: Coefficients for CP-to-flavor final configurations, for the $(\mid q/p \mid, \lambda, z)$ formalism.

$$
\begin{aligned}
\mathrm{Im}\lambda_f &= -\eta_{CP,f}\mathrm{Im}\lambda \\
\mathrm{Re}\lambda_f &= \eta_{CP,f}\mathrm{Re}\lambda .
\end{aligned}
\tag{51}
$$

Coefficient	(B_r^0, B_t^0)	$(\bar{B}_r^0, \bar{B}_t^0)$	$(B_r^0, \bar{B}_t^0)$	$(\bar{B}_r^0, B_t^0)$
a	$\mid q/p \mid^{-2}$	$\mid q/p \mid^2$	1	1
b	$-\mid q/p \mid^{-2}$	$-\mid q/p \mid^2$	1	1
c	0	0	$-2\mathrm{Re}z$	$2\mathrm{Re}z$
d	0	0	$-2\mathrm{Im}z$	$2\mathrm{Im}z$

Table 5: Coefficients of the various time dependencies in $(B_r^0/\bar{B}_r^0, B_t^0/\bar{B}_t^0)$ events, to leading order in the CPT parameter z, for the $(\mid q/p \mid, \lambda, z)$ formalism.

Coefficient	$(B_{r\pm}, \bar{B}_t^0)$
a	$\frac{1}{2}\left(1 + \mid \lambda_f \mid^2\right) + \mathrm{Re}z\mathrm{Re}\lambda_f + \mathrm{Im}z\mathrm{Im}\lambda_f$
b	$\frac{1}{2}\left(1 - \mid \lambda_f \mid^2\right) - \mathrm{Re}z\mathrm{Re}\lambda_f - \mathrm{Im}z\mathrm{Im}\lambda_f$
c	$-\left(\mathrm{Re}z + \mathrm{Re}\lambda_f\right)$
d	$-\left(\mathrm{Im}z + \mathrm{Im}\lambda_f\right)$

Coefficient	$(B_{r\pm}, B_t^0)$
a	$\mid q/p \mid^{-2}\left[\frac{1}{2}\left(1 + \mid \lambda_f \mid^2\right) - \mathrm{Re}z\mathrm{Re}\lambda_f + \mathrm{Im}z\mathrm{Im}\lambda_f\right]$
b	$\mid q/p \mid^{-2}\left[\frac{1}{2}\left(\mid \lambda_f \mid^2 - 1\right) + \mathrm{Re}z\mathrm{Re}\lambda_f - \mathrm{Im}z\mathrm{Im}\lambda_f\right]$
c	$-\mid q/p \mid^{-2}\left[\mathrm{Re}\lambda_f - \mid \lambda_f \mid^2 \mathrm{Re}z\right]$
d	$\mid q/p \mid^{-2}\left[\mathrm{Im}\lambda_f + \mid \lambda_f \mid^2 \mathrm{Im}z\right]$

Table 6: Coefficients for CP-to-flavor final configurations, to leading order in the CPT parameter z, for the $(\mid q/p \mid, \lambda, z)$ formalism.

It should be noted that in the above coefficients we have contributions from $\mid \lambda \mid$, $\mathrm{Im}\lambda$ and $\mathrm{Re}\lambda$, which are related. This closure relation is exactly the same as it was described in section 2.5 for the ε, δ formalism, giving rise to the same problematics [37]. The option chosen here is the same as it was adopted for the (ε, δ) formalism. $\mathrm{Re}\lambda$ is expressed in terms of $\mathrm{Im}\lambda$ and $\mid \lambda \mid$,

$$
\mathrm{Re}\lambda = \pm\sqrt{\mid \lambda \mid^2 - (\mathrm{Im}\lambda)^2} .
\tag{52}
$$

The parameter $\mathrm{Re}z\mathrm{Re}\lambda$ is then insensitive to the sign choice in (52), but $\Delta\Gamma$ does not, and the actual parameter

to which the analysis will be sensitive is $\Delta\Gamma \times sign(\text{Re}\lambda)$. As in the previous section, $\text{Re}\lambda$ is constrained to be within the physical region, i.e. $|\lambda|^2 - (\text{Im}\lambda)^2 \geq 0$.

Therefore, the choice of seven independent real physics parameters that model CPT/CP, CP/T and mixing in the $(|q/p|, \lambda, z)$ formalism is:

$$\frac{\text{Re}\lambda}{|\lambda|}\text{Re}z \; , \; \text{Im}z \; , \; \frac{\text{Im}\lambda}{\lambda} \; , \; |q/p| \; , \; \Delta\Gamma/\Gamma \times sign(\text{Re}\lambda) \; , \; \Delta m \; , \; \tau$$

The correspondence between the above parameters and those defined in section 2.5 is apparent.

2.7 (ε, δ) versus $(|q/p|, \lambda, z)$

Some useful relations connecting the (ε, δ) and $(|q/p|, \lambda, z)$ formalisms are derived here. Beyond the straightforward algebra to find the relations, it should be empathized the fundamental differences between the two approaches. The (ε, δ) formalism is requires the application of a *CP tag*, while $(|q/p|, \lambda, z)$ is based on a *flavor tag*. This implies in the $(|q/p|, \lambda, z)$ formalism the need of a specific decay process to unambiguosly define the unphysical relative phase between B^0 and $\bar{B}^0$. In the case of the (ε, δ) approach the specific process enters in by the need to unambiguosly define the CP tag, requiring a CP-conserving decay into a definite CP final state (CP final state free of direct violation), and not to define the quark phases as before [15]. This is possible to $O(\lambda^3)$ in the quark flavor-mixing parameter of the CKM matrix [16]. The determination is based on the requirement of CP conservation, to $O(\lambda^3)$, in the (sd) and (bs) sectors. If the decay does not fall into a CP-conserving direction, corrections are needed in order to define the CP tag (see appendix A). In the context of $(|q/p|, \lambda, z)$ this means that one is unable (up to additional corrections) disentangle whether the symmetry violation is due to the effective hamiltonian of evolution or the one responsible of the decay.

From equation (11) one can easily obtain the well known relation

$$\frac{2\text{Re}\varepsilon}{1+|\varepsilon|^2} = \frac{1-|q/p|^2}{1+|q/p|^2} \tag{53}$$

or equivalently,

$$|q/p|^2 = \frac{1 - \frac{2\text{Re}(\varepsilon)}{1+|\varepsilon|^2}}{1 + \frac{2\text{Re}(\varepsilon)}{1+|\varepsilon|^2}}. \tag{54}$$

If there is no CP violation in the decay to f, $|\bar{A}_f| = |A_f|$, so that A_f and $\bar{A}_f$ are the same up to the reference phase, CP_{12}, times the CP charge, $\eta_{CP,f}$: $\bar{A}_f = A_f \, \eta_{CP,f} CP_{12}$. We can then write

$$\lambda_f = \eta_{CP,f}\frac{q}{p}CP_{12} = \eta_{CP,f}\frac{1-\varepsilon}{1+\varepsilon} \tag{55}$$

From equation (55) it can then easily be shown the following relations:

$$\text{Re}\lambda_f \equiv \eta_{CP,f}\text{Re}\left(\frac{q}{p}CP_{12}\right) = \eta_{CP,f}\frac{\frac{1-|\varepsilon|^2}{1+|\varepsilon|^2}}{1+2\frac{\text{Re}\varepsilon}{1+|\varepsilon|^2}} \tag{56}$$

18

$$\text{Im}\lambda_f \quad \equiv \quad -\eta_{CP,f}\text{Im}\left(\frac{q}{p}CP_{12}\right) = -\eta_{CP,f}\frac{2\frac{\text{Im}\varepsilon}{1+|\varepsilon|^2}}{1+2\frac{\text{Re}\varepsilon}{1+|\varepsilon|^2}} \tag{57}$$

and

$$|\lambda_f|^2 \quad \equiv \quad |q/p|^2 = \frac{1-2\frac{\text{Re}\varepsilon}{1+|\varepsilon|^2}}{1+2\frac{\text{Re}\varepsilon}{1+|\varepsilon|^2}} \; . \tag{58}$$

In the limit $\Delta\Gamma = 0$, equations (56), (57) and (58) become

$$\text{Re}\lambda_f \quad = \quad \eta_{CP,f}\frac{1-|\varepsilon|^2}{1+|\varepsilon|^2} \tag{59}$$

$$\text{Im}\lambda_f \quad = \quad -\eta_{CP,f}\frac{2\text{Im}\varepsilon}{1+|\varepsilon|^2} \tag{60}$$

and

$$|\lambda_f|^2 \quad = \quad 1 \tag{61}$$

respectively.

From (19), (20), (23) and (24), it can be obtained the following relation,

$$\frac{\delta}{1-\varepsilon^2} \quad = \quad \frac{\Delta}{\Delta m + i\Delta\Gamma/2} \equiv z \; . \tag{62}$$

To linear order in $\frac{\text{Re}\varepsilon}{1+|\varepsilon|^2}$ and δ,

$$\frac{\delta}{1+|\varepsilon|^2} \quad \equiv \quad z \tag{63}$$

2.8 Building the asymmetries

By comparing the intensities corresponding to the different processes we can build several time-dependent asymmetries.

2.8.1 Flavor-to-flavor asymmetries

From the flavor-to-flavor processes three non-trivial asymmetries arise.

The first, well known mixing asymmetry,

$$A(Mixing) \equiv \frac{f(B_r^0, \bar{B}_t^0) + f(\bar{B}_r^0, B_t^0) - f(B_r^0, B_t^0) - f(\bar{B}_r^0, \bar{B}_t^0)}{f(B_r^0, \bar{B}_t^0) + f(\bar{B}_r^0, B_t^0) + f(B_r^0, B_t^0) + f(\bar{B}_r^0, \bar{B}_t^0)} = \frac{\cos(\Delta m \Delta t)}{\cosh(\Delta\Gamma\Delta t/2)} \tag{64}$$
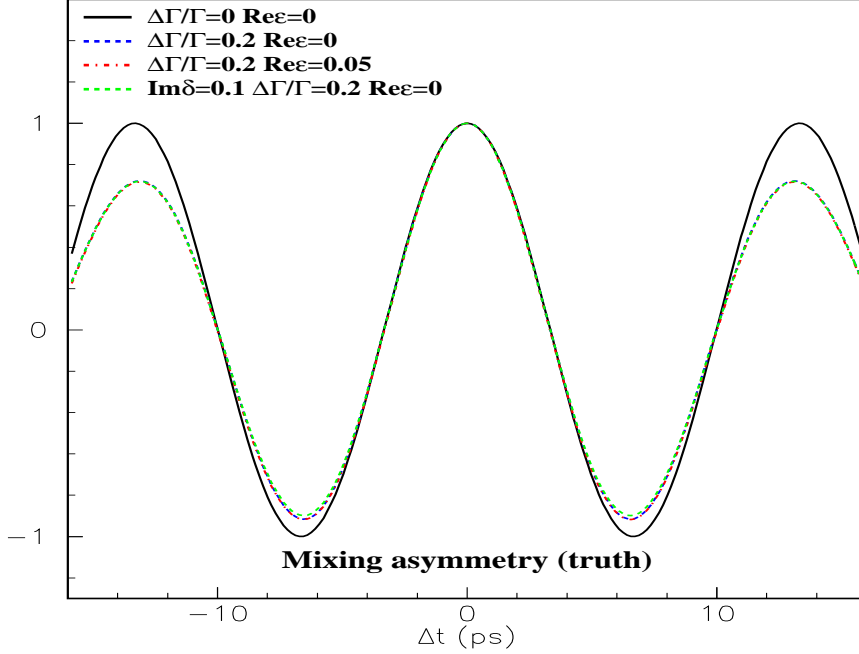
Figure 3: Mixing asymmetry as defined in equation (64). The different curves correspond to different values of $\Delta\Gamma/\Gamma$, $\frac{\text{Re}\varepsilon}{1+|\varepsilon|^2}$ and $\frac{\text{Im}\delta}{1+|\varepsilon|^2}$. Δm is assumed to be 0.472 ps^{-1} and $\frac{1-|\varepsilon|^2}{1+|\varepsilon|^2}\frac{\text{Re}\delta}{1+|\varepsilon|^2} = 0$. No mistag and time resolution have been included.

is ilustrated in figure 3. The different curves show how the asymmetry is modified by the presence of $\Delta\Gamma \neq 0$, assuming Δm=0.472 ps^{-1}. Non negligible values of $\frac{\text{Re}\varepsilon}{1+|\varepsilon|^2}$ and δ do not affect the asymmetry, as given by equation (64).

The second asymmetry can be constructed comparing the rates of mixed events for B^0 and $\bar{B}^0$,

$$A(T) \equiv \frac{f(B^0_r, B^0_t) - f(\bar{B}^0_r, \bar{B}^0_t)}{f(B^0_r, B^0_t) + f(\bar{B}^0_r, \bar{B}^0_t)} = 4\frac{\text{Re}\varepsilon}{1+|\varepsilon|^2} \ . \tag{65}$$

This Kabir asymmetry [7] is time independent. It is a genuine CP and T asymmetry, since the second process corresponds to the CP-, or T-transformed of the first one. Thus the asymmetry cannot be faked by $\Delta\Gamma \neq 0$ in absence of true T violation. However, in the exact limit $\Delta\Gamma = 0$, Reε vanishes, and this quantity will be zero, even if CP and T violation exist. So this observable also needs, in order to be non-zero, the presence of $\Delta\Gamma \neq 0$. For B^0_d mesons the negligible value of $\Delta\Gamma$ predicts that this asymmetry will be small and difficult to observe [10]. Figure 4 ilustrates this asymmetry for different values of $\frac{\text{Re}\varepsilon}{1+|\varepsilon|^2}$ (0,0.05) and $\Delta\Gamma/\Gamma$ (0,0.2), assuming Δm=0.472 ps^{-1}. The asymmetry is insensitive to δ.

The third asymmetry can be constructed from the comparison of unmixed rates for B^0 and $\bar{B}^0$ [17]:
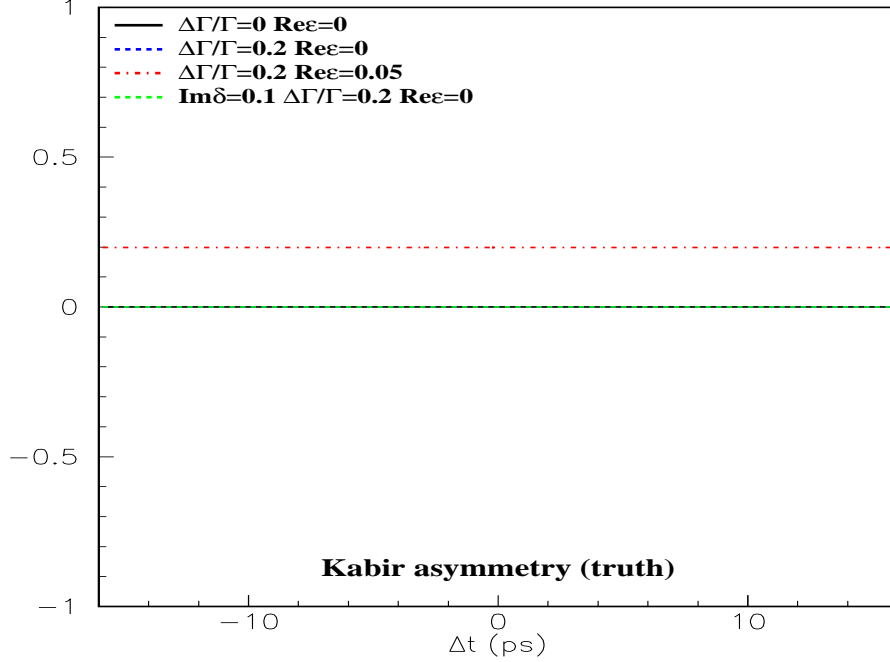
Figure 4: Kabir asymmetry as defined in equation (65). The different curves correspond to different values of $\Delta\Gamma/\Gamma$, $\frac{\mathrm{Re}\varepsilon}{1+|\varepsilon|^2}$ and $\frac{\mathrm{Im}\delta}{1+|\varepsilon|^2}$. Δm is assumed to be 0.472 ps^{-1} and $\frac{1-|\varepsilon|^2}{1+|\varepsilon|^2}\frac{\mathrm{Re}\delta}{1+|\varepsilon|^2}=0$. No mistag and time resolution have been included.

$$
\begin{aligned}
A(CPT) &\equiv \frac{f(B_r^0,\bar{B}_t^0)-f(\bar{B}_r^0,B_t^0)}{f(B_r^0,\bar{B}_t^0)+f(\bar{B}_r^0,B_t^0)} \\
&= 2\frac{\frac{\mathrm{Re}\delta}{1+|\varepsilon|^2}\sinh\left(\frac{\Delta\Gamma\Delta t}{2}\right)+\frac{\mathrm{Im}\delta}{1+|\varepsilon|^2}\sin\left(\Delta m\Delta t\right)}{\cosh\left(\frac{\Delta\Gamma\Delta t}{2}\right)+\cos\left(\Delta m\Delta t\right)} \quad .
\end{aligned}
\tag{66}
$$

Contrary to the Kabir asymmetry, this depends on time as an odd function of Δt. If we keep only terms of $O(\Delta\Gamma)$ this asymmetry vanishes, as it is linear in both $\Delta\Gamma$ and δ. We see that it corresponds to a genuine CP and CPT asymmetry, but due to the proportionality of both terms to $\Delta\Gamma$, measuring a small limit for this asymmetry does not give a straightforward bound on CPT violation. Figure 5 ilustrates this asymmetry for different values of $\frac{\mathrm{Re}\varepsilon}{1+|\varepsilon|^2}$ (0,0.05) and $\Delta\Gamma/\Gamma$ (0,0.2), assuming Δm=0.472 ps^{-1} and $\frac{1-|\varepsilon|^2}{1+|\varepsilon|^2}\frac{\mathrm{Re}\delta}{1+|\varepsilon|^2}=0$.

2.8.2 CP-to-flavor asymmetries

The comparison of decay rates with CP-to-flavor/flavor-to-CP transtions provides both *genuine* and *non-genuine* asymmetries [12]. The first type corresponds to pure symmetry violating quantities, i.e. asymmetries between conjugated mesonic processes, that will always vanish if the relating symmetry is respected. The second category does not correspond to purely conjugated pairs of processes, so that a non-vanishing value can arise due to the presence of off-diagonal absorptive parts in the effective hamiltonian, although

21
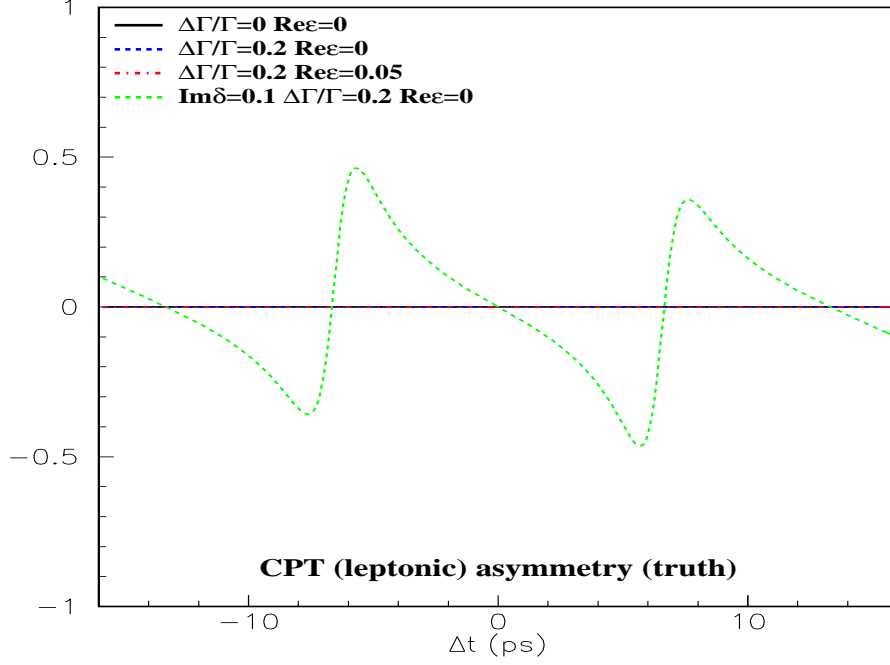
Figure 5: CPT flavor-to-flavor (leptonic) asymmetry as defined in equation (66). The different curves correspond to different values of $\Delta\Gamma/\Gamma$, $\frac{\mathrm{Re}\varepsilon}{1+|\varepsilon|^2}$ and $\frac{\mathrm{Im}\delta}{1+|\varepsilon|^2}$. Δm is assumed to be 0.472 ps^{-1} and $\frac{1-|\varepsilon|^2}{1+|\varepsilon|^2}\frac{\mathrm{Re}\delta}{1+|\varepsilon|^2} = 0$. No mistag and time resolution have been included.

in the exact limit $\Delta\Gamma = 0$ they turn out to be equivalent to the genuine observables, and the deviations are governed by $\Delta\Gamma$ if it is not null. The advantage of the second group of asymmetries is that they can be constructed from events with the same CP charge (for example, with reconstructed $J/\psi K_S^0$ in the final state only), not needing the reconstruction of both, CP+ and CP− states (which involve the experimentally more challenging and less statistically and systematically powerful $J/\psi K_L^0$ mode).

Genuine asymmetries

One can construct genuine asymmetries of the form

$$A(X,Y) = \frac{f(J/\psi K_s^0, B_t^0) - f(X,Y)}{f(J/\psi K_s^0, B_t^0) + f(X,Y)} \tag{67}$$

by comparing the intensity of $(J/\psi K_s^0, B_t^0)$ with those of the configurations that correspond to conjugated mesonic processes via de different fundamental symmetry transformations, as shown in table 7.

Transition	$B_+ \to B^0$	$B_+ \to \bar{B}^0$	$\bar{B}^0 \to B_+$	$B^0 \to B_+$
(X, Y)	$(J/\psi K_S^0, B_t^0)$	$(J/\psi K_S^0, \bar{B}_t^0)$	$(B_t^0, J/\psi K_L^0)$	$(\bar{B}_t^0, J/\psi K_L^0)$
Transformation		CP	CPT	T

Table 7: Transitions and final configurations connected to $B_+ \to B^0$ by symmetry transformations.

The resulting asymmetries are, to linear order in $\Delta\Gamma$ and neglecting $\frac{\text{Im}\delta}{1+|\epsilon|^2}$ terms [12]:

- The CP asymmetry,

$$
\begin{aligned}
A_{\text{CP}} &= A(J/\psi K_s^0, \overline{B}_t^0) \\
&\simeq -\frac{2\text{Im}\epsilon}{1+|\epsilon|^2}\sin(\Delta m \Delta t) + \frac{2\text{Re}\delta}{1+|\epsilon|^2}\frac{1-|\epsilon|^2}{1+|\epsilon|^2}\sin^2\left(\frac{\Delta m \Delta t}{2}\right) \\
&\quad + \frac{4\text{Re}\epsilon}{1+|\epsilon|^2}\left[1+2\left(\frac{2\text{Im}\epsilon}{1+|\epsilon|^2}\right)^2\right]\sin^2\left(\frac{\Delta m \Delta t}{2}\right) \\
&\quad - \frac{\Delta\Gamma\Delta t}{2}\frac{1-|\epsilon|^2}{1+|\epsilon|^2}\frac{2\text{Im}\epsilon}{1+|\epsilon|^2}\sin(\Delta m \Delta t) \\
&\quad - \frac{8\text{Re}\epsilon}{1+|\epsilon|^2}\left(\frac{2\text{Im}\epsilon}{1+|\epsilon|^2}\right)^2\sin^4\left(\frac{\Delta m \Delta t}{2}\right),
\end{aligned}
\tag{68}
$$

has contributions from CP-violating and CPT-violating terms. The first two terms in equation (68) correspond to the limit $\Delta\Gamma = 0$. The first term, odd in Δt, is governed by the CP-violating $\text{Im}\epsilon$, whereas the second one, which is even in Δt, is sensitive to CPT violation through the parameter $\text{Re}\delta$. Linear $\Delta\Gamma$ corrections induce both Δt even and odd functions.

- The T asymmetry,

$$
\begin{aligned}
A_{\text{T}} &= A(\overline{B}_t^0, J/\psi K_L^0) \\
&\simeq -\frac{2\text{Im}\epsilon}{1+|\epsilon|^2}\sin(\Delta m \Delta t)\left[1-\frac{2\text{Re}\delta}{1+|\epsilon|^2}\frac{1-|\epsilon|^2}{1+|\epsilon|^2}\sin^2\left(\frac{\Delta m \Delta t}{2}\right)\right] \\
&\quad + \frac{4\text{Re}\epsilon}{1+|\epsilon|^2}\left[1-2\left(\frac{2\text{Im}\epsilon}{1+|\epsilon|^2}\right)^2\right]\sin^2\left(\frac{\Delta m \Delta t}{2}\right) \\
&\quad + \frac{\Delta\Gamma\Delta t}{2}\frac{1-|\epsilon|^2}{1+|\epsilon|^2}\frac{2\text{Im}\epsilon}{1+|\epsilon|^2}\sin(\Delta m \Delta t) \\
&\quad + \frac{8\text{Re}\epsilon}{1+|\epsilon|^2}\left(\frac{2\text{Im}\epsilon}{1+|\epsilon|^2}\right)^2\sin^4\left(\frac{\Delta m \Delta t}{2}\right),
\end{aligned}
\tag{69}
$$

includes even and odd terms, needs $\epsilon \neq 0$. In the exact limit $\Delta\Gamma = 0$, given by the first term in equation (69), the T asymmetry is purely odd in Δt. Contrary to what happens for A_{CP}, all the new terms in A_{T} from linear $\Delta\Gamma$ corrections have different Δt dependencies than those of zero order.

- The CPT asymmetry,

$$
\begin{aligned}
A_{\text{CPT}} &= A(B_t^0, J/\psi K_L^0) \\
&\simeq -\frac{1-|\epsilon|^2}{1+|\epsilon|^2}\frac{2\text{Re}\delta}{1+|\epsilon|^2}\frac{1}{1-2\frac{\text{Im}\epsilon}{1+|\epsilon|^2}\sin(\Delta m \Delta t)}\sin^2\left(\frac{\Delta m \Delta t}{2}\right),
\end{aligned}
\tag{70}
$$

needs $\delta \neq 0$, and includes both even and odd time dependencies, so that there is no definite symmetry under a change of sign of Δt. To the order considered in our perturbation expansion, A_{CPT} has no linear $\Delta\Gamma$ corrections. The genuine character of the asymmetry would put them in higher order terms. Therefore, a non-vanish value of $\text{Re}\delta$ will genuinely manisfest in A_{CPT}.

If $\Delta\Gamma = 0$ is a good limit, the asymmetries above present odd Δt dependency in the CP/T paramater $\frac{\mathrm{Im}\varepsilon}{1+|\varepsilon|^2}$, and even Δt dependency in the CP/CPT parameter $\frac{1-|\varepsilon|^2}{1+|\varepsilon|^2}\frac{2\mathrm{Re}\delta}{1+|\varepsilon|^2}$. The separation of ε and δ is therefore associated with resolving odd and even functions of Δt, respectively. Corrections due to $\Delta\Gamma \neq 0$ add an even Δt dependency in the CP/T parameter $\frac{\mathrm{Re}\varepsilon}{1+|\varepsilon|^2}$ in A_{CP} and A_{T}, as well as a linear (odd) dependency in $\Delta\Gamma$ which is proporcional to $\frac{\mathrm{Im}\varepsilon}{1+|\varepsilon|^2}$. It is therefore verified that even in the case of $\Delta\Gamma \neq 0$ the asymmetries above vanish if the fundamental symmetries are satisfied.

Figures 6, 7 and 8 show, respectively, these A_{CP} (for CP$-$ and CP$+$), A_{T} and A_{CPT} asymmetries. The different curves ilustrate how the asymmetries are modified by the presence of CPT violation ($\frac{1-|\varepsilon|^2}{1+|\varepsilon|^2}\frac{\mathrm{Re}\delta}{1+|\varepsilon|^2}\neq 0$), $\Delta\Gamma \neq 0$ and T violation ($\frac{\mathrm{Re}\varepsilon}{1+|\varepsilon|^2}\neq 0$), assuming Δm=0.472 ps^{-1}, $\frac{\mathrm{Im}\varepsilon}{1+|\varepsilon|^2} = 0.35$ and $\frac{\mathrm{Im}\delta}{1+|\varepsilon|^2} = 0$.

Non-genuine asymmetries

The previous asymmetries are defined as a comparison between intensities for a conjugated pair of mesonic processes. Nevertheless, there is a fourth discrete transformation, whose relation to the symmetries of the problem is not straightforward. It consists in the exchange of the order of appearance of the decay products X and Y, i.e. $\Delta t \to -\Delta t$. Thus, this transformation relates processes involving transitions with the same CP charge, for example $(J/\psi, K_S^0, B_t^0)$ to $(B_t^0, J/\psi, K_S^0)$. At the mesonic level, $(B_+ \to B^0) \overset{\Delta t}{\to} (\bar{B}^0 \to B_-)$, so that Δt reversal cannot be associated with any fundamental symmetry. But, in the limit $\Delta\Gamma = 0$ it turns out to be equivalent to the time reversal asymmetry,

$$A_{\Delta t}(\Delta\Gamma = 0) \equiv A(B_t^0, J/\psi\, K_S^0)\big|_{\Delta\Gamma=0} \equiv A(\bar{B}_t^0, J/\psi\, K_L^0)\big|_{\Delta\Gamma=0} \tag{71}$$

In general, the equivalence of T and Δt inversions is only valid for hamiltonians with the property of hermiticity, up to a global (proportional to unity) absorptive part.

There are four possible configurations of the final state with the same CP charge (e.g. $J/\psi K_S^0$), depending on the flavor of the opposite side (sign of the charged lepton) and on the order of appearance of the decay products. The relation between these final configurations and the mesonic transitions and the 'symmetry' transformations are detailed in table 8.

Transition	$B_+ \to B^0$	$B_+ \to \bar{B}^0$	$\bar{B}^0 \to B_-$	$B^0 \to B_-$
(X, Y)	$(J/\psi K_S^0, B_t^0)$	$(J/\psi K_S^0, \bar{B}_t^0)$	$(B_t^0, J/\psi K_S^0)$	$(\bar{B}_t^0, J/\psi K_S^0)$
Transformation		CP	Δt	CPΔt

Table 8: (X, Y) configurations involving a single final state with the same CP charge (e.g. $J/\psi K_S^0$) and their relation with the mesonic transitions and the 'symmetry' transformations.

The resulting asymmetries involving the Δt temporal transformation are, to linear order in $\Delta\Gamma$ and neglecting $\frac{\mathrm{Im}\delta}{1+|\varepsilon|^2}$ terms [12]:

24
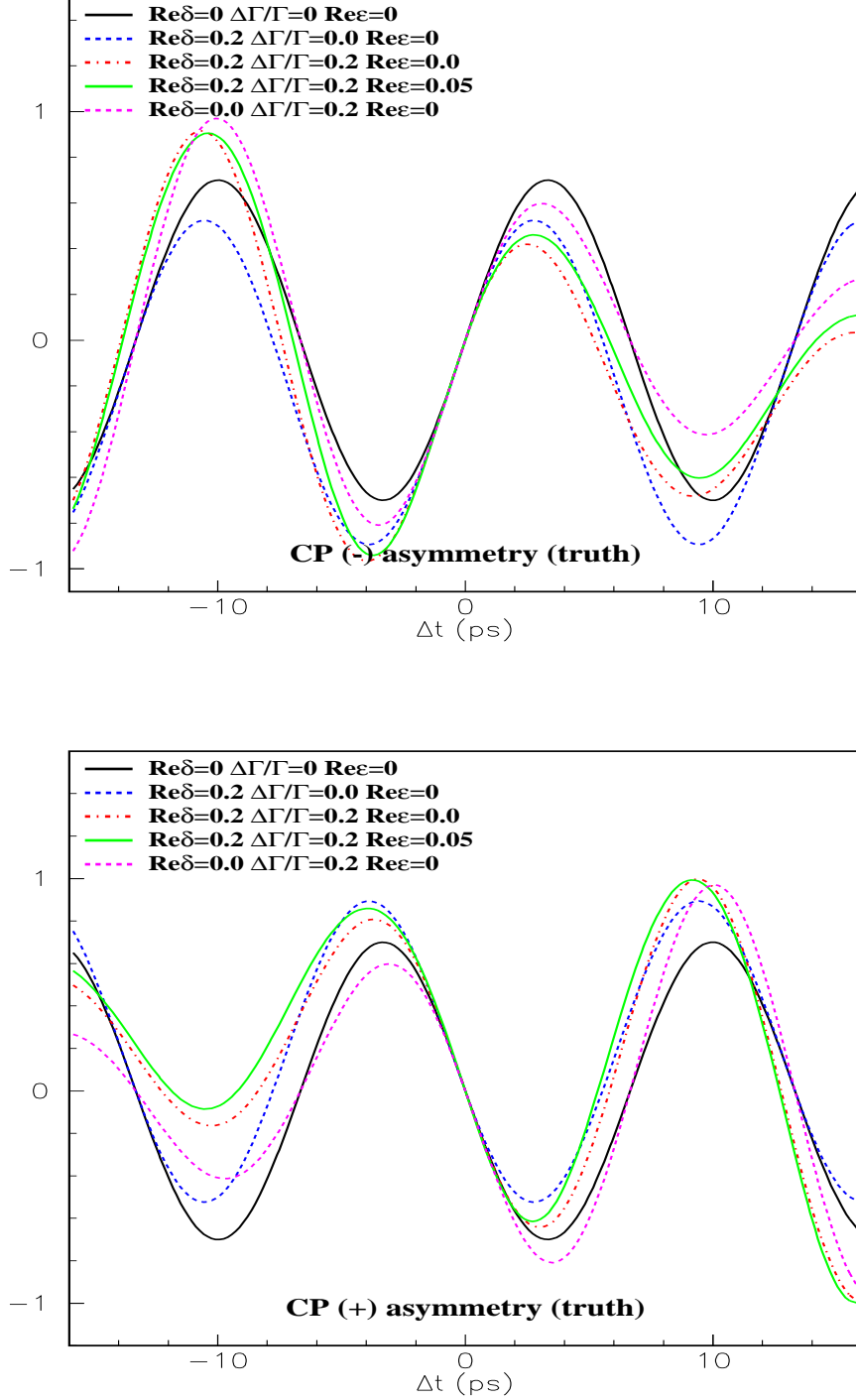
Figure 6: The A_{CP} asymmetry, as defined in equation (68), for CP− (top) and CP+ (bottom). The different curves correspond to different values of $\frac{1-|\varepsilon|^2}{1+|\varepsilon|^2}\frac{\mathrm{Re}\delta}{1+|\varepsilon|^2}$ (0, 0.2), $\Delta\Gamma/\Gamma$ (0, 0.2) and $\frac{\mathrm{Re}\varepsilon}{1+|\varepsilon|^2}$ (0, 0.05). Δm, $\frac{\mathrm{Im}\varepsilon}{1+|\varepsilon|^2}$ and $\frac{\mathrm{Im}\delta}{1+|\varepsilon|^2}$ are assumed to be 0.472 ps^{-1}, 0.35 and 0, respectively. No mistag and time resolution have been included.
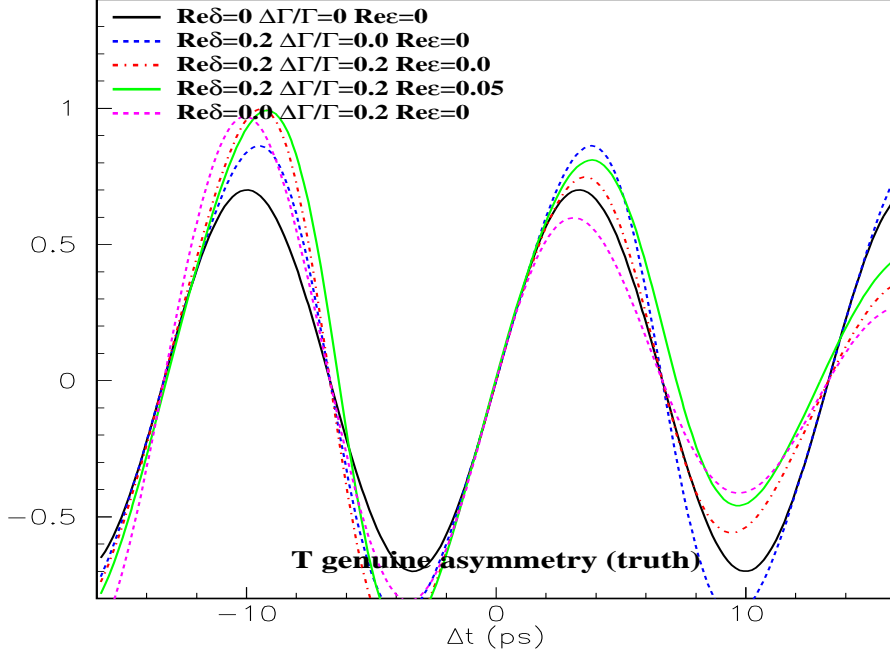
Figure 7: The A_T asymmetry, as defined in equation (69). The different curves correspond to different values of $\frac{1-|\varepsilon|^2}{1+|\varepsilon|^2}\frac{\mathrm{Re}\delta}{1+|\varepsilon|^2}$ (0,0.2), $\Delta\Gamma/\Gamma$ (0,0.2) and $\frac{\mathrm{Re}\varepsilon}{1+|\varepsilon|^2}$ (0,0.05). Δm, $\frac{\mathrm{Im}\varepsilon}{1+|\varepsilon|^2}$ and $\frac{\mathrm{Im}\delta}{1+|\varepsilon|^2}$ are assumed to be 0.472 ps^{-1}, 0.35 and 0, respectively. No mistag and time resolution have been included.

- The Δt asymmetry,

$$
\begin{aligned}
A_{\Delta t} &= A(B_t^0, J/\psi K_s^0) \\
&\simeq -2\frac{\mathrm{Im}\varepsilon}{1+|\varepsilon|^2}\sin(\Delta m \Delta t)\left[1 - 2\frac{\mathrm{Re}\delta}{1+|\varepsilon|^2}\frac{1-|\varepsilon|^2}{1+|\varepsilon|^2}\sin^2\left(\frac{\Delta m \Delta t}{2}\right)\right] \\
&\quad +\frac{\Delta\Gamma\Delta t}{2}\frac{1-|\varepsilon|^2}{1+|\varepsilon|^2} \\
&\quad -\frac{2\mathrm{Re}\varepsilon}{1+|\varepsilon|^2}\frac{2\mathrm{Im}\varepsilon}{1+|\varepsilon|^2}\sin(\Delta m \Delta t)\left[1 - 2\sin^2\left(\frac{\Delta m \Delta t}{2}\right)\right],
\end{aligned}
\tag{72}
$$

- The CPΔt asymmetry,

$$
\begin{aligned}
A_{CP\Delta t} &= A(\bar{B}_t^0, J/\psi K_s^0) \\
&\simeq \frac{1}{1 - \frac{2\mathrm{Im}\varepsilon}{1+|\varepsilon|^2}\sin(\Delta m \Delta t)}\left[\frac{2\mathrm{Re}\delta}{1+|\varepsilon|^2}\frac{1-|\varepsilon|^2}{1+|\varepsilon|^2} + \frac{\Delta\Gamma\Delta t}{2}\frac{1-|\varepsilon|^2}{1+|\varepsilon|^2}\right. \\
&\quad \left. +\frac{4\mathrm{Re}\varepsilon}{1+|\varepsilon|^2}\sin^2\left(\frac{\Delta m \Delta t}{2}\right) - \frac{2\mathrm{Im}\varepsilon}{1+|\varepsilon|^2}\frac{2\mathrm{Re}\varepsilon}{1+|\varepsilon|^2}\sin(\Delta m \Delta t)\right].
\end{aligned}
\tag{73}
$$

The non-genuine character of $A_{\Delta t}$ and $A_{CP\Delta t}$ are explicit in expressions (72) and (73), as in the limit of exact symmetry, $\varepsilon = 0$ and $\delta = 0$, there are surviving terms, linear in $\Delta\Gamma$. Thus off-diagonal absorptive parts in

26
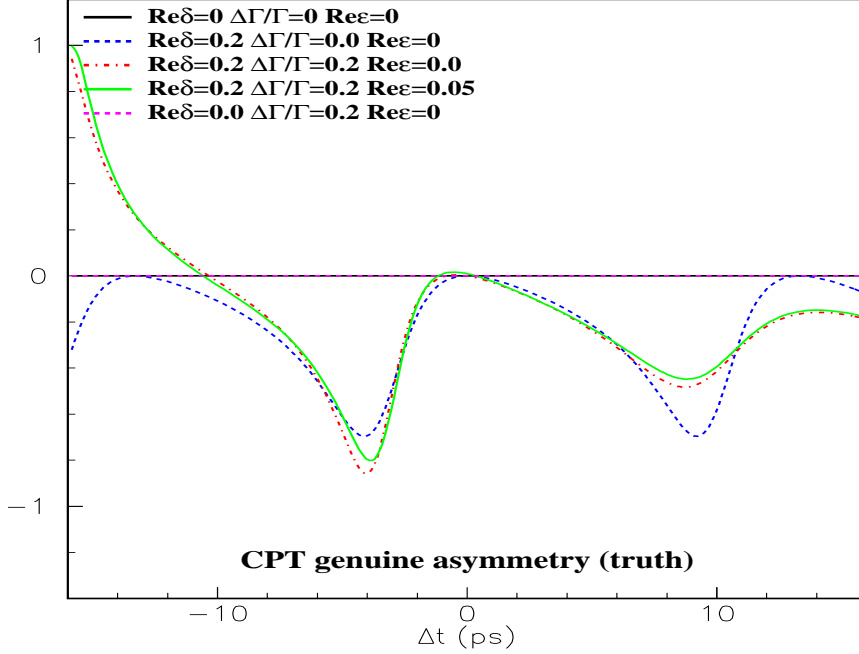
Figure 8: The A_{CPT} asymmetry, as defined in equation 70. The different curves correspond to different values of $\frac{1-|\varepsilon|^2}{1+|\varepsilon|^2}\frac{\text{Re}\delta}{1+|\varepsilon|^2}$ (0,0.2), $\Delta\Gamma/\Gamma$ (0,0.2) and $\frac{\text{Re}\varepsilon}{1+|\varepsilon|^2}$ (0,0.05). Δm, $\frac{\text{Im}\varepsilon}{1+|\varepsilon|^2}$ and $\frac{\text{Im}\delta}{1+|\varepsilon|^2}$ are assumed to be 0.472 ps^{-1}, 0.35 and 0, respectively. No mistag and time resolution have been included.

the effective hamiltonian may originate fake contributions to these non-genuine asymmetries. In the limit $\Delta\Gamma = 0$, these terms disappear, and $A_{\Delta t}$ and $A_{\text{CP}\Delta t}$ become equivalent to A_T and A_{CPT}, as given in equations (69) and (70), respectively.

Figures 9 and 10 show, respectively, the $A_{\Delta t}$ and and $A_{\text{CP}\Delta t}$ asymmetries. The different curves ilustrate how the asymmetries are modified by the presence of CPT violation ($\frac{1-|\varepsilon|^2}{1+|\varepsilon|^2}\frac{\text{Re}\delta}{1+|\varepsilon|^2} \neq 0$), $\Delta\Gamma \neq 0$ and T violation ($\frac{\text{Re}\varepsilon}{1+|\varepsilon|^2} \neq 0$), assuming Δm=0.472 ps^{-1}, $\frac{\text{Im}\varepsilon}{1+|\varepsilon|^2} = 0.35$ and $\frac{\text{Im}\delta}{1+|\varepsilon|^2} = 0$. The fake effects introduced by the absortive part Γ_{12} are apparent.

3 Extraction of the CPT, CP and T violation parameters

In the previous section we have derived the general time dependent decay rate expressions which govern mixing and the CP/CPT, CP/T violation, as well as the asymmetries which reveal the different effects.

In this section, we describe how do we incorporate the various experimental effects to the theoretical intensities (42): mistag rates, limited time resolution, detector asymmetries (differences in $B^0/\bar{B}^0$ reconstruction and tagging efficiencies). The final form of the likelihood function and its technical implementation will also be described here. The section will finish with a discussion about which are the final free parameters used to describe signal and background, as well as the underlying assumptions of the nominal unbinned maximum likelihood fit. The content of this section took extensive profit of the work developped for the
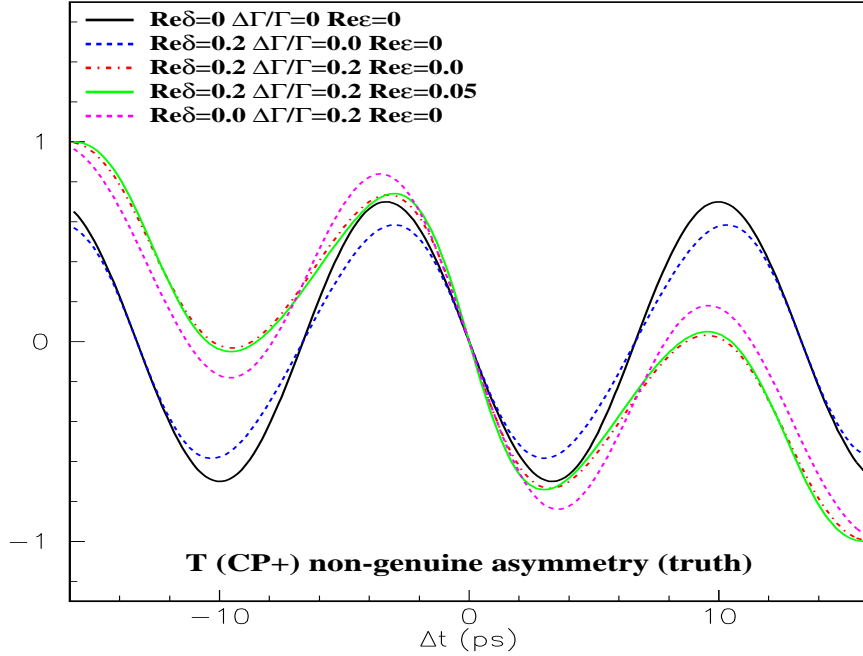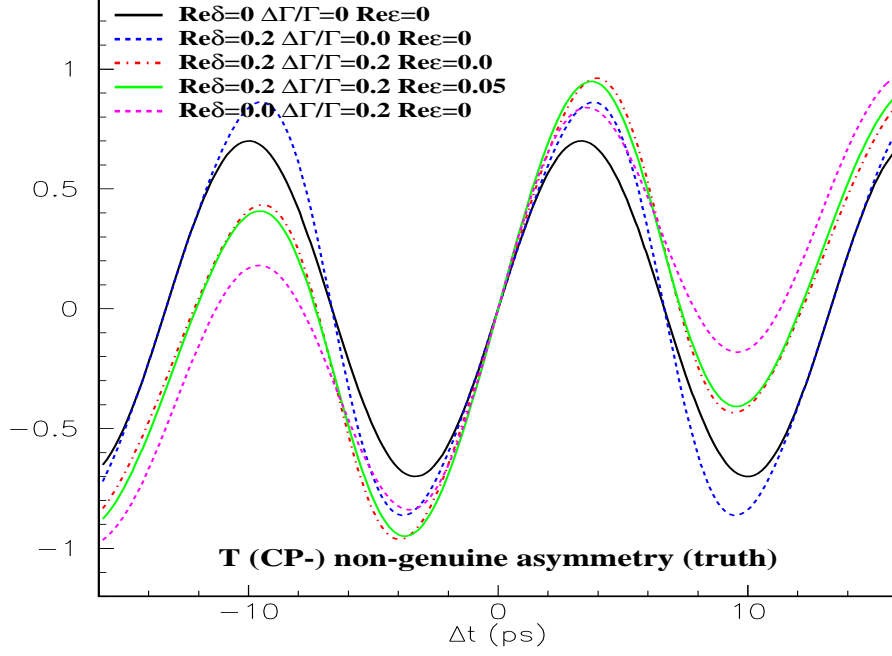
Figure 9: The $A_{\Delta t}$ asymmetry, as defined in equation (72), for CP− (top) and CP+ (bottom) events. The different curves correspond to different values of $\frac{1-|\varepsilon|^2}{1+|\varepsilon|^2}\frac{\mathrm{Re}\delta}{1+|\varepsilon|^2}$ (0, 0.2), $\Delta\Gamma/\Gamma$ (0, 0.2) and $\frac{\mathrm{Re}\varepsilon}{1+|\varepsilon|^2}$ (0, 0.05). Δm, $\frac{\mathrm{Im}\varepsilon}{1+|\varepsilon|^2}$ and $\frac{\mathrm{Im}\delta}{1+|\varepsilon|^2}$ are assumed to be 0.472 ps^{-1}, 0.35 and 0, respectively. No mistag and time resolution have been included.
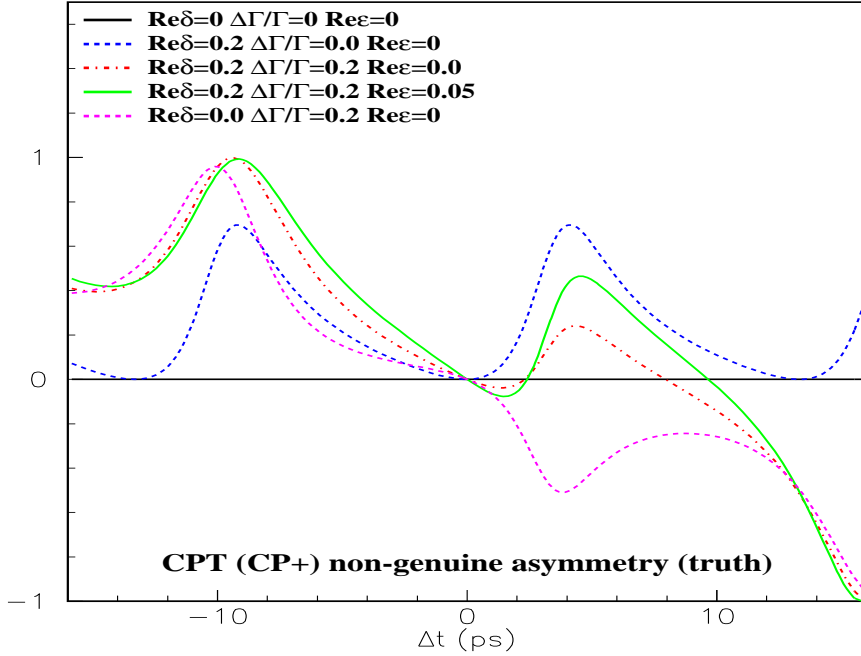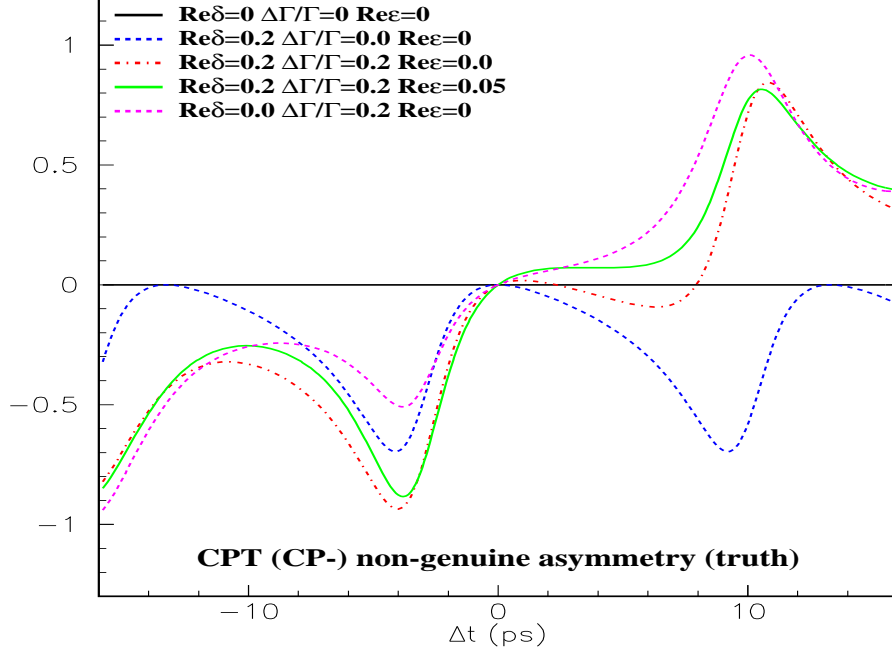
Figure 10: The $A_{\mathrm{CP}\Delta t}$ asymmetry, as defined in equation (73), for CP− (top) and CP+ (bottom) events. The different curves correspond to different values of $\frac{1-|\varepsilon|^2}{1+|\varepsilon|^2}\frac{\mathrm{Re}\delta}{1+|\varepsilon|^2}$ $(0, 0.2)$, $\Delta\Gamma/\Gamma$ $(0, 0.2)$ and $\frac{\mathrm{Re}\varepsilon}{1+|\varepsilon|^2}$ $(0, 0.05)$. Δm, $\frac{\mathrm{Im}\varepsilon}{1+|\varepsilon|^2}$ and $\frac{\mathrm{Im}\delta}{1+|\varepsilon|^2}$ are assumed to be 0.472 ps^{-1}, 0.35 and 0, respectively. No mistag and time resolution have been included.

$\sin 2\beta$ analysis [19, 20, 21, 22].

3.1 Mistag fractions and B^0-$\bar{B}^0$ differences in reconstruction and tagging efficiencies

The time dependent intensities given in equation (42) have to be corrected by the fraction w^α of events with wrongly assigned flavor in tagging category α (Lepton, Kaon, NT1, NT2 [26]), the *mistag fraction*. On the other hand, differences in reconstruction and tagging efficiencies for B^0 and $\bar{B}^0$ can induce biases in the decay time distributions due to the presence of odd terms in Δt (even terms do not contribute). Let us define first the quantities used to parameterize all these effects (we use the same definitions as in [19, 20]).

$w^\alpha_{B^0}$ is defined as the fraction of true B^0 but are incorrectly tagged as $\bar{B}^0$ for tagging category α, and similarly for $w^\alpha_{\bar{B}^0}$ [26]. As the mistag fraction can be different for B^0 and $\bar{B}^0$ due to differences in the material interactions (especially for kaons), it is convenient to define

$$w^\alpha = \frac{w^\alpha_{B^0} + w^\alpha_{\bar{B}^0}}{2} \tag{74}$$

and

$$\Delta w^\alpha = w^\alpha_{B^0} - w^\alpha_{\bar{B}^0} \tag{75}$$

which give, respectively, the mean value and the difference of the mistag fractions for B^0 and $\bar{B}^0$. With these definitions,

$$w^\alpha_{B^0} = w^\alpha + \Delta w^\alpha/2 \tag{76}$$

and

$$w^\alpha_{\bar{B}^0} = w^\alpha - \Delta w^\alpha/2 \ . \tag{77}$$

Let us define now

$$\mu^\alpha \quad = \quad \frac{t^\alpha_{B^0} - t^\alpha_{\bar{B}^0}}{t^\alpha_{B^0} + t^\alpha_{\bar{B}^0}} \tag{78}$$

and

$$\nu \quad = \quad \frac{r_{B^0} - r_{\bar{B}^0}}{r_{B^0} + r_{\bar{B}^0}} \tag{79}$$

where t^α_Y is the tagging efficiency for $Y = B^0, \bar{B}^0$ and tagging category α. Similarly r_X is the overall reconstruction efficiency for $X = B^0, \bar{B}^0$. If we call T^α and R the average tagging and reconstruction efficiencies, we have

$$t^\alpha_{B^0} = T^\alpha(1 + \mu^\alpha) \quad , \quad t^\alpha_{\bar{B}^0} = T^\alpha(1 - \mu^\alpha) \tag{80}$$

and

$$r_{B^0} = R(1+\nu) \quad , \quad r_{\bar{B}^0} = R(1-\nu) \tag{81}$$

The corrected expressions read, for B_{flav} processes:

$$f^\alpha(X,Y;\Delta t) = r_X \left\{ t^\alpha_Y (1-w^\alpha_Y) f(X,Y;\Delta t) + t^\alpha_{\bar{Y}} w^\alpha_{\bar{Y}} f(X,\bar{Y};\Delta t) \right\} \tag{82}$$

and for B_{CP}:

$$f^\alpha(X,Y;\Delta t) = t^\alpha_Y (1-w^\alpha_Y) f(X,Y;\Delta t) + t^\alpha_{\bar{Y}} w^\alpha_{\bar{Y}} f(X,\bar{Y};\Delta t) \tag{83}$$

where t^α_Y, r_X are the quantities defined in (80), (81), and $Y = B^0_t, \bar{B}^0_t$ and $X = B_{r-}, B_{r+}, B^0_t, \bar{B}^0_t$. $(\bar{X}, \bar{Y})$ denotes the conjugate state of (X,Y), and w^α_Y is the mistag fraction as given by equations (76) and (77). The difference among equations (82) and (83) is because $CP-$ and $CP+$ states are normalized separately.

As it is described in section 3.2, the reconstructed event-by-event Δt error is used to weight the events in the fitting procedure. It is therefore important to make sure that there are no significant correlations among this variable and the variables parameterizing the tagging performance, w^α and Δw^α, and if there are, then model them properly. It was found [30] an almost perfect linear correlation between the mean wrong tag fraction, w^α, and the Δt error, especially for the Kaon tagging category, being much weaker or negligible for the other categories. We then model the wrong tag fraction according to the following model:

$$w^\alpha = w^\alpha_0 + w^\alpha_{slope} \sigma_{\Delta t} . \tag{84}$$

Detailed studies to explain the mechanism of this observed correlation can be found in [31]. The difference of the mistag fractions for B^0 and $\bar{B}^0$, Δw^α, is well constant over the full $\sigma_{\Delta t}$ range, for all tagging categories [30]. The tagging performance for each tagging category is therefore characterized by a set of three parameters, w^α_0, w^α_{slope} and Δw^α.

μ^α, ν and T^α can be calculated from time integrated flavor-to-flavor rates according to the prescription documented in [32]. This prescription has to be generalized in order to account for non-vanishing values of $\Delta\Gamma$ as well as Reϵ. As described in appendix B, the parameters μ^α, ν and T^α depend on the number of $B^0/\bar{B}^0$/mixed/unmixed events (x,y,z,w) and the theoretical total rates, independently of mistags and Δt resolution (a,b,c,d). Terms with odd Δt dependence do not contribute, so finally the dependence is with Δm, $\Delta\Gamma$ and $\frac{\text{Re}\epsilon}{1+|\epsilon|^2}$. This dependence (the exact expression can be found in appendix B) has to be taken into account since Δm, $\Delta\Gamma$ and $\frac{\text{Re}\epsilon}{1+|\epsilon|^2}$ are parameters in which we are interested for, otherwise an unsuitable circularity would be induced. The solution adopted to overcome this problem is discussed and validated in section 4.1.10. Assuming $\Delta m = 0.472$ ps^{-1}, $\Delta\Gamma = 0$ and $\frac{\text{Re}\epsilon}{1+|\epsilon|^2} = 0$, the measured values of ν, μ^α and T^α from the Monte Carlo simulation (anal10h ASCII files) are given in tables 9, 10 and 11, respectively.

3.2 Δt resolution function

The decay time difference Δt between the two decaying B mesons is calculated from the z positions of the reconstructed vertices, using the *average τ_B approximation* [23], which uses the measured $\Upsilon(4S)$ boost

Sample	ν
B^0 cocktail MC	0.006 ± 0.004
B^+ cocktail MC	0.010 ± 0.004

Table 9: Measured ν values from the B_{flav} sample for the Monte Carlo simulation (`anal0h` ASCII files).

Sample	Lepton	Kaon	NT1	NT2
B^0 cocktail MC	-0.014 ± 0.015	0.016 ± 0.008	-0.022 ± 0.018	0.011 ± 0.013
B^+ cocktail MC	0.010 ± 0.011	0.011 ± 0.006	0.035 ± 0.015	0.006 ± 0.011

Table 10: Measured μ^α values from the B_{flav} sample for the Monte Carlo simulation (`anal0h` ASCII files).

(determined on a run-by-run basis) as well as the polar angle of the reconstructed B, therefore accounting for the boost of the B mesons with respect to the $\Upsilon(4S)$. The standard *BABAR* algorithm, `BtaSelFit`, with default configuration (beam constraints) is used for the Δz reconstruction [23]. Only events satisfying that $|\Delta t| < 20$ ps and $\sigma_{\Delta t} < 2.4$ ps are accepted. The overall Δt reconstruction efficiency is about 97% and the resolution is about 1.1 ps for more than 99% of the events.

The Δt resolution is modelled using two different parameterizations.

The first approach, called thereafter *GG model*, asumes three Gaussians [24]. The *core* component tries to describe well measured vertices, meanwhile the *tail* part accounts for poorly measured decay times. Finally, there is a small fraction of *outliers* (a few per mille) where Δt is badly reconstructed, partly due to mistakes in the track reconstruction, partly to tracks from secondary decays (long living particles and hard scatters). As the reconstructed Δt error provides a good (approximate) representation of the resolution for the core (tail) Gaussian, it is used to weight the events on a event-by-event basis, rather than to use a global resolution, therefore increasing the sensitivity of the analysis to well measured events. As the error is still not a perfect representation of the resolution (especially for the tail component) we allow for two global scale factors. On the contrary, the event-by-event Δt error is not a good representation of the resolution for the outliers component, and in this case a global and fixed (8 ps) resolution is used instead. In addition to the increase of the sensitivity, the weighting of the events according to the reconstructed Δt error largely eliminates small differences in resolution between the different classes of events entering in the analysis. Very small residual effects due to differences in the scale factors can then be considered as part of the systematic uncertainties. Figure 11 shows the distributions of the per-event error on Δt for the B_{flav} and CP samples in the Monte Carlo simulation. The curves correspond to the unbinned maximum likelihood fit to a Crystal Ball shape. The results of these fits are the basis to define the probability density function used to generate realistic Δt error distributions in toy Monte Carlo exercises, but they do not enter in the definition of the likelihood function (section 3.4).

Sample	Lepton	Kaon	NT1	NT2
B^0 cocktail MC	0.1195 ± 0.0011	0.3451 ± 0.0017	0.0825 ± 0.0010	0.1483 ± 0.0013
B^+ cocktail MC	0.1232 ± 0.0014	0.3720 ± 0.0020	0.0736 ± 0.0011	0.1320 ± 0.0014

Table 11: Measured T^α values from the B_{flav} sample for the Monte Carlo simulation (`anal0h` ASCII files).
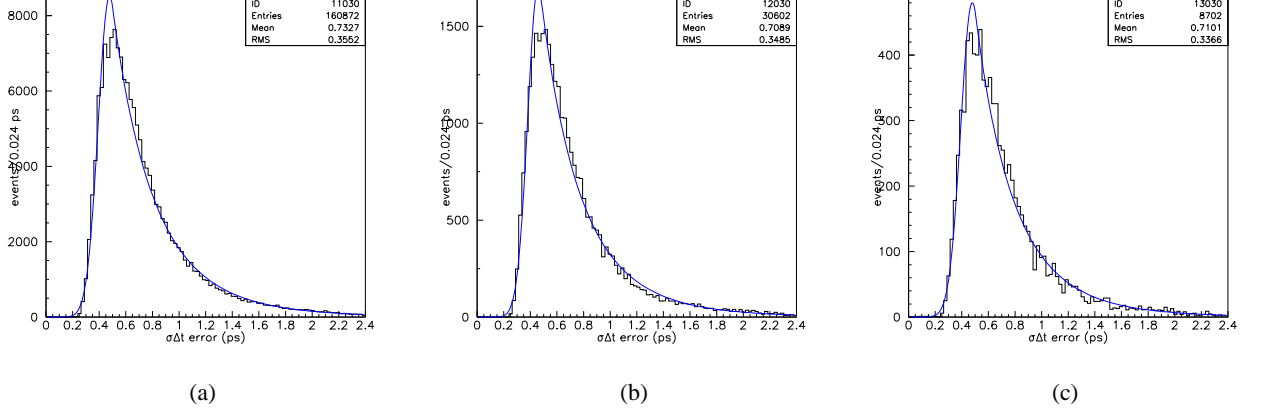
Figure 11: Event-by-event error on Δt for the (a) B_{flav}, (b) $B_{CPK_S^0}$ and (c) $B_{CPK_L^0}$ samples in the Monte Carlo simulation (`anal10h` ASCII files).

Although the vertex reconstruction algorithm minimizes biases due to the secondary charm decays and V^0's in the tagging side, the z_{TAG} position is on average biased towards positive z values, resulting in a negative shift in Δt. This effect is accounted in the resolution function by introducing a shift in the central value of the core and tail Gaussians. Due to the different B decay channels populating the different tagging categories, the average bias is category dependent [27]. It was found that introducing a different bias in each tagging category for the core component but having a common tail bias provides the optimal trade-off between systematic effects and number of different parameters in the resolution [24]. The resolution was also found not to be sensitive to possible biases in the outliers component.

The second parameterization, called *GExp*, uses one Gaussian with variable width and zero bias plus the same Gaussian convoluted with an exponential which effective lifetime is intended to describe the charm bias [25]. Similarly to the *GG* model, the reconstructed Δt error is used to weight the events, and different effective lifetimes and fractions of the exponential part are assumed for each tagging category, in order to take into account the different B decay channels populating each tagging category. The outlier component in this model is assumed the same as in the *GG* parameterization.

In summary, for an event with reconstructed $(\Delta t, \sigma_{\Delta t})$, the *GG* resolution function for tagging category α reads

$$
\begin{aligned}
\mathcal{R}(\Delta t - \Delta t', \sigma_{\Delta t}; \vec{q}_\alpha) &= (1 - f_{tail} - f_{outlier})h_G(\Delta t - \Delta t'; \delta_{core}^\alpha, S_{core}\sigma_{\Delta t}) + \\
&\quad f_{tail}h_G(\Delta t - \Delta t'; \delta_{tail}, S_{tail}\sigma_{\Delta t}) + \\
&\quad f_{outlier}h_G(\Delta t - \Delta t', ; \delta_{outlier}, \sigma_{outlier})
\end{aligned}
\tag{85}
$$

where

$$
h_G(t; \delta, \sigma) = \frac{1}{\sqrt{2\pi}\sigma} \exp(-(t-\delta)^2/(2\sigma^2))
\tag{86}
$$

The equivalent *GExp* resolution function for tagging category α reads

$$\mathcal{R}(\Delta t - \Delta t', \sigma_{\Delta t}; \vec{q}_\alpha) = (1 - f_{Exp}^\alpha - f_{outlier}) h_G(\Delta t - \Delta t'; \delta = 0, S\sigma_{\Delta t}) +$$

$$f_{Exp}^\alpha \frac{1}{2\sigma_{\Delta t}\tau_r^\alpha} \left[\exp\left(\frac{S^2}{2(\tau_r^\alpha)^2} + \frac{\Delta t - \Delta t'}{\sigma_{\Delta t}\tau_r^\alpha} \right) erfc\left(\frac{S}{\sqrt{2}\tau_r^\alpha} + \frac{\Delta t - \Delta t'}{\sqrt{2}S\sigma_{\Delta t}} \right) \right] +$$

$$f_{outlier} h_G(\Delta t - \Delta t',; \delta_{outlier}, \sigma_{outlier}) \tag{87}$$

The complete signal resolution function for all tagging categories is therefore represented by 11 parameters in the *GG* model,

$$\vec{q} = \left\{ S_{core}, \delta_{core}^{leptons}, \delta_{core}^{kaons}, \delta_{core}^{NT1}, \delta_{core}^{NT2}, f_{tail}, \delta_{tail}, S_{tail}, f_{outlier}, \delta_{outlier}, \sigma_{outlier} \right\} \tag{88}$$

and 12 in the *GExp* parameterization,

$$\vec{q} = \left\{ S, \tau_r^{leptons}, \tau_r^{kaons}, \tau_r^{NT1}, \tau_r^{NT2}, f_{Exp}^{leptons}, f_{Exp}^{kaons}, f_{Exp}^{NT1}, f_{Exp}^{NT2}, f_{outlier}, \delta_{outlier}, \sigma_{outlier} \right\} \,. \tag{89}$$

$\sigma_{outlier}$ and $\delta_{outlier}$ are fixed, respectively, to 8 and 0 ps.

In the *GG* model all offsets δ_{core}^α and δ_{tail} are modeled to be proportional to the reconstructed error $\sigma_{\Delta t}$, since it was found that events with high $\sigma_{\Delta t}$ tend to have high Δt residual [28]. The *GExp* model accounts implicitly for this effect.

The introduction of the resolution effects requires the convolution of equations (82/83) with (85/87),

$$f_{resol}^\alpha(X, Y; \Delta t, \sigma_{\Delta t}) = \int_{-\infty}^{+\infty} \mathcal{R}(\Delta t - \Delta t', \sigma_{\Delta t}; \vec{q}_\alpha) f^\alpha(X, Y; \Delta t') d\Delta t' \,. \tag{90}$$

The problem can be reduced to the convolution of a set of basis functions,

$$\frac{1}{2\tau} \exp\left(\mp \tau_{eff} \Delta t' \right) \exp\left(i\Delta m \Delta t' \right) \tag{91}$$

with (86), where

$$\tau_{eff} = \frac{2\tau}{2 \mp \tau \Delta \Gamma} = \frac{\tau}{1 \mp \Delta\Gamma/2\Gamma} \tag{92}$$

and $\tau = 1/\Gamma$. The $-(+)$ sign applies for $\Delta t' > 0$ ($\Delta t' < 0$). The normalization of (90) over a finite domain $[\Delta t_1, \Delta t_2]$ can then be calculated from the integral

$$F_{resol}^\alpha(X, Y; \sigma_{\Delta t}) = \int_{\Delta t_1}^{\Delta t_2} f_{resol}^\alpha(X, Y; \Delta t, \sigma_{\Delta t}) d\Delta t \tag{93}$$

All the integrals (90) and their normalizations (93) can be calculated analytically, and expressed in terms of complex exponentials and the complementary complex error function. The analytical expresions used in this analysis have been taken from [29].

Figures 12 and 13 ilustrate the shape of the time dependent intensities (90) for B_{flav} and B_{CP} transitions (the equivalent to figures 1 and 2, respectively) after introducing the Δt resolution effects (realistic values) and a mistag rate of 10%. The corresponding mixing, Kabir, leptonic, A_{CP}, A_T, A_{CPT}, $A_{\Delta t}$ and $A_{CP\Delta t}$ asymmetries, are shown in figures 14, 15, 16, 17, 18, 19, 20 and 21, respectively. It is worth noting the fake effects introduced by the offset of the resolution function in the CPT asymmetries. The apparent time dependence in the Kabir asymmetry (figure 15) is due to the mistag rate.
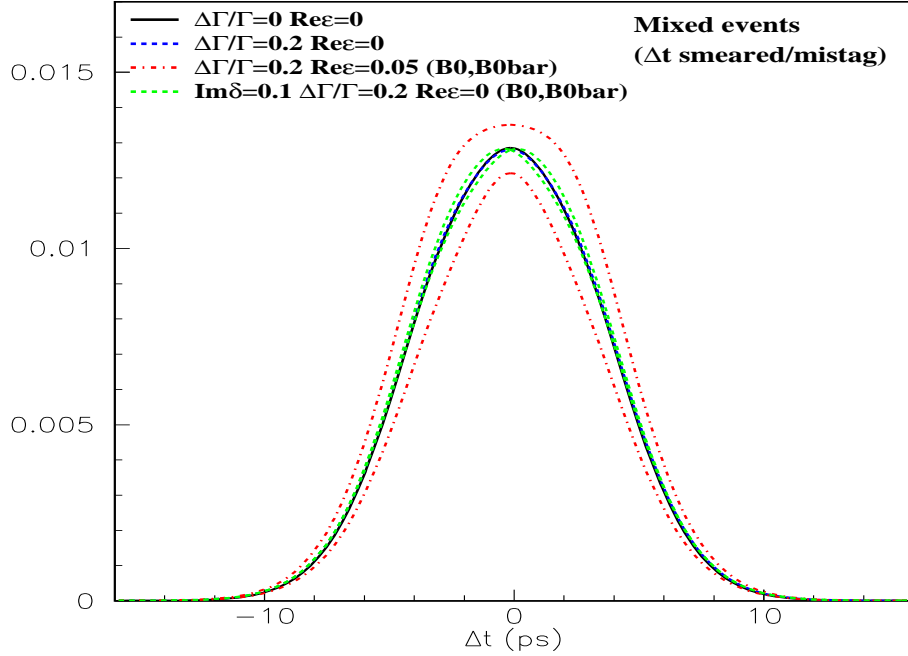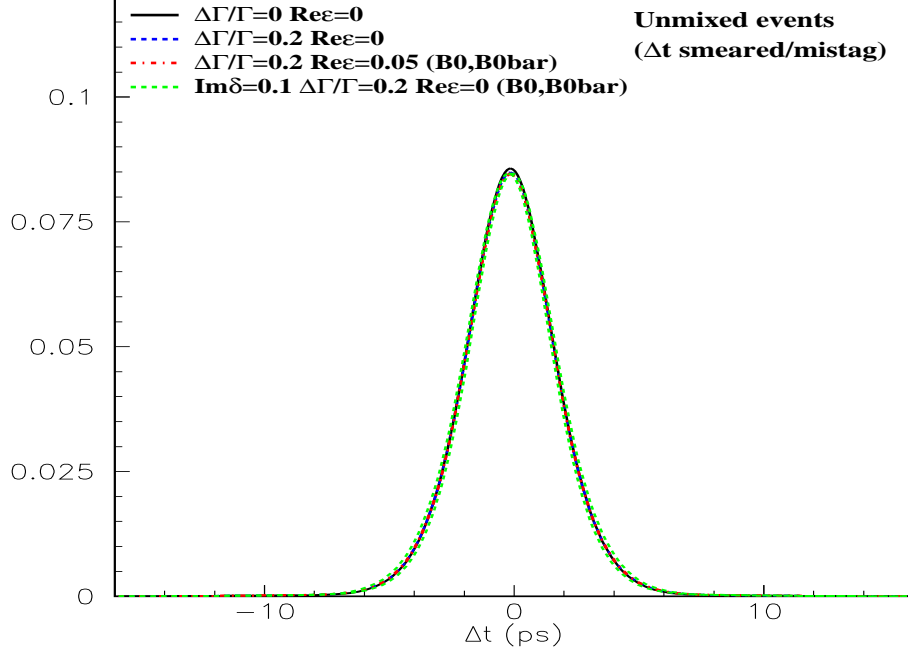
Figure 12: Decay time distributions for $(B^0_f/\bar{B}^0_f/\ell)$ transitions for (top) unmixed and (bottom) mixed events, after time resolution smearing and with a mistag rate of 10%. The different curves correspond to different values of $\Delta\Gamma/\Gamma$, $\frac{Re\varepsilon}{1+|\varepsilon|^2}$ and $\frac{Im\delta}{1+|\varepsilon|^2}$. Δm is assumed to be 0.472 ps^{-1} and $\frac{1-|\varepsilon|^2}{1+|\varepsilon|^2}\frac{Re\delta}{1+|\varepsilon|^2} = 0$. The corresponding theoretical distributions were shown in figure 1.
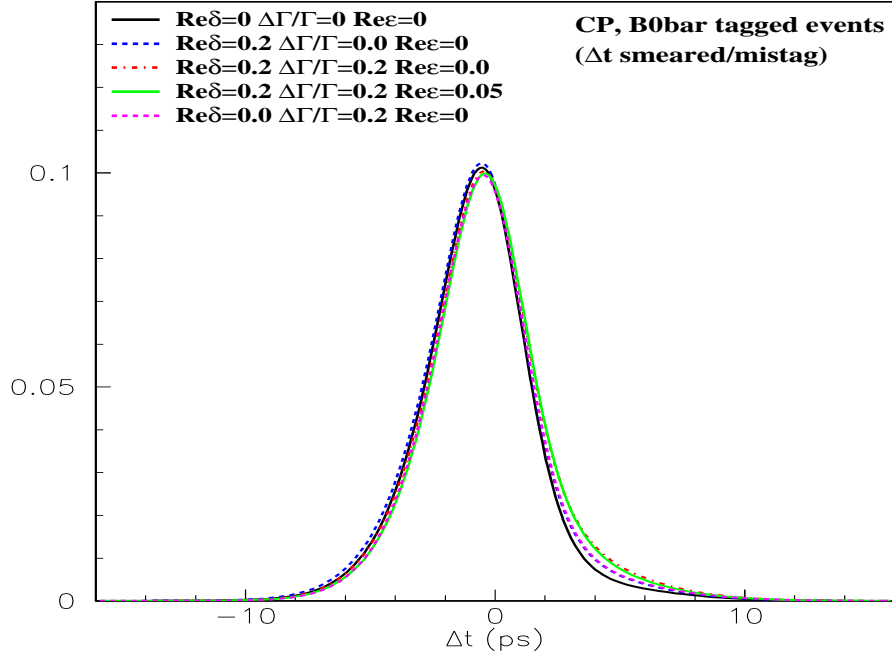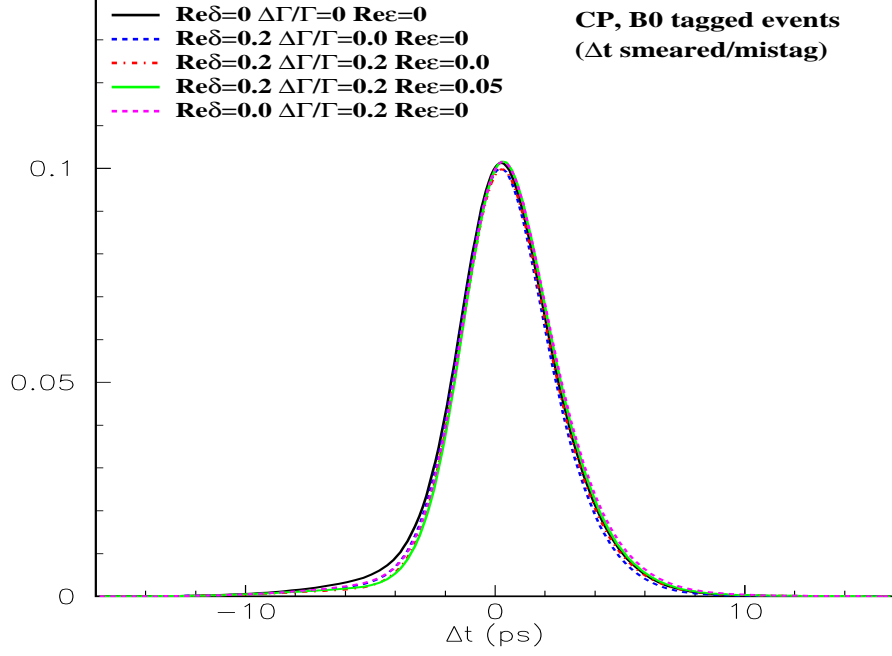
Figure 13: Decay time distributions for $(B_{f\pm}, \ell)$ transitions, for (top) B^0 and (bottom) $\bar{B}^0$ tagged events (CP=−), after time resolution smearing and with a mistag rate of 10%. The different curves correspond to different values of $\frac{1-|\varepsilon|^2}{1+|\varepsilon|^2} \frac{\mathrm{Re}\delta}{1+|\varepsilon|^2}$, $\Delta\Gamma/\Gamma$ and $\frac{\mathrm{Re}\varepsilon}{1+|\varepsilon|^2}$. Δm is assumed to be 0.472 ps^{-1}, and $\frac{\mathrm{Im}\delta}{1+|\varepsilon|^2} = 0$. The corresponding theoretical distributions were shown in figure 2.
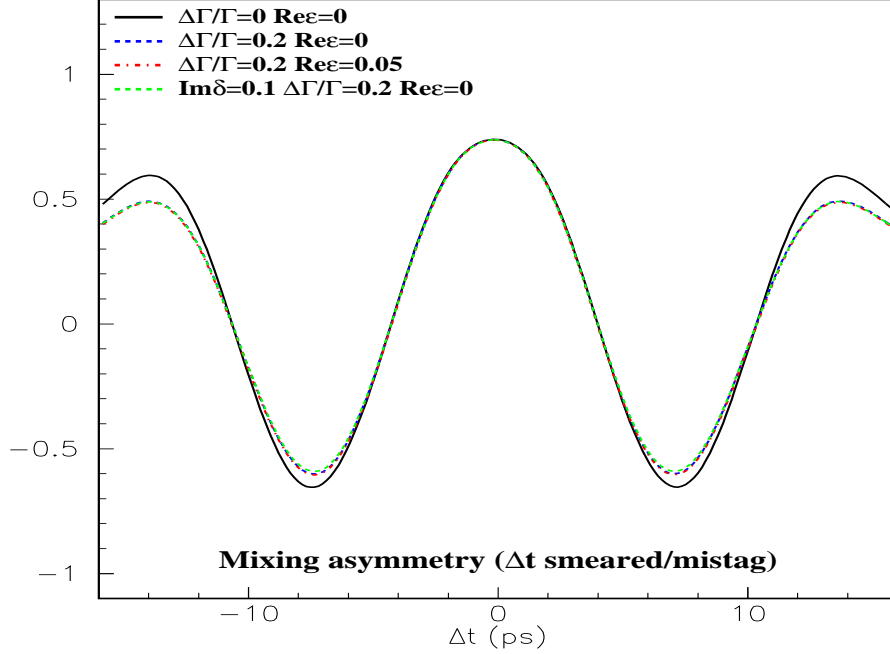
Figure 14: Mixing asymmetry as defined in equation (64), after time resolution smearing and with a mistag rate of 10%. The different curves correspond to different values of $\Delta\Gamma/\Gamma$, $\frac{\mathrm{Re}\varepsilon}{1+|\varepsilon|^2}$ and $\frac{\mathrm{Im}\delta}{1+|\varepsilon|^2}$. Δm is assumed to be 0.472 ps^{-1} and $\frac{1-|\varepsilon|^2}{1+|\varepsilon|^2}\frac{\mathrm{Re}\delta}{1+|\varepsilon|^2}=0$. No mistag and time resolution have been included. The corresponding theoretical asymmetry was shown in figure 3.

3.3 Background treatment

In the presence of backgrounds, the PDF has to be extended to include a term for each significant background source:

$$
\begin{aligned}
f_{obs}^{\alpha}(X,Y;\Delta t,\sigma_{\Delta t}) &= (1-f_{peak}^{\alpha}-f_{DCSD}^{\alpha})p_{sig}^{\alpha}(m_{ES})f_{resol,sig}^{\alpha}(X,Y;\Delta t,\sigma_{\Delta t}) + \\
&\quad f_{peak}^{\alpha}p_{sig}^{\alpha}(m_{ES})f_{resol,peak}^{\alpha}(X,Y;\Delta t,\sigma_{\Delta t}) + \\
&\quad f_{DCSD}^{\alpha}p_{sig}^{\alpha}(m_{ES})f_{resol,sig}^{\alpha}(\bar{X},Y;\Delta t,\sigma_{\Delta t}) + \\
&\quad \left\{1-p_{sig}^{\alpha}(m_{ES})\right\}\sum_{\beta}f_{\beta}^{\alpha}f_{resol,\beta}^{\alpha}(X,Y;\Delta t,\sigma_{\Delta t})
\end{aligned}
\tag{94}
$$

where f_{β}^{α}, f_{peak}^{α}, f_{DCSD}^{α} are the combinatorial, peaking and double Cabbibo supresed (DCSD) background component fractions for the given sample (the latter only exists for flavor-to-flavor states). It is verified that

$$
\sum_{\beta}f_{\beta}^{\alpha} = 1 \; .
\tag{95}
$$

37
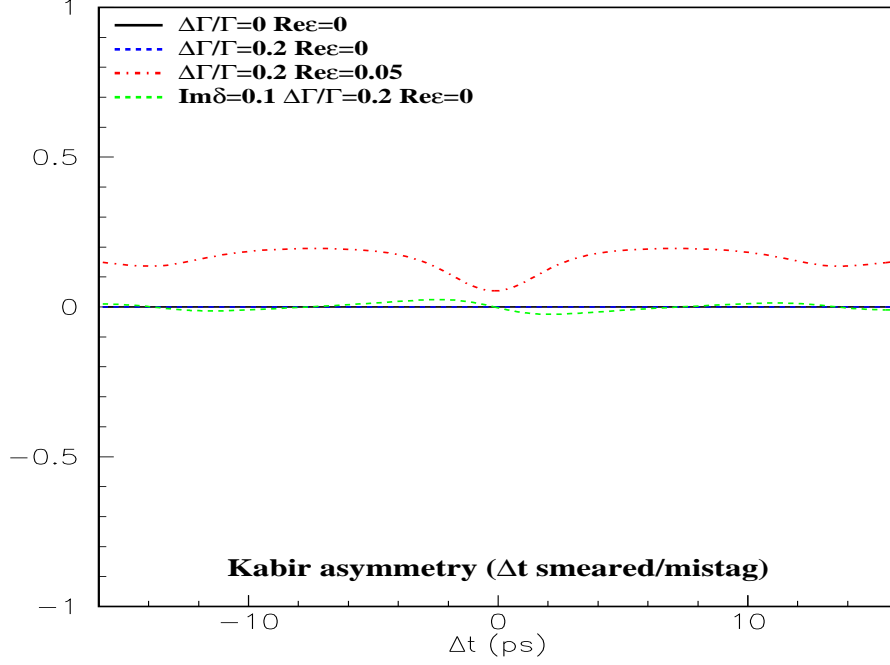
Figure 15: Kabir asymmetry as defined in equation (65), after time resolution smearing and with a mistag rate of 10%. The different curves correspond to different values of $\Delta\Gamma/\Gamma$, $\frac{\text{Re}\varepsilon}{1+|\varepsilon|^2}$ and $\frac{\text{Im}\delta}{1+|\varepsilon|^2}$. Δm is assumed to be 0.472 ps^{-1} and $\frac{1-|\varepsilon|^2}{1+|\varepsilon|^2}\frac{\text{Re}\delta}{1+|\varepsilon|^2} = 0$. No mistag and time resolution have been included. The corresponding theoretical asymmetry was shown in figure 4.

The backgrounds for the B_{flav} and B_{f-} states are small and mostly combinatoric. They are estimated from the beam-energy substituted mass (m_{ES}) side band, assuming a single Gaussian distribution for the signal and an Argus parameterization for the background. From unbinned maximum likelihood fits to the m_{ES} spectrum, the event-by-event signal probability, $p_{sig}^{\alpha}(m_{ES})$, is calculated and then borrowed to (94). Examples of m_{ES} fits for each tagging category in the Monte Carlo simulation for the B_{flav} and B_{f-} samples are shown in figures 22 and 23 respectively. The signal probability is calculated separately for each tagging category.

For each individual signal and background component, $j = sig, peak, DCSD, \beta$, and tagging category, α, the distributions (94) are normalized so that:

$$\sum_{Y=B_t^0,\bar{B}_t^0} \int_{-\infty(\Delta t_1)}^{+\infty(\Delta t_2)} f_{resol,j}^{\alpha}(X,Y;\Delta t,\sigma_{\Delta t})d\Delta t \;\; = \;\; 1 \tag{96}$$

for B_{CP} events, and

$$\sum_{X=B_r^0,\bar{B}_r^0} \sum_{Y=B_t^0,\bar{B}_t^0} \int_{-\infty(\Delta t_1)}^{+\infty(\Delta t_2)} f_{resol,j}^{\alpha}(X,Y;\Delta t,\sigma_{\Delta t})d\Delta t \;\; = \;\; 1 \tag{97}$$
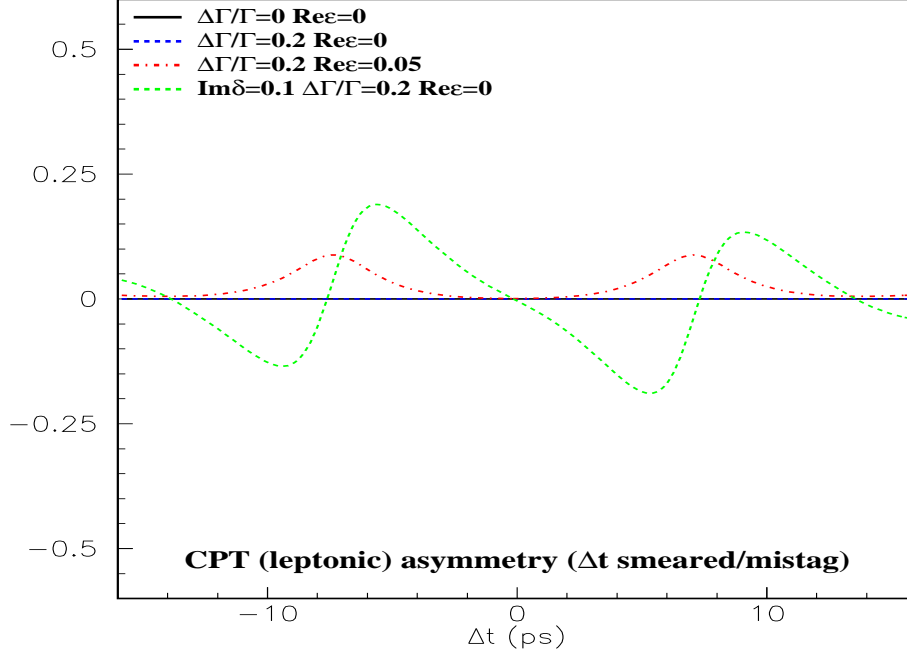
Figure 16: CPT flavor-to-flavor (leptonic) asymmetry as defined in equation (66), after time resolution smearing and with a mistag rate of 10%. The different curves correspond to different values of $\Delta\Gamma/\Gamma$, $\frac{\mathrm{Re}\varepsilon}{1+|\varepsilon|^2}$ and $\frac{\mathrm{Im}\delta}{1+|\varepsilon|^2}$. Δm is assumed to be 0.472 ps^{-1} and $\frac{1-|\varepsilon|^2}{1+|\varepsilon|^2}\frac{\mathrm{Re}\delta}{1+|\varepsilon|^2} = 0$. No mistag and time resolution have been included. The corresponding theoretical asymmetry was shown in figure 5.

for B_{flav} events. The integration limits, $-\infty(\Delta t_1)$ and $+\infty(\Delta t_2)$ correspond to asymptotic (finite) normalization, where Δt_1 ps and Δt_2 are the acceptance cuts on Δt. Asymptotic normalization is used by default in this study.

For the $B^0 \to J/\psi K_L^0$ channel the background level is significantly higher with significant non-combinatorial component, therefore requiring an special treatment [21, 22]. Through the studies presented in this document, signal only $B^0 \to J/\psi K_L^0$ fits are used.

3.4 The log-likelihood function

The likelihood function for tagging category α is finally defined as
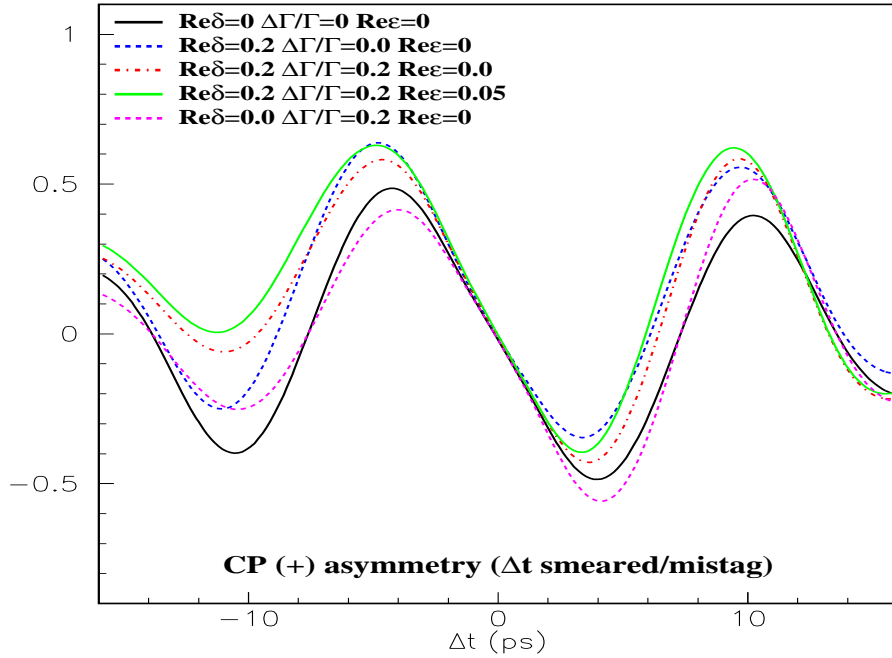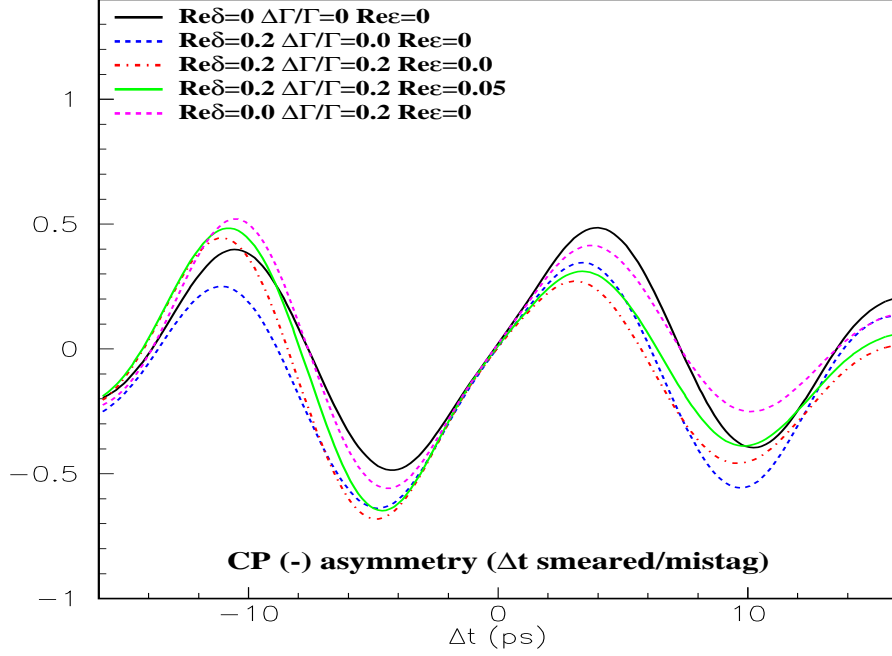
Figure 17: The A_{CP} asymmetry, as defined in equation (68), for CP− (top) and CP+ (bottom), after time resolution smearing and with a mistag rate of 10%. The different curves correspond to different values of $\frac{1-|\varepsilon|^2}{1+|\varepsilon|^2}\frac{\text{Re}\delta}{1+|\varepsilon|^2}$ (0,0.2), $\Delta\Gamma/\Gamma$ (0,0.2) and $\frac{\text{Re}\varepsilon}{1+|\varepsilon|^2}$ (0,0.05). Δm, $\frac{\text{Im}\varepsilon}{1+|\varepsilon|^2}$ and $\frac{\text{Im}\delta}{1+|\varepsilon|^2}$ are assumed to be 0.472 ps^{-1}, 0.35 and 0, respectively. The corresponding theoretical asymmetry was shown in figure 6.

40
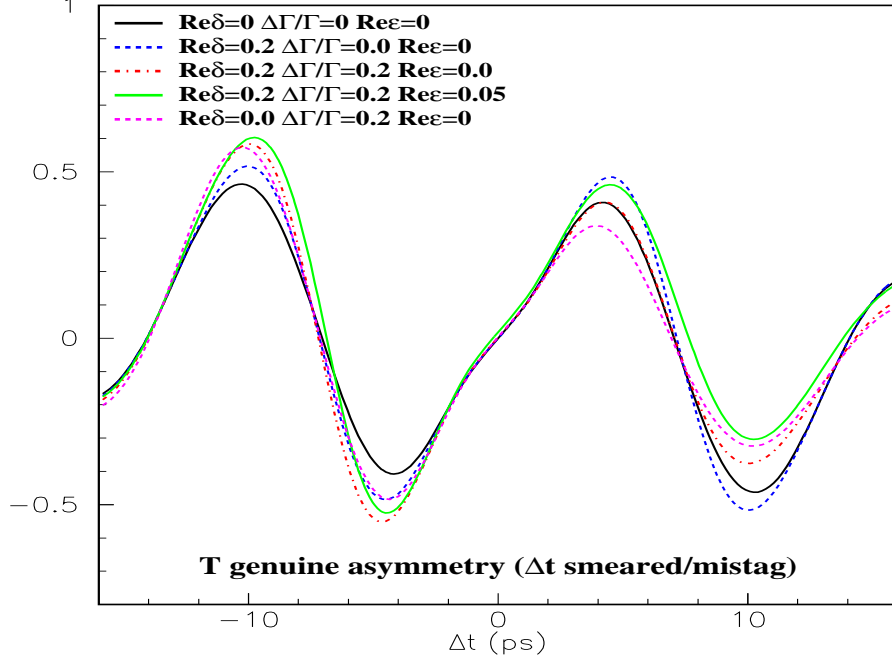
Figure 18: The A_{T} asymmetry, as defined in equation (69), after time resolution smearing and with a mistag rate of 10%. The different curves correspond to different values of $\frac{1-|\varepsilon|^2}{1+|\varepsilon|^2}\frac{\mathrm{Re}\delta}{1+|\varepsilon|^2}$ (0, 0.2), $\Delta\Gamma/\Gamma$ (0, 0.2) and $\frac{\mathrm{Re}\varepsilon}{1+|\varepsilon|^2}$ (0, 0.05). Δm, $\frac{\mathrm{Im}\varepsilon}{1+|\varepsilon|^2}$ and $\frac{\mathrm{Im}\delta}{1+|\varepsilon|^2}$ are assumed to be 0.472 ps^{-1}, 0.35 and 0, respectively. The corresponding theoretical asymmetry was shown in figure 7.

$$
\begin{aligned}
\ln\mathcal{L}_\alpha \;=\; & \sum_i^{N^\alpha_{B_{r-}B^0_t}} \ln f^\alpha_{obs}(B_{r-},B^0_t;\Delta t_i,\sigma_{\Delta t,i}) + \sum_i^{N^\alpha_{B_{r-}\bar{B}^0_t}} \ln f^\alpha_{obs}(B_{r-}\bar{B}^0_t;\Delta t_i,\sigma_{\Delta t,i}) + \\
& \sum_i^{N^\alpha_{B_{r+}B^0_t}} \ln f^\alpha_{obs}(B_{r+},B^0_t;\Delta t_i,\sigma_{\Delta t,i}) + \sum_i^{N^\alpha_{B_{r+}\bar{B}^0_t}} \ln f^\alpha_{obs}(B_{r+},\bar{B}^0_t;\Delta t_i,\sigma_{\Delta t,i}) + \\
& \sum_i^{N^\alpha_{B^0_r B^0_t}} \ln f^\alpha_{obs}(B^0_r,B^0_t;\Delta t_i,\sigma_{\Delta t,i}) + \sum_i^{N^\alpha_{\bar{B}^0_r \bar{B}^0_t}} \ln f^\alpha_{obs}(\bar{B}^0_r,\bar{B}^0_t;\Delta t_i,\sigma_{\Delta t,i}) + \\
& \sum_i^{N^\alpha_{\bar{B}^0_r B^0_t}} \ln f^\alpha_{obs}(\bar{B}^0_r,B^0_t;\Delta t_i,\sigma_{\Delta t,i}) + \sum_i^{N^\alpha_{B^0_r \bar{B}^0_t}} \ln f^\alpha_{obs}(B^0_r,\bar{B}^0_t;\Delta t_i,\sigma_{\Delta t,i})
\end{aligned}
\tag{98}
$$

where $f^\alpha_{obs}(X,Y;\Delta t,\sigma_{\Delta t})$ was defined in (94), with $f^\alpha_{resol,j}(X,Y;\Delta t,\sigma_{\Delta t})$ as defined in (82) and (83). The global likelihood function for all tagging categories is then calculated as

$$
\ln\mathcal{L} = \sum_\alpha \ln\mathcal{L}_\alpha \,.
\tag{99}
$$

41
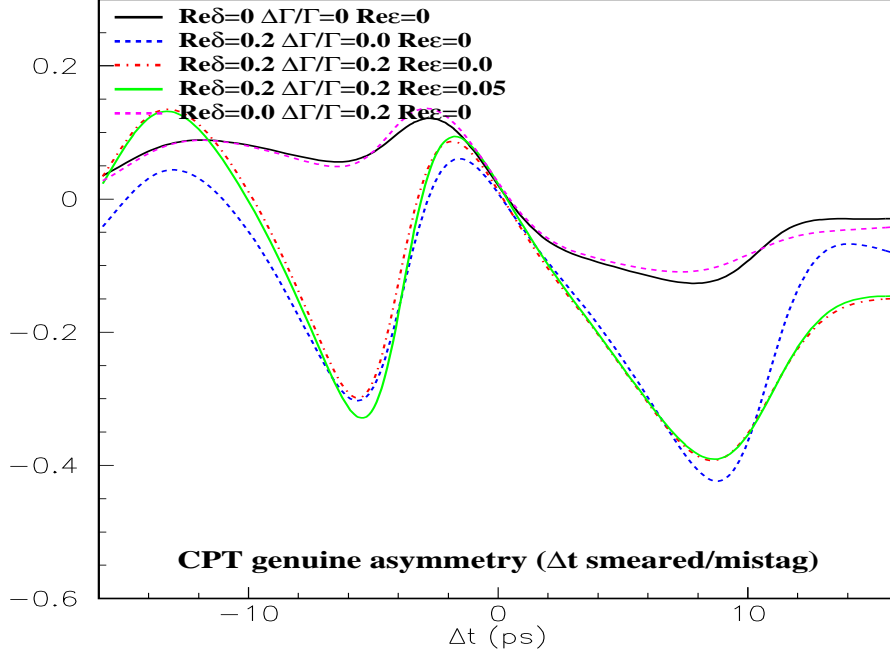
Figure 19: The A_{CPT} asymmetry, as defined in equation 70, after time resolution smearing and with a mistag rate of 10%. The different curves correspond to different values of $\frac{1-|\varepsilon|^2}{1+|\varepsilon|^2}\frac{\text{Re}\delta}{1+|\varepsilon|^2}$ $(0, 0.2)$, $\Delta\Gamma/\Gamma$ $(0, 0.2)$ and $\frac{\text{Re}\varepsilon}{1+|\varepsilon|^2}$ $(0, 0.05)$. Δm, $\frac{\text{Im}\varepsilon}{1+|\varepsilon|^2}$ and $\frac{\text{Im}\delta}{1+|\varepsilon|^2}$ are assumed to be 0.472 ps^{-1}, 0.35 and 0, respectively. The corresponding theoretical asymmetry was shown in figure 8.

The categories of events considered in (99) are the following:

- B_{r-}: $B^0 \to J/\psi K_S^0 (\pi^+\pi^-$ and $\pi^0\pi^0)$, $B^0 \to \psi(2S)K_S^0$ ($B_{CPK_S^0}$ sample);

- B_{r+}: $B^0 \to J/\psi K_L^0$ ($B_{CPK_L^0}$ sample);

- B_{flav}: $B^0 \to D^{(*)}\pi(\rho, a_1)$;

- Control sample for B_{CP} transitions: $B^0 \to J/\psi K^{*0}(K^\pm\pi^\mp)$.

Each of these samples is separated by tagging category, with a total of 4 tagging categories [26, 19, 20] (Lepton, Kaon, NT1, NT2).

In the calculation of the likelihood function, the exact expressions for the theoretical distributions are used for the two formalisms, therefore we are not making assumptions about the size of the effects to be measured.

An standalone fitting program, called `cptNagFit`, has been developed to find the solution of (99) and the errors on the fitted parameters. The program has been interfaced to the NAG library [33] and the MINUIT package [34]. All the numerical and minimization routines are based on the NAG library, and

42
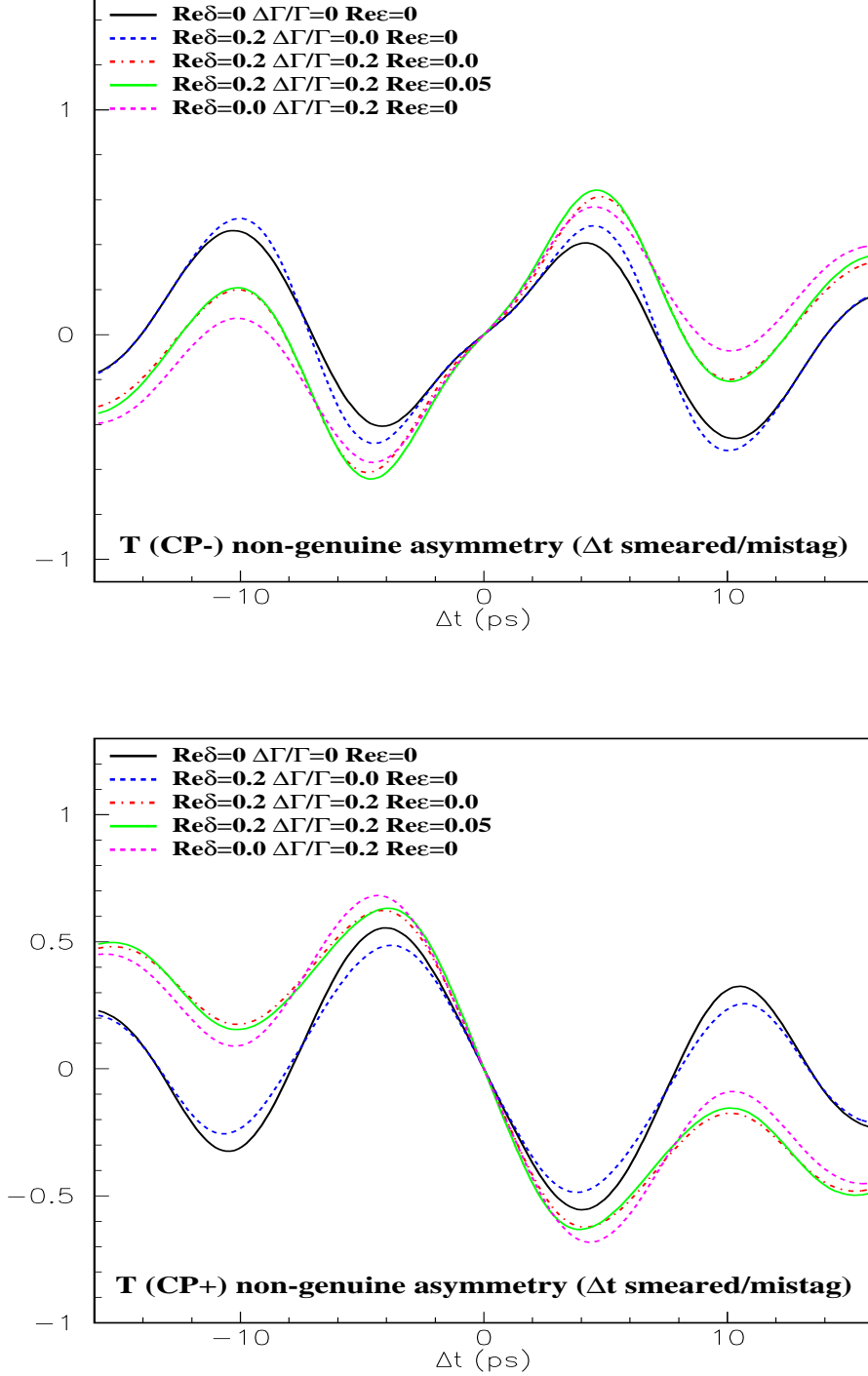
Figure 20: The $A_{\Delta t}$ asymmetry, as defined in equation (72), for CP− (top) and CP+ (bottom) events, after time resolution smearing and with a mistag rate of 10%. The different curves correspond to different values of $\frac{1-|\varepsilon|^2}{1+|\varepsilon|^2} \frac{\mathrm{Re}\delta}{1+|\varepsilon|^2}$ $(0, 0.2)$, $\Delta\Gamma/\Gamma$ $(0, 0.2)$ and $\frac{\mathrm{Re}\varepsilon}{1+|\varepsilon|^2}$ $(0, 0.05)$. Δm, $\frac{\mathrm{Im}\varepsilon}{1+|\varepsilon|^2}$ and $\frac{\mathrm{Im}\delta}{1+|\varepsilon|^2}$ are assumed to be 0.472 ps^{-1}, 0.35 and 0, respectively. The corresponding theoretical asymmetry was shown in figure 9.
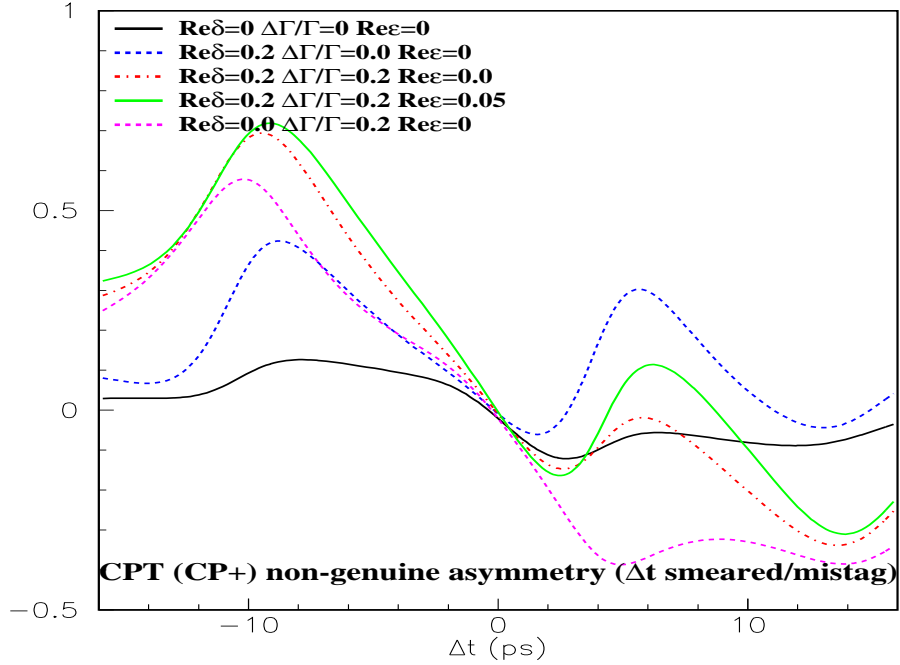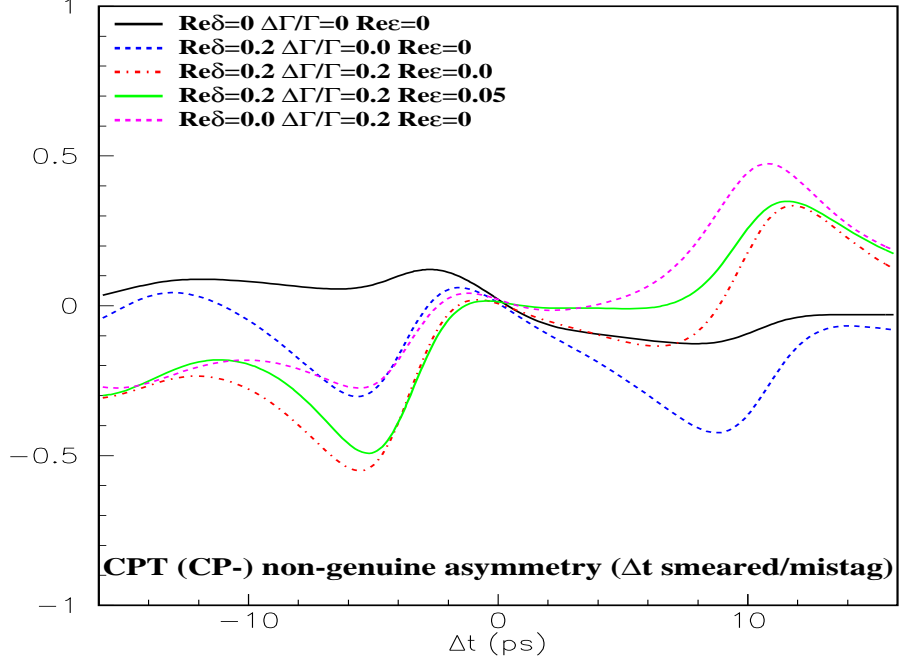
Figure 21: The $A_{\text{CP}\Delta t}$ asymmetry, as defined in equation (73), for CP− (top) and CP+ (bottom) events, after time resolution smearing and with a mistag rate of 10%. The different curves correspond to different values of $\frac{1-|\varepsilon|^2}{1+|\varepsilon|^2}\frac{\text{Re}\delta}{1+|\varepsilon|^2}$ (0,0.2), $\Delta\Gamma/\Gamma$ (0,0.2) and $\frac{\text{Re}\varepsilon}{1+|\varepsilon|^2}$ (0,0.05). Δm, $\frac{\text{Im}\varepsilon}{1+|\varepsilon|^2}$ and $\frac{\text{Im}\delta}{1+|\varepsilon|^2}$ are assumed to be 0.472 ps^{-1},0.35 and 0, respectively. The corresponding theoretical asymmetry was shown in figure 10.

44
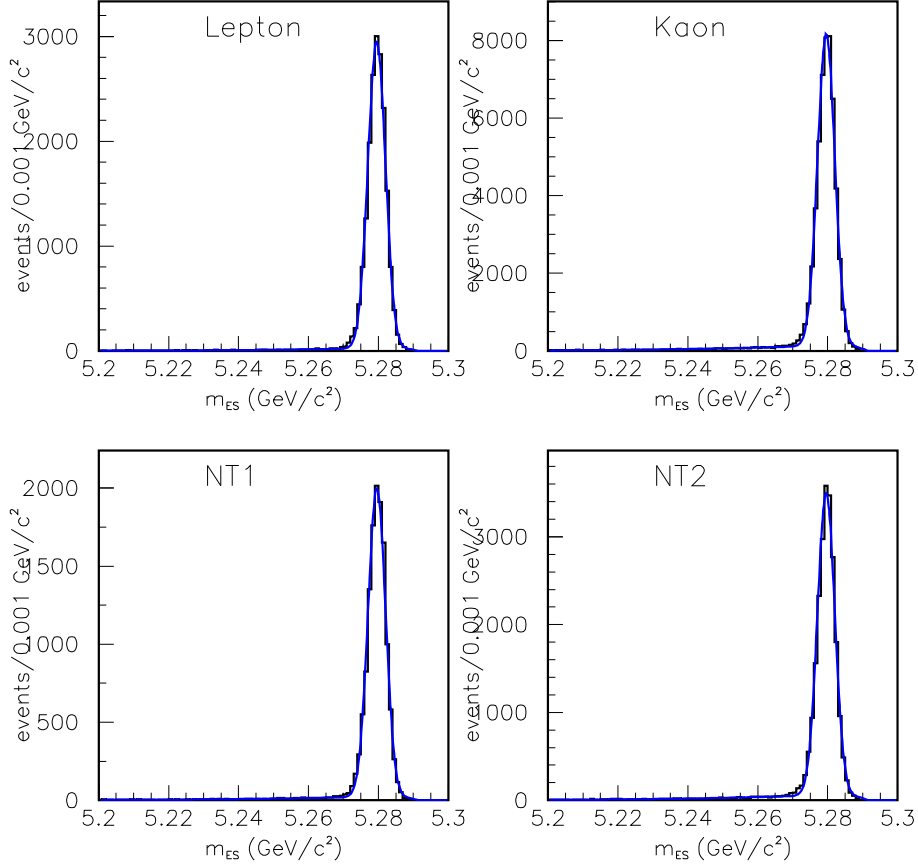
Figure 22: m_{ES} fits to each tagging category for the B_{flav} Monte Carlo sample.

the error estimation relies on the HESSE and MINOS methods of MINUIT. This simultaneous interfacing allows direct comparison and cross-checking of the fitting results using two completely different libraries.

The NAG library is a comercial and modern (end 80's - begining 90's) numerical library which use in HEP is becoming more and more popular, with a very large number of numerical routines. NAG is already part of the kernel of large HEP projects, like LHC++ at CERN [35]. Among many different available minimization routines, the `e04jyf` routine was chosen, which is based on a quasi-Newton algorithm [36], one of the most powerful methods available for general problems. For the nominal global CPT/CP/T fits (see section 3.5), MINUIT requires close to twice more iterations than NAG to find the solution. In toy Monte Carlo exercises the rate of failed fits is also significantly larger when using MINUIT. However, when both approaches report converged fits the agreement among them in both, the solution and reported errors, is satisfactory. NAG is also used, among other service and utility functions, to calculate the error function (`s15aef`), the complementary error function (`s15adf`) and the complementary complex error function (`s15ddf`).
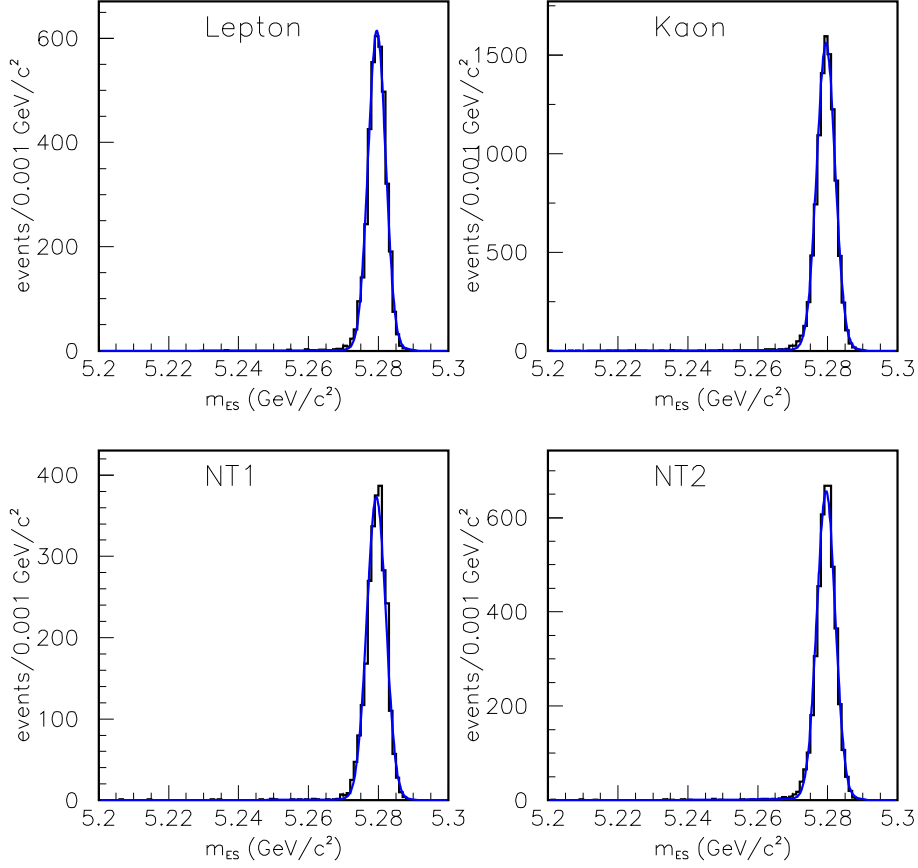
Figure 23: m_{ES} fits to each tagging category for the $B_{CPK_S^0}$ Monte Carlo sample.

3.5 Assumptions in the nominal fit

The nominal CPT/CP/T fit used in these studies has finally a total of 42(44) free parameters, for the *GG*(*GExp*) model, with the following assumptions:

- fit simultaneously for the 6 physics parameters (formalism dependent):

  (ε, δ) **formalism:** $\frac{\mathrm{Re}\delta}{1+|\varepsilon|^2}\frac{1-|\varepsilon|^2}{1+|\varepsilon|^2}$, $\frac{\mathrm{Im}\delta}{1+|\varepsilon|^2}$, $\frac{\mathrm{Im}\varepsilon}{1+|\varepsilon|^2}$, $\frac{\mathrm{Re}\varepsilon}{1+|\varepsilon|^2}$, $\Delta\Gamma/\Gamma$ and Δm;

  $(|q/p|, \lambda, z)$ **formalism:** $\frac{\mathrm{Re}\lambda}{|\lambda|}\mathrm{Re}z$, $\mathrm{Im}z$, $\frac{\mathrm{Im}\lambda}{|\lambda|}$, $|q/p|$, $\Delta\Gamma/\Gamma$ and Δm;

- a total of 9(11) parameters are used to describe the signal resolution function with the *GG*(*GExp*) model:

  GG: scale factors of the core and tails components, S_{core} and S_{tail}; tagging category dependent core bias, δ_{core}^{α}; common tail bias, δ_{tail}; fraction of tail and outlier Gaussians, f_{tail} and $f_{outlier}$; the width and bias of the outlier Gaussian were fixed to 8 ps and 0 respectively;

GExp: scale factor of the Gaussian, *S*, tagging category dependent effective lifetime (τ_r^α) and exponential component fraction (f_{Exp}^α); the width and bias of the outlier Gaussian were fixed to 8 ps and 0 respectively;

- a total of 9 parameters are used to describe the signal wrong tag fractions: for each tagging category, w_0^α, w_{slope}^α and Δw^α, where w_{slope}^α is fixed to zero for the `Lepton,` `NT1` and `NT2` categories;

- 3 background components are assumed for the B_{flav} sample (16 parameters):

  - a prompt (zero lifetime) and non-prompt (non-vanishing and free lifetime -1 parameter-) components, with their own effective wrong tag fraction (w_{slope}^α and Δw^α fixed to zero) (8 parameters) and a common resolution function, described as a common single Gaussian distribution with a scale factor S_{backg} and a bias δ_{backg} (*GG* model) or a common single unbiassed Gaussian with a scale factor S_{backg} plus the same Gaussian convoluted with an exponential function with effective lifetime $\tau_{r,backg}$ (*GExp* model), and an outlier fraction $f_{backg,outlier}$ (3 parameters); the width of the outlier component is taken to be fixed at 8 ps with zero bias; the relative $f_{prompt,B_{flav}}^\alpha$ fraction of prompt background for each tagging category are also considered as free parameters (4 parameters);

  - a peaking contribution, which resolution function is the same as that of the signal, with B^+ fixed lifetime; the peaking background fraction is fixed;

  - no oscillatory background component is assumed;

  - no DCSD background component is assumed;

- 3 background components are also assumed for the $B_{CPK_S^0}$ sample (2 parameters):

  - prompt, non-prompt and peaking background, where the peaking background fraction is also fixed, and a common (averaged over tagging categories) prompt fraction is assumed (1 parameter); the wrong tag fraction parameters, lifetime and resolution function of the peaking background component is assumed to be the same as those of the signal; the lifetime of the non-prompt background is left free (1 parameter) and assumed the same for all tagging categories; the effective wrong tag fractions for the prompt and non-prompt background components are assumed to be 0.5 (i.e. effective dilutions zero), which correspond to no CPT, CP and T asymmetries in the background; finally, the resolution function parameters of the prompt and non-prompt components are assumed the same as those of the B_{flav} sample.

- signal only component is assumed for $B_{CPK_L^0}$;

- the $B^0\overline{B}^0$ differences in reconstruction and tagging efficiencies, ν and μ^α, are fixed to the values extracted from the B_{flav} sample, assuming for Δm, $\Delta\Gamma$ and $\frac{\text{Re}\varepsilon}{1+|\varepsilon|^2}$ the generated values. In section 4.1.10 it is described and validated an alternative approach which avoids the circularity between ν, μ^α and the fitted values of Δm, $\Delta\Gamma$ and $\frac{\text{Re}\varepsilon}{1+|\varepsilon|^2}$;

- $\Delta\Gamma/\Gamma$ is assumed zero for all background components;

- direct CP contribution assumed to be zero, $|\bar{A}_f/A_f| = 1$;

- in the global fit, the parameters of the signal probablity obtained from the m_{ES} fits are taken as fixed.

4 Validation of the fitting procedure

In order to validate the nominal fit procedure described in the previous section and to study its feasibility we have performed toy and full Monte Carlo studies which are described in the following.

4.1 Toy Monte Carlo

Toy Monte Carlo events are generated in order to validate the fit and study its feasibility, and finally to have an estimation of the sensitivity on the physical parameters and their correlation. In appendix C we describe the details of the CPT/CP/T/Mixing Toy Monte Carlo generator used for these studies. Typically, toy Monte Carlo validation and reach studies have been based on sets of at least 600 experiments with an statistics per experiment of about $60 \, fb^{-1}$, assuming the yields shown in table 12, which correspond roughly to our current yields [20]. The m_{ES} shapes for the different samples in signal only experiments correspond to the distributions shown in figures 22 and 23 (ΔE distributions are similarly generated for the $B_{CPK_L^0}$ sample, but they are not actually used in the fits). When backgrounds were considered in the B_{flav} and $B_{CPK_S^0}$ samples, the generated m_{ES} distributions are those shown in figure 24. Peaking background components of 1.5% and 1.0% were assumed for the B_{flav} and $B_{CPK_S^0}$ samples, respectively.

Sample	Signal only	Signal+background
B_{flav}	21000	48000
$B_{CPK_S^0}$	1500	1800
$B_{CPK_L^0}$	450	450

Table 12: Assumed yields used in the toy Monte Carlo studies (equivalent to roughly $60 \, fb^{-1}$) for each data sample, signal only and signal with backgrounds.

The generated tagging efficiencies per category were 0.095, 0.359, 0.080 and 0.139 for the `Lepton`, `Kaon`, `NT1` and `NT2` tagging categories respectively. The assumed mistag rates w_0^α were, respectively, 0.070, 0.068, 0.190 and 0.349. For the `Kaon` category, the linear tagging/vertexing correlation slope, w_{slope}^{kaon}, was assumed to be 0.135. The resolution function parameters were similar to that obtained from a fit to the full Monte Carlo sample (section 4.2). The $B^0 \bar{B}^0$ reconstruction and tagging efficiency differences included were those given in tables 9 and 10.

4.1.1 Log-likelihood shape

It is very useful before to do any other study to scan the shape of the likelihood function (99), in order to identify possible pathological behavior of the PDF. This exercise was performed running two high statistics experiments (≈ 200 fb^{-1}) with the following values for the physics parameters:

- Experiment 1: reference (table 13);

- Experiment 2: reference with $\Delta\Gamma/\Gamma$=0.2.

The scan of each physics parameter in a wide interval (about 15 standard deviations, assuming Gaussian errors) around the maximum for both single experiments, as shown in figure 25, reveals a well behaved
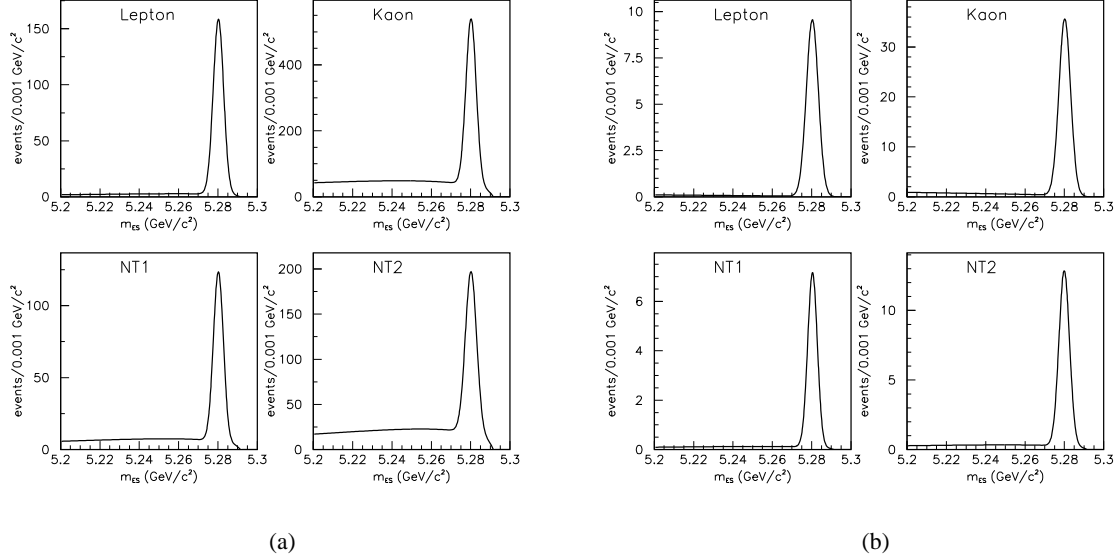
Figure 24: Generated m_{ES} fits to each tagging category for the B_{flav} (a) and $B_{CPK_S^0}$ (b) samples in presence of background.

lihelihood function. An slightly asymmetric shape is observed for $\Delta\Gamma/\Gamma$. As will be shown later in more detail, the sampling of the 60 fb^{-1} experiments confirmed this behavior. This gave us a first indication of the feasibility of the simultaneous extraction of all the 6 physics paramaters.

Parameter	Generated value
$\frac{1-|\varepsilon|^2}{1+|\varepsilon|^2}\frac{\mathrm{Re}\delta}{1+|\varepsilon|^2}$	0.00
$\frac{\mathrm{Im}\delta}{1+|\varepsilon|^2}$	0.00
$\frac{\mathrm{Re}\varepsilon}{1+|\varepsilon|^2}$	0.00
$\frac{\mathrm{Im}\varepsilon}{1+|\varepsilon|^2}$	0.35
$\Delta\Gamma/\Gamma$	0.00
$\Delta m(\mathrm{ps}^{-1})$	0.472

Table 13: Generated physics parameter values for the reference configuration, (ε, δ) formalism.

4.1.2 Residual distributions and Gaussian errors

The residual, defined as the fitted value minus the generated one, and Gaussian error distributions for all the physics parameters from signal only fits in the reference configuration (table 13) are shown in figures 26 and 27, for the *GG* and *GExp* resolution models, respectively. The average and RMS of the residual distribution as well as the average Gaussian error and its coverage are summarized in tables 14 and 15. In figure 28 the residuals for each physics parameter is plotted against the corresponding Gaussian error coming from the fit. The highest correlation coefficient refers to $\frac{\mathrm{Im}\delta}{1+|\varepsilon|^2}$ and it is around 10%, while all the other parameters are well below 10%.
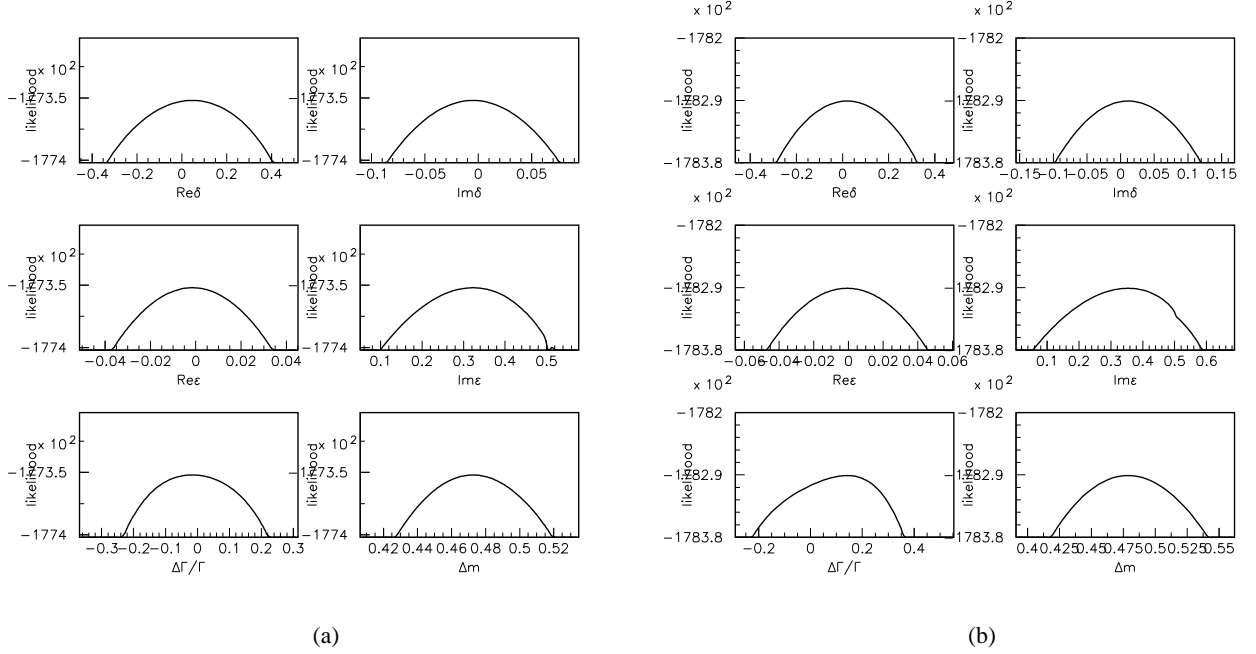
Figure 25: Scanning of the log-likelihood function (99) around the solution for a high statistics experiment (≈ 200 fb^{-1}) for $\Delta\Gamma/\Gamma$=0 (a) and $\Delta\Gamma/\Gamma$=0.2 (b).

These results show that there is no evidence of biases in the estimation of all the physics parameters, for the two resolution models and the truth values given in table 13. For $\frac{\mathrm{Im}\delta}{1+|\varepsilon|^2}$, $\frac{\mathrm{Re}\varepsilon}{1+|\varepsilon|^2}$, $\frac{\mathrm{Im}\varepsilon}{1+|\varepsilon|^2}$ and Δm the estimated Gaussian error is a good estimator of the resolution with which each parameter is determined. However, the Gaussian errors for $\Delta\Gamma/\Gamma$ and $\frac{1-|\varepsilon|^2}{1+|\varepsilon|^2}\frac{\mathrm{Re}\delta}{1+|\varepsilon|^2}$ underestimate slightly the resolution ($\sim 10\%$). The non-Gaussian effects, particularly in $\Delta\Gamma/\Gamma$, where already apparent in figure 25. Non-Gaussian errors are investigated in section 4.1.4.

	Reference configuration, *GG* model				
	$\frac{1-|\varepsilon|^2}{1+|\varepsilon|^2}\frac{\mathrm{Re}\delta}{1+|\varepsilon|^2}$	$\frac{\mathrm{Im}\varepsilon}{1+|\varepsilon|^2}$	$\frac{\mathrm{Re}\varepsilon}{1+|\varepsilon|^2}$	$\Delta\Gamma/\Gamma$	Δm
Mean residual	$(1.9\pm2.6)\cdot10^{-3}$	$(1.9\pm1.3)\cdot10^{-3}$	$(-0.4\pm2.4)\cdot10^{-4}$	$(1.9\pm2.1)\cdot10^{-3}$	$(-1\pm3.1)\cdot10^{-4}$
RMS residual	$(7.6\pm0.2)\cdot10^{-2}$	$(3.9\pm0.1)\cdot10^{-2}$	$(7\pm0.2)\cdot10^{-3}$	$(6.3\pm0.2)\cdot10^{-2}$	$(9.2\pm0.3)\cdot10^{-3}$
Average error (Gauss)	$6.8\cdot10^{-2}$	$3.9\cdot10^{-2}$	$7.1\cdot10^{-3}$	$5.3\cdot10^{-2}$	$9.5\cdot10^{-3}$
Gaussian error coverage	$(59.9\pm3.3)\%$	$(69.3\pm3.7)\%$	$(68.5\pm3.7)\%$	$(58.7\pm3.3)\%$	$(70.9\pm3.7)\%$

Table 14: Summary of results for the reference configuration from signal only fits (*GG* resolution model, $\approx$ 60 fb^{-1}).

4.1.3 $\Delta\Gamma/\Gamma \neq 0$ effects

The behavior of the fit was also studied for non-vanishing values of $\Delta\Gamma/\Gamma$. Figure 29 shows the residual and Gaussian error distributions for the physics parameters from signal only fits in the reference configuration with $\Delta\Gamma/\Gamma$=0.2 (*GExp* resolution model). The asymmetry of the residual distribution, consequence of the asymmetry of the log-likelihood function (figure 25) for $\Delta\Gamma/\Gamma$ is apparent. The average and RMS of the
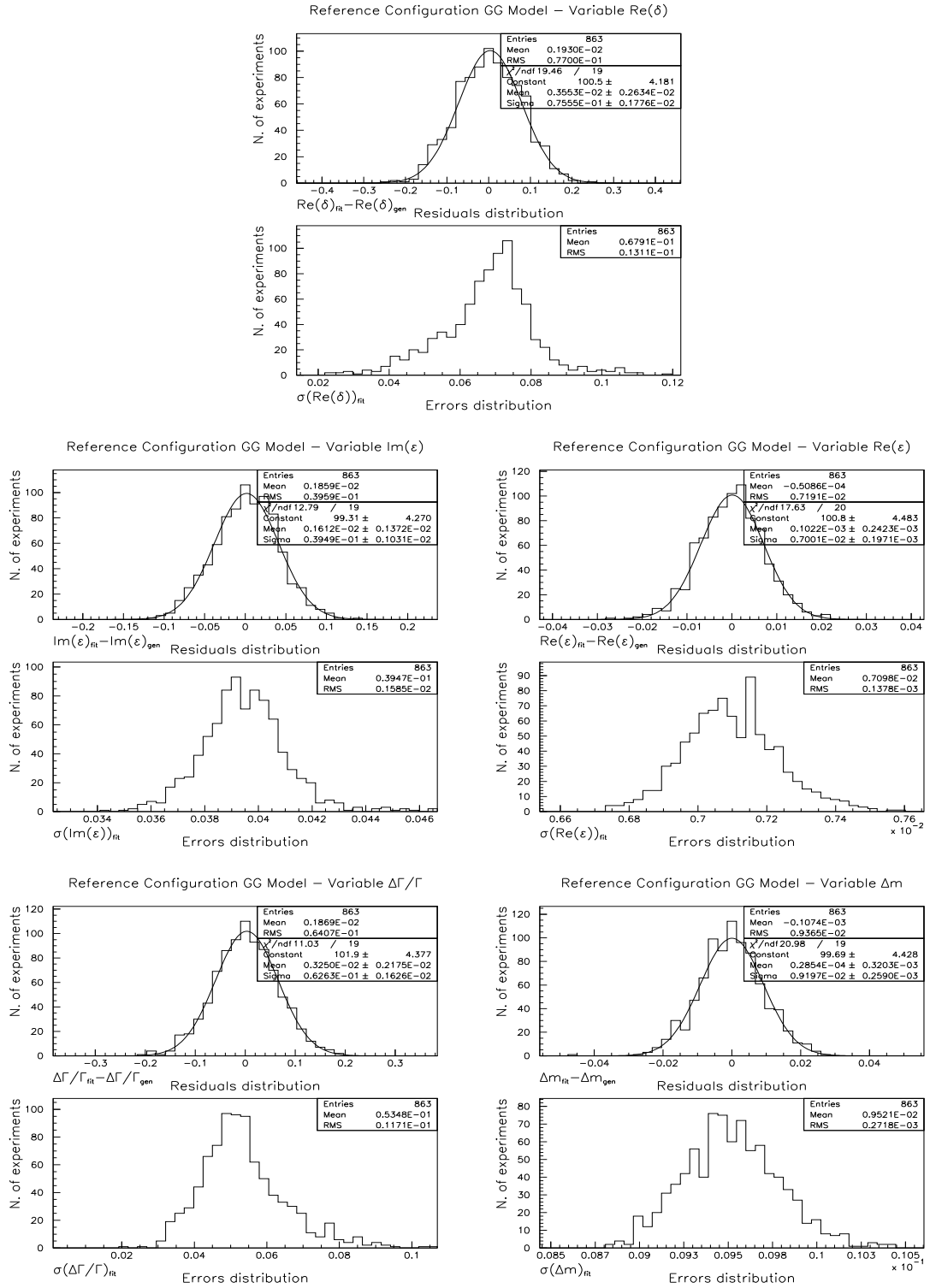
Figure 26: Residual and Gaussian error distributions for the physics parameters from signal only fits (GG resolution model, ≈ 60 fb^{-1}). The generated values correspond to our reference configuration given in table 13. $\frac{\mathrm{Im}\delta}{1+|\varepsilon|^2}$ was fixed in this set of experiments.

51
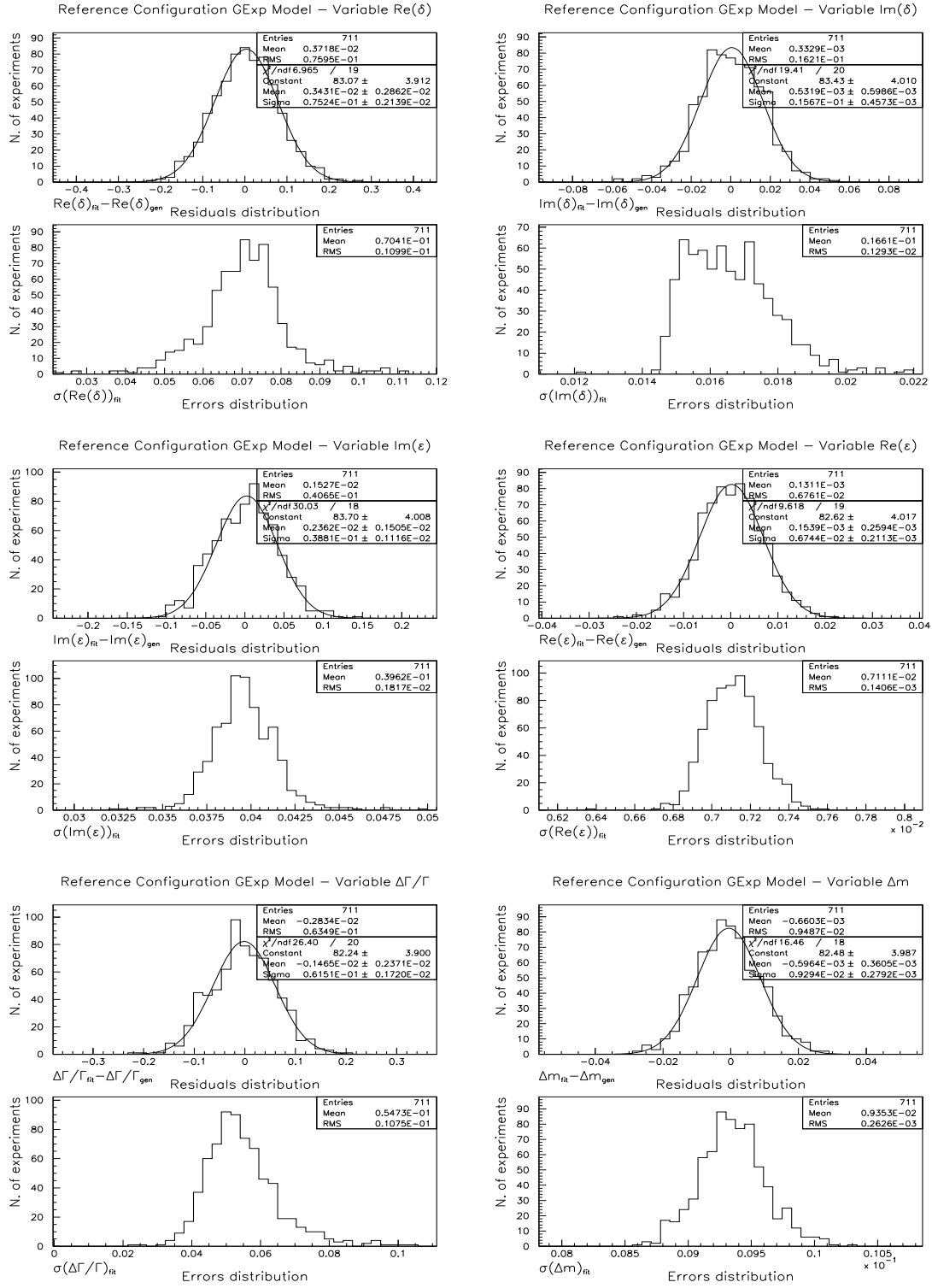
Figure 27: Residual and Gaussian error distributions for the physics parameters from signal only fits (*GExp* resolution model, $\approx 60 \ \mathrm{fb}^{-1}$). The generated values correspond to our reference configuration given in table 13.
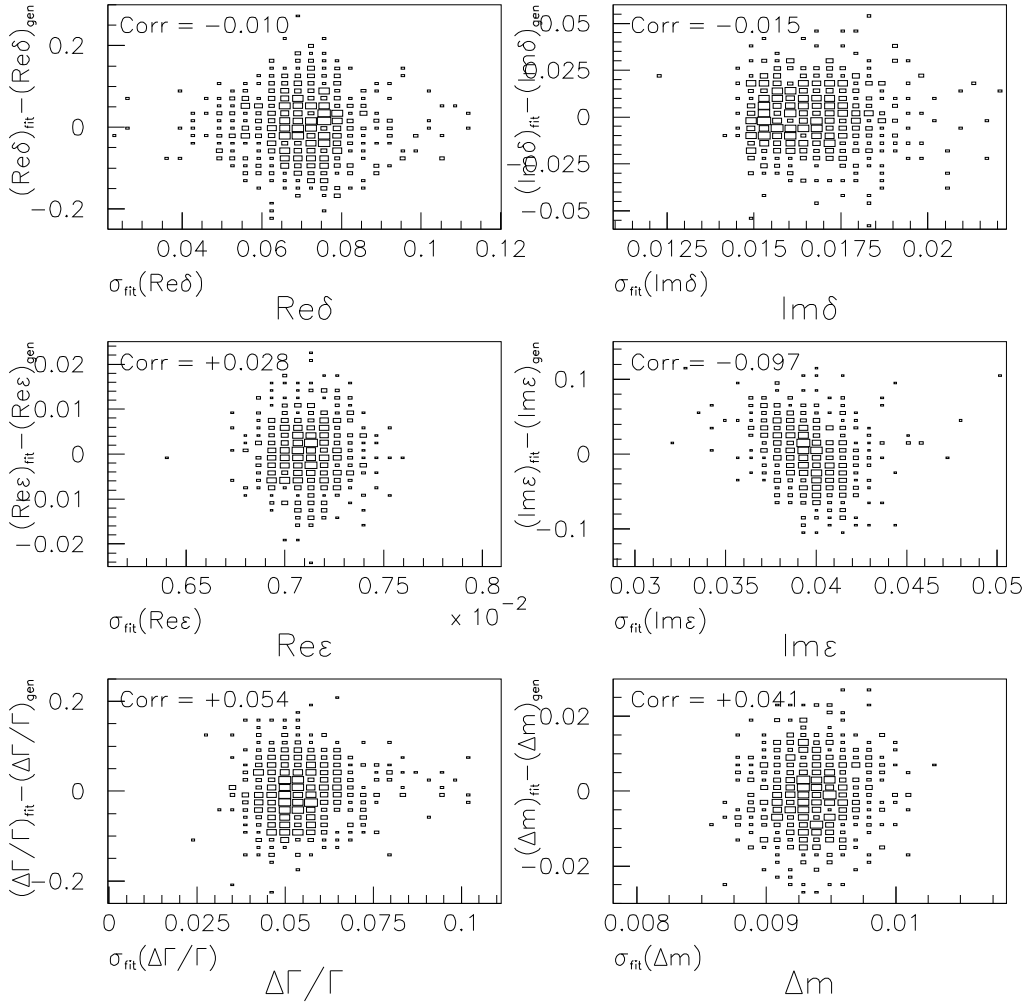
Figure 28: Residual vs. Gaussian error for the physics parameters from signal only fits (*GExp* resolution model, ≈ 60 fb^{-1}). The correlation coefficient is reported on each plot. The sample is the same that used in figure 27.

Reference configuration, *GExp* model						
	$\frac{1-|\varepsilon|^2}{1+|\varepsilon|^2}\ \frac{Re\delta}{1+|\varepsilon|^2}$	$\frac{Im\delta}{1+|\varepsilon|^2}$	$\frac{Im\varepsilon}{1+|\varepsilon|^2}$	$\frac{Re\varepsilon}{1+|\varepsilon|^2}$	$\Delta\Gamma/\Gamma$	Δm
Mean residual	$(3.7\pm2.8)\cdot10^{-3}$	$(3.3\pm5.9)\cdot10^{-4}$	$(1.5\pm1.5)\cdot10^{-3}$	$(1.3\pm2.5)\cdot10^{-4}$	$(-2.7\pm2.3)\cdot10^{-3}$	$(-6.5\pm3.5)\cdot10^{-4}$
RMS residual	$(7.5\pm0.2)\cdot10^{-2}$	$(1.57\pm0.05)\cdot10^{-2}$	$(3.9\pm0.1)\cdot10^{-2}$	$(6.7\pm0.2)\cdot10^{-3}$	$(6.2\pm0.2)\cdot10^{-2}$	$(9.3\pm0.3)\cdot10^{-3}$
Av. error (Gauss)	$7.0\cdot10^{-2}$	$1.7\cdot10^{-2}$	$4.0\cdot10^{-2}$	$7.1\cdot10^{-3}$	$5.5\cdot10^{-2}$	$9.4\cdot10^{-3}$
Gauss. error cov.	$(62.7\pm3.8)\%$	$(70.3\pm4.1)\%$	$(66.1\pm3.9)\%$	$(72.2\pm4.2)\%$	$(60.1\pm3.7)\%$	$(66.9\pm4.0)\%$

Table 15: Summary of results for the reference configuration from signal only fits (*GExp* resolution model, ≈ 60 fb^{-1}).

residual distribution as well as the average Gaussian error and its coverage are summarized in tables 16 and 17, for the *GG* and *GExp* resolution models. Figure 30(a) shows the mean residuals as a function of several values of the true value of $\Delta\Gamma/\Gamma$. From this scan we conclude that the extraction of $\Delta\Gamma/\Gamma$ over a wide range of truth values is, for both the *GG* and *GExp* resolution models, unbiased at 5×10^{-3} level, about one order of magnitude smaller than the statistical reach, as seen in figure 30(b) where it is shown the RMS of the residuals for the same various values of the generated $\Delta\Gamma/\Gamma$. The corresponding mean residuals for all the other physics parameters are shown in figure 31. Again, no biases are seen up to one order of magnitude below the statistical reach of each parameter.

$\Delta\Gamma/\Gamma$=0.2 configuration, *GG* model						
	$\frac{1-|\varepsilon|^2}{1+|\varepsilon|^2}\ \frac{Re\delta}{1+|\varepsilon|^2}$	$\frac{Im\delta}{1+|\varepsilon|^2}$	$\frac{Im\varepsilon}{1+|\varepsilon|^2}$	$\frac{Re\varepsilon}{1+|\varepsilon|^2}$	$\Delta\Gamma/\Gamma$	Δm
Mean residual	$(1.7\pm2.0)\cdot10^{-3}$	$(3.6\pm9.2)\cdot10^{-4}$	$(-2.8\pm1.9)\cdot10^{-3}$	$(-2.6\pm3.3)\cdot10^{-4}$	$(-4.4\pm2.1)\cdot10^{-3}$	$(0.3\pm4.6)\cdot10^{-4}$
RMS residual	$(4.4\pm0.2)\cdot10^{-2}$	$(2.0\pm0.1)\cdot10^{-2}$	$(4.1\pm0.1)\cdot10^{-2}$	$(7.1\pm0.2)\cdot10^{-3}$	$(4.4\pm0.1)\cdot10^{-2}$	$(9.9\pm0.3)\cdot10^{-3}$
Av. error (Gauss)	$4.6\cdot10^{-2}$	$2.0\cdot10^{-2}$	$3.9\cdot10^{-2}$	$7.0\cdot10^{-3}$	$4.6\cdot10^{-2}$	$9.9\cdot10^{-3}$
Gauss. error cov.	$(68.8\pm5.0)\%$	$(69.0\pm5.0)\%$	$(67.9\pm5.0)\%$	$(66.4\pm4.9)\%$	$(70.7\pm5.1)\%$	$(66.4\pm4.9)\%$

Table 16: Summary of results for the $\Delta\Gamma/\Gamma$=0.2 configuration from signal only fits (*GG* resolution model, ≈ 60 fb^{-1}).

$\Delta\Gamma/\Gamma$=0.2 configuration, *GExp* model						
	$\frac{1-|\varepsilon|^2}{1+|\varepsilon|^2}\ \frac{Re\delta}{1+|\varepsilon|^2}$	$\frac{Im\delta}{1+|\varepsilon|^2}$	$\frac{Im\varepsilon}{1+|\varepsilon|^2}$	$\frac{Re\varepsilon}{1+|\varepsilon|^2}$	$\Delta\Gamma/\Gamma$	Δm
Mean residual	$(-2.0\pm1.6)\cdot10^{-3}$	$(-2.6\pm7.4)\cdot10^{-4}$	$(1.4\pm1.5)\cdot10^{-3}$	$(0.0\pm2.7)\cdot10^{-4}$	$(0.7\pm1.7)\cdot10^{-3}$	$(-4.4\pm3.5)\cdot10^{-4}$
RMS residual	$(4.2\pm0.1)\cdot10^{-2}$	$(1.9\pm0.1)\cdot10^{-2}$	$(4.0\pm0.1)\cdot10^{-2}$	$(7.1\pm0.2)\cdot10^{-3}$	$(4.6\pm0.2)\cdot10^{-2}$	$(9.4\pm0.3)\cdot10^{-3}$
Av. error (Gauss)	$4.3\cdot10^{-2}$	$2.0\cdot10^{-2}$	$3.9\cdot10^{-2}$	$7.0\cdot10^{-3}$	$4.4\cdot10^{-2}$	$9.6\cdot10^{-3}$
Gauss. error cov.	$(67.6\pm4.0)\%$	$(66.9\pm4.0)\%$	$(68.1\pm4.0)\%$	$(67.3\pm4.0)\%$	$(62.3\pm3.8)\%$	$(70.2\pm4.1)\%$

Table 17: Summary of results for the $\Delta\Gamma/\Gamma$=0.2 configuration from signal only fits (*GExp* resolution model, ≈ 60 fb^{-1}).

The behaviour of the $\Delta\Gamma$ error shown in figure 30(b) confirms the expectations discussed in [38]. Due to the linear (second order) dependence of the time dependence with $\Delta\Gamma$ for CP (flavor) events, CP events dominate its determination for small values of $\Delta\Gamma/\Gamma$, while the larger weight is from the flavor events for large values. For CP events, the precision on $\Delta\Gamma/\Gamma$ scales as $1/\sqrt{N}$, constant as a function of $\Delta\Gamma/\Gamma$. In the case of flavor events, due to the second order dependence, the error scales as $1/N^{1/4}$ for small values, while for large values it goes as $1/\sqrt{N}\ 1/\Delta\Gamma$, as seen is figure 30(b). With the relative statistics of flavor and CP events assumed in these studies (table 12), we have evaluated the $\Delta\Gamma/\Gamma$ point where the relative weight of both samples equals. This has been evaluated running toy Monte Carlo experiments for several values of $\Delta\Gamma/\Gamma$ by fitting the flavor and CP samples together and comparing the results to CP only fits, fixing in both cases the resolution function and mistag parameters to those generated. Table 18 summarizes the RMS of the residual distributions for all the physics parameters and three configurations, $\Delta\Gamma/\Gamma$=0.0,0.1,0.2. For $\Delta\Gamma/\Gamma\approx0$ the CP sample dominates the sensitivity, and at $\Delta\Gamma/\Gamma\approx0.1$ is where the statistical power of
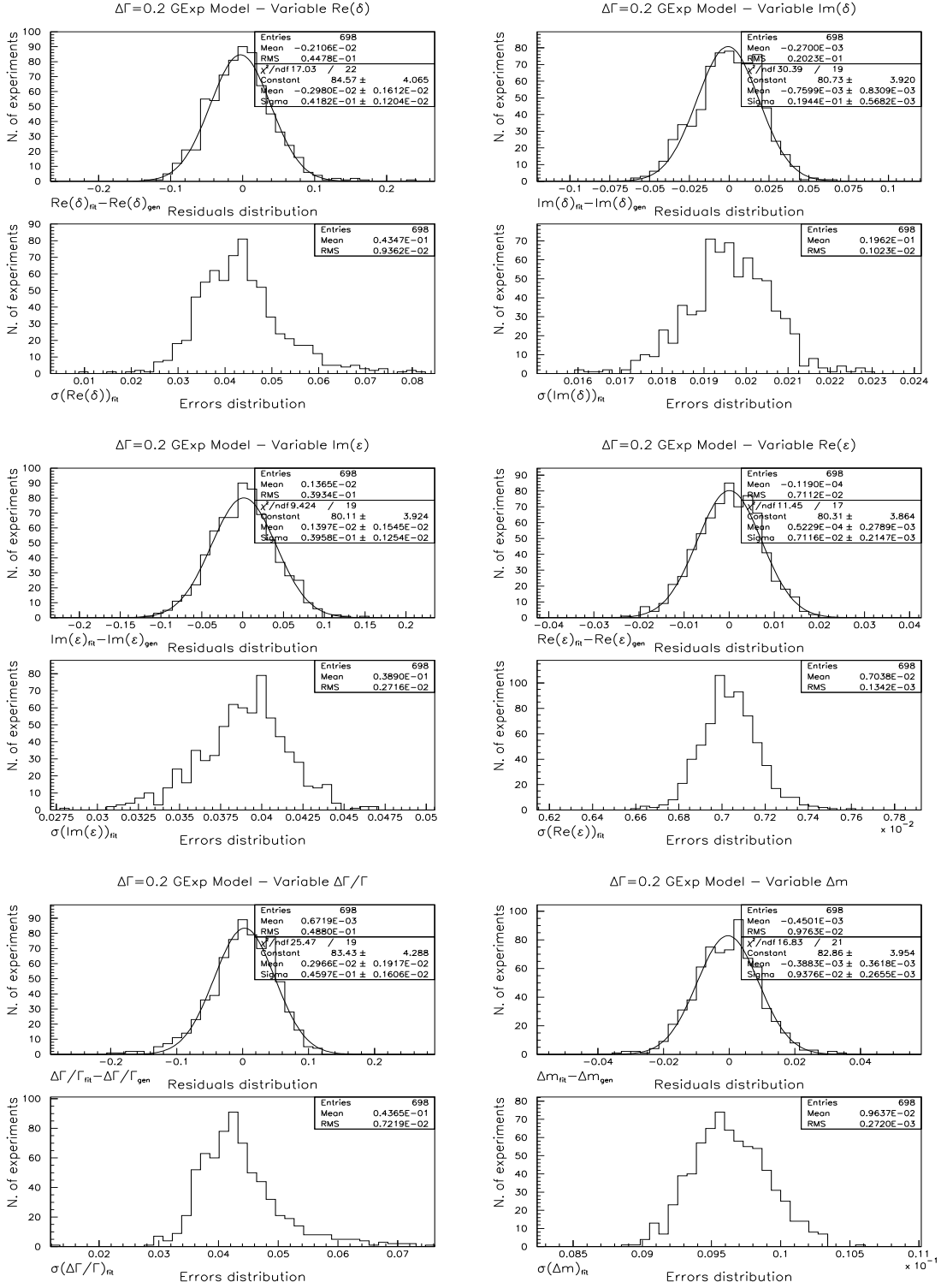
Figure 29: Residual and Gaussian error distributions for the physics parameters from signal only fits (*GExp* resolution model, $\approx 60 \text{ fb}^{-1}$). The generated values correspond to the reference configuration given in table 13 with $\Delta\Gamma/\Gamma=0.2$.
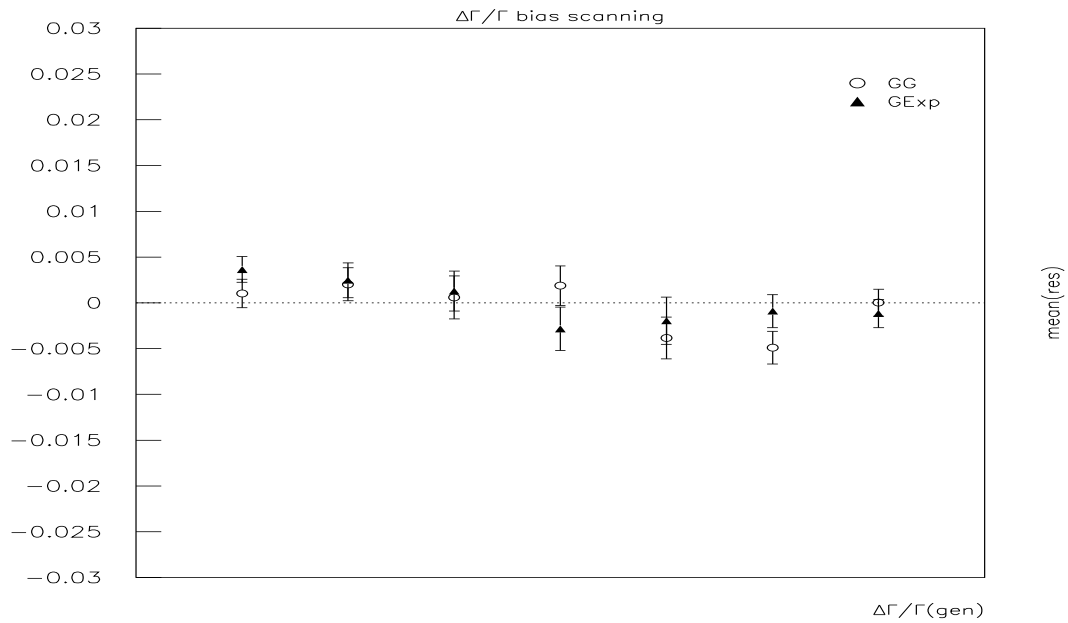
(a)
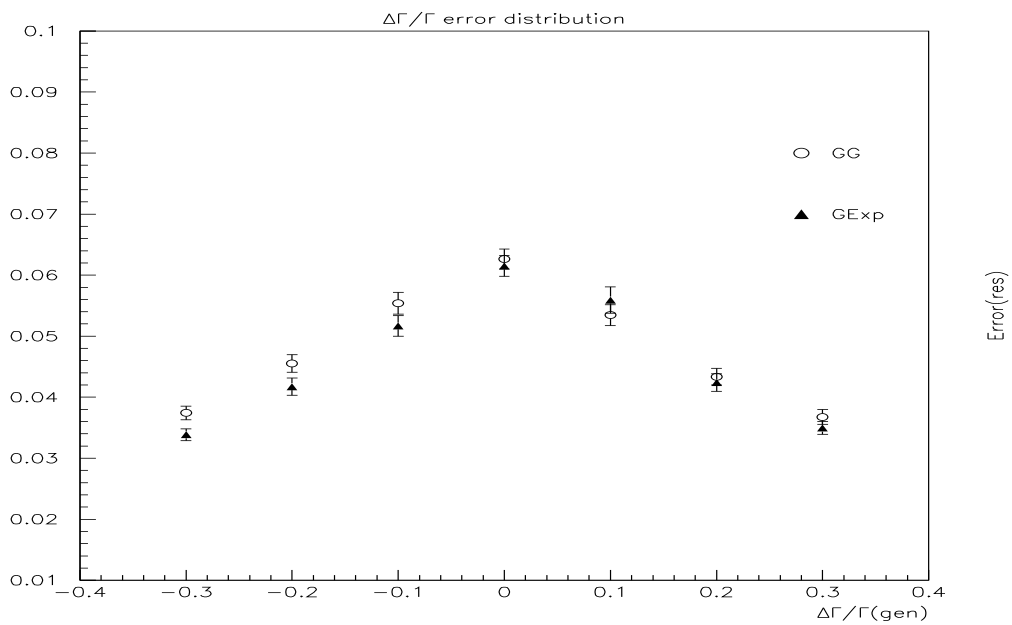
(b)

Figure 30: $\Delta\Gamma/\Gamma$ mean residuals (a) and RMS (b) as a function of the generated $\Delta\Gamma/\Gamma$, for the *GG* and *GExp* resolution models, for an equivalent luminosity of ≈ 60 fb^{-1}.
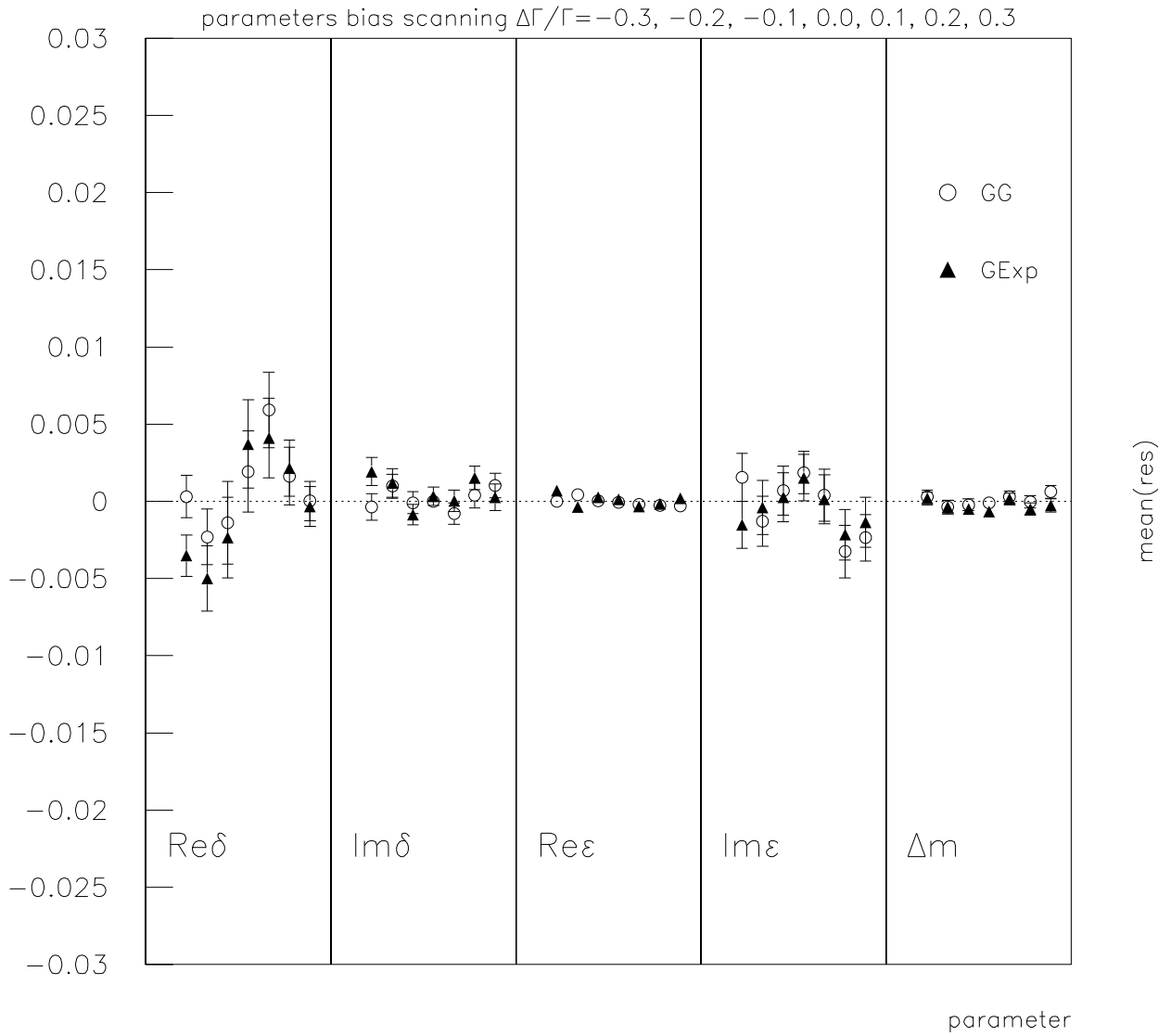
Figure 31: $\frac{\mathrm{Re}\delta}{1+|\varepsilon|^2}$, $\frac{\mathrm{Im}\delta}{1+|\varepsilon|^2}$, $\frac{\mathrm{Re}\varepsilon}{1+|\varepsilon|^2}$, $\frac{\mathrm{Im}\varepsilon}{1+|\varepsilon|^2}$ and Δm mean residuals from the same experiments/fits as those used in figure 30, for the *GG* and *GExp* resolution models. For each parameter the ordering from left to right matches the scanning points in the previous figure.

the CP sample equals to that of the flavor events (estimated from the combined flavor+CP fits using simple quadratic differences), ≈ 0.073. The relative contribution from each sample for all the other parameters is also seen in table 18, in agreement with the discussion of the last paragraph of section 4.1.5.

	Flavor+CP		
	$\Delta\Gamma/\Gamma = 0.0$	$\Delta\Gamma/\Gamma = 0.1$	$\Delta\Gamma/\Gamma = 0.2$
$\Delta\Gamma/\Gamma$	0.0680 ± 0.0018	0.0517 ± 0.0018	0.0354 ± 0.0010
$\frac{1-|\varepsilon|^2}{1+|\varepsilon|^2}\frac{\mathrm{Re}\delta}{1+|\varepsilon|^2}$	0.0771 ± 0.0020	0.0620 ± 0.0022	0.0452 ± 0.0015
$\frac{\mathrm{Im}\delta}{1+|\varepsilon|^2}$	0.0160 ± 0.0004	0.0168 ± 0.0005	0.0182 ± 0.0006
$\frac{\mathrm{Im}\varepsilon}{1+|\varepsilon|^2}$	0.0382 ± 0.0011	0.0410 ± 0.0012	0.0379 ± 0.0011
$\frac{\mathrm{Re}\varepsilon}{1+|\varepsilon|^2}$	0.00632 ± 0.00019	0.00628 ± 0.00018	0.00617 ± 0.00020
Δm	0.00800 ± 0.00024	0.00812 ± 0.00027	0.00832 ± 0.00025
	CP only		
	$\Delta\Gamma/\Gamma = 0.0$	$\Delta\Gamma/\Gamma = 0.1$	$\Delta\Gamma/\Gamma = 0.2$
$\Delta\Gamma/\Gamma$	0.0749 ± 0.0024	0.0737 ± 0.0021	0.0737 ± 0.0024
$\frac{1-|\varepsilon|^2}{1+|\varepsilon|^2}\frac{\mathrm{Re}\delta}{1+|\varepsilon|^2}$	0.0854 ± 0.0024	0.0833 ± 0.0030	0.0812 ± 0.0028
$\frac{\mathrm{Im}\delta}{1+|\varepsilon|^2}$	0.0797 ± 0.0024	0.0844 ± 0.0024	0.0812 ± 0.0027
$\frac{\mathrm{Im}\varepsilon}{1+|\varepsilon|^2}$	0.0412 ± 0.0014	0.0451 ± 0.0013	0.0462 ± 0.0014
$\frac{\mathrm{Re}\varepsilon}{1+|\varepsilon|^2}$	0.0403 ± 0.0012	0.0381 ± 0.0014	0.0382 ± 0.0012
Δm	0.0510 ± 0.0019	0.0546 ± 0.0017	0.0574 ± 0.0018

Table 18: RMS of the residual distributions for all the physics parameters from combined flavor+CP and CP only fits. The resolution function and mistag parameters were fixed to those generated. The statistics corresponds to ≈ 60 fb^{-1}.

The even $\cosh(\Delta\Gamma\Delta t/2)$ ($\Delta\Gamma^2$ to first order) dependence of the flavor sample has another important consequence: the log-likelihood function is symmetric with respect to $\Delta\Gamma=0$, so we expect two symmetric maxima [39]. On the contrary the CP sample has a non-vanishing odd $\sinh(\Delta\Gamma\Delta t/2)$ dependence, and therefore it is sensitive to the sign of $\Delta\Gamma/\Gamma$. We expect that the measurement made with the two samples combined breaks the ambiguity, as shown also in the likelihood scan in figure 25, in the case of $\Delta\Gamma/\Gamma = 0.2$. In order to check this guess, we fitted 100 toy Monte Carlo samples with the equivalent statistics of 60 fb^{-1}, generated with $\Delta\Gamma/\Gamma = 0.2$, giving as starting point for the fit three different values of $\Delta\Gamma/\Gamma$: -0.2, 0.0 and 0.2. The number of converged fits reduces if the starting point is different from the generated value, but, if the fit converges, it gives the right value. In none of the cases the fit converged to $\Delta\Gamma/\Gamma = -0.2$. If we compare the fitted value in the three different cases for the same experiment, we found that the difference is negligible with respect to the statistical error, at the level of the numerical precision, as shown in figure 32.

Another set of tests has been performed to evaluate the improvement in the $\Delta\Gamma/\Gamma$ measurement due to the complementary use of the flavour and the CP sample. We generated and fitted ~ 600 low statistics toy Monte Carlo experiments (30 fb^{-1}) using just the flavour sample with the *GG* resolution model. In figure 33 the residual distributions of $\Delta\Gamma/\Gamma$ variable are reported for three different values of generated $\Delta\Gamma/\Gamma$: 0.1, 0.2 and 0.3. In the first two cases a large part of the fits (30% and 15% respectively) converged to the value of $\Delta\Gamma/\Gamma=0$, corresponding to the high spike at the value of -0.1 on the first residual plot and -0.2 on the second one. Few of the fits converged also at the opposite of the generated value corresponding to the bins at -0.2 and -0.4 on the residual plots. These effects are due to the mentioned symmetric shape around zero of the likelihood function for the mixing sample. In the case of $\Delta\Gamma/\Gamma=0.3$ the two maxima should be well separated and we don't see any effect since we used the generated values as a starting point for the fit. In all the three cases the distribution showed a large negative bias of 5–6 standard deviations from the central
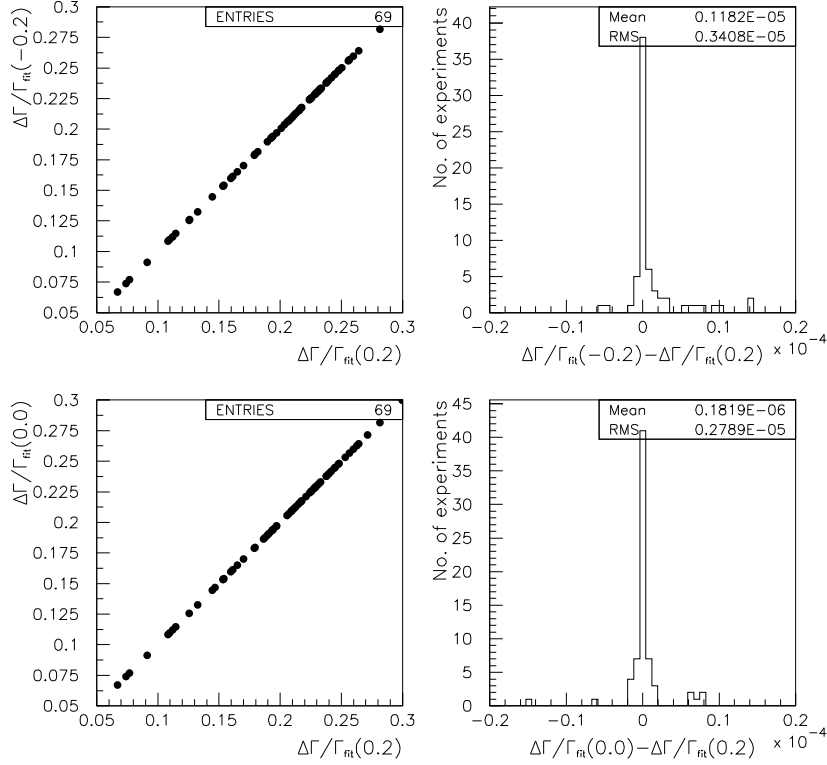
Figure 32: Comparison between the results obtained fitting the same 60 fb^{-1} samples generated with $\Delta\Gamma/\Gamma=0.2$, using different starting points for $\Delta\Gamma/\Gamma$. The upper left plot shows the correlation among the fitted values starting from $\Delta\Gamma/\Gamma=0.2$ and $\Delta\Gamma/\Gamma=0.0$, while the upper right shows the distribution of the difference between the two fitted parameters. The lower plots shows the analogous for the comparison between $\Delta\Gamma/\Gamma=0.2$ and $\Delta\Gamma/\Gamma=-0.2$.

value, never seen in all the tests made using the flavour and the CP samples together.

In order to check how these effects change with the statistics, we repeated the experiment with a much larger data sample size (150 fb^{-1}). In figure 34, top plots, the residual distributions for $\Delta\Gamma/\Gamma$ show that the situation is pretty similar to the low statistics case for $\Delta\Gamma/\Gamma=0.1$, but much better for $\Delta\Gamma/\Gamma=0.2$: no fits converged to the negative value and just a couple of them collapsed to zero. Nevertheless in all the three cases we had a confirmation of the negative bias of the fitted values (7.5, 3.5 and 2 standard deviations respectively).

We explored also the possibility of measuring $\Delta\Gamma/\Gamma$ using the CP sample alone, performing similar toy Monte Carlo experiments. In figure 34, bottom plots, the residual distributions give another confirmation of the fact that the CP sample is sensitive to the sign of $\Delta\Gamma$. The distributions in this case show no evidences of bias.

30 fb^{-1} experiments mixing events only

$\Delta\Gamma/\Gamma_{gen}$=0.1	Entries 632
	Mean −0.1380E−01 ± 0.41E−02

Residuals distribution

$\Delta\Gamma/\Gamma_{gen}$=0.2	Entries 590
	Mean −0.2550E−01 ± 0.44E−02

Residuals distribution

$\Delta\Gamma/\Gamma_{gen}$=0.3	Entries 548
	Mean −0.2078E−01 ± 0.35E−02

Residuals distribution
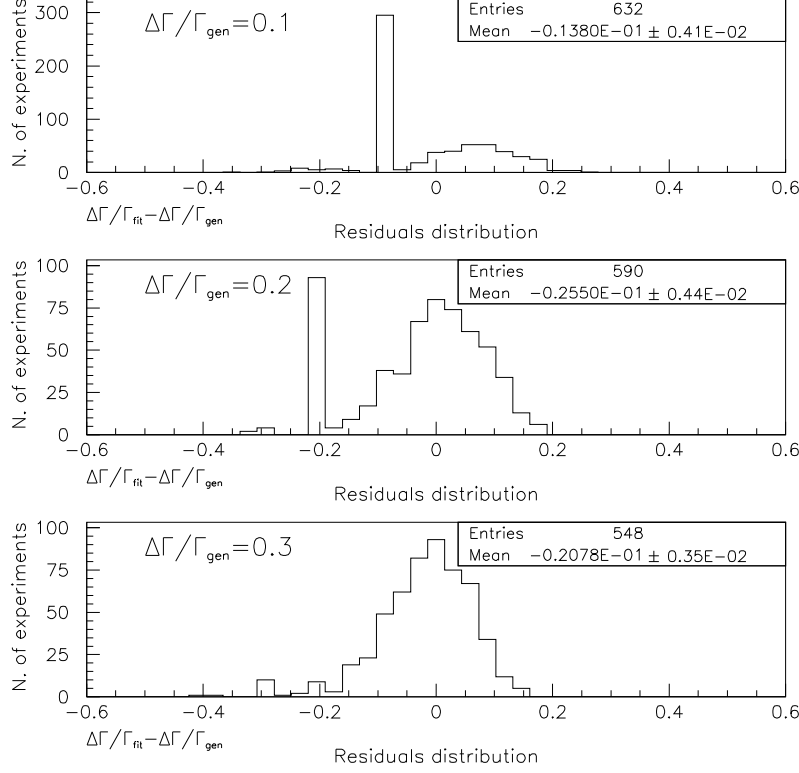
Figure 33: Residual distribution for three different values of $\Delta\Gamma/\Gamma$generated (0.1, 0.2 and 0.3 from top to bottom) using the flavour sample alone. Each of the plots comes from $\sim$600 experiments with the equivalent statistics of 30 fb^{-1}. *GG* resolution model has been used. Variables $\frac{1-|\varepsilon|^2}{1+|\varepsilon|^2}\frac{\mathrm{Re}\delta}{1+|\varepsilon|^2}$ and $\frac{\mathrm{Im}\varepsilon}{1+|\varepsilon|^2}$ were fixed in the fit since the sample is not sensitive to them.

4.1.4   Non-Gaussian errors

The non-Gaussian behavior of the physics parameters has been investigated for $\Delta\Gamma/\Gamma$ and $\frac{1-|\varepsilon|^2}{1+|\varepsilon|^2}\frac{\mathrm{Re}\delta}{1+|\varepsilon|^2}$. Figures 35 and 36 show the distribution of the positive and negative asymmetric errors for these two parameters (*GExp* model) and their correlation, for the reference and $\Delta\Gamma/\Gamma$=0.2 configurations. Tables 19 and 20 summarize the average and RMS of the residual distribution together with the average Gaussian, positive and negative errors and the corresponding confidence interval coverages. Let us note that the set of experiments used for this check is statistically independent of that used in section 4.1.2. For the $\Delta\Gamma/\Gamma$=0.2 configuration, the $\Delta\Gamma/\Gamma$ negative error is about 10% larger than the positive, reflecting the systematic asymmetry of the log-likelihood function ilustrated in figure 25(b), which origin was discussed in last paragraph of section 4.1.3. Within the precision of our statistics, the asymmetric confidence intervals provide the correct coverage.
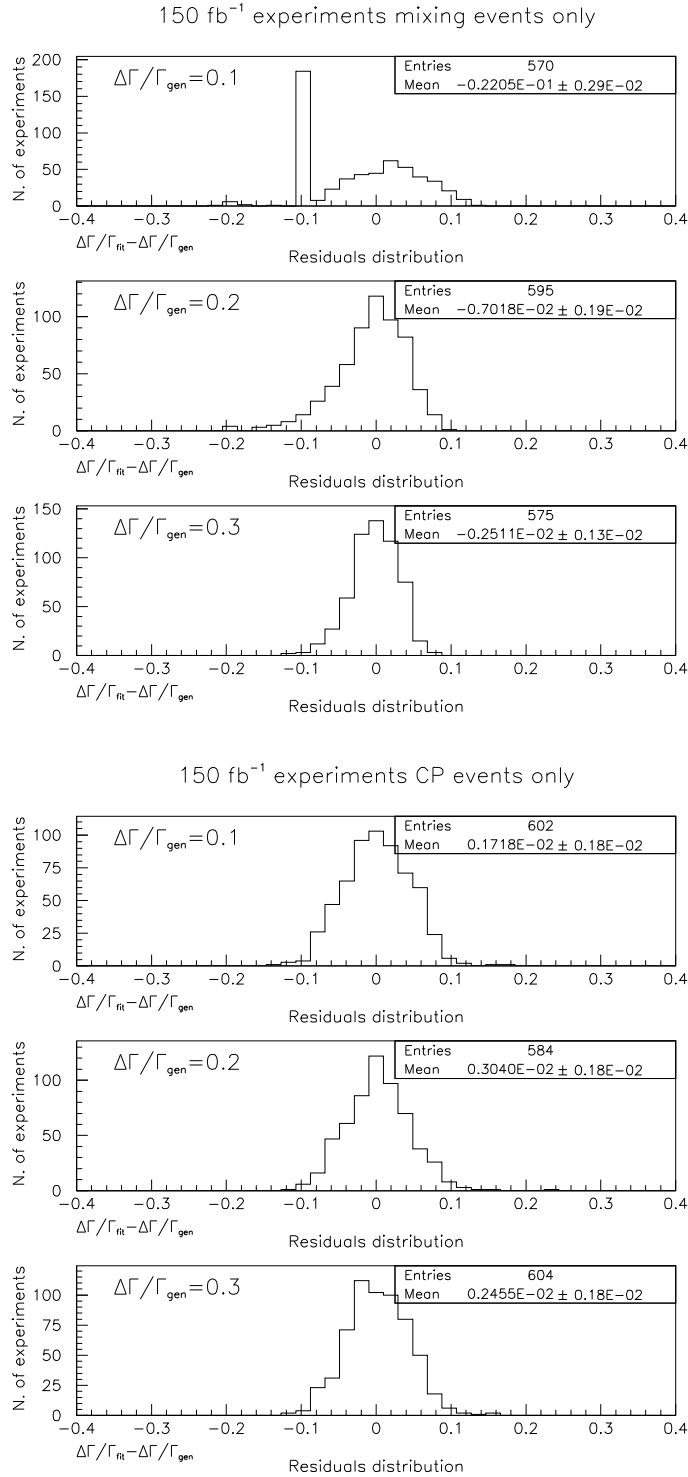
Figure 34: Top three plots: Residual distribution for three different values of generated $\Delta\Gamma/\Gamma$(0.1, 0.2 and 0.3 from top to bottom) using the flavour sample alone. Each of the plots comes from $\sim$600 experiments with the equivalent statistics of 150 fb^{-1}. *GG* resolution model has been used. Variables $\frac{1-|\varepsilon|^2}{1+|\varepsilon|^2}\frac{\text{Re}\delta}{1+|\varepsilon|^2}$ and $\frac{\text{Im}\varepsilon}{1+|\varepsilon|^2}$ were fixed in the fit since the sample is not sensitive to them. Bottom three plots: The same for CP sample. In this case we fixed $\frac{\text{Re}\varepsilon}{1+|\varepsilon|^2}$, $\frac{\text{Im}\delta}{1+|\varepsilon|^2}$ and tagging efficiencies and asymmetries.
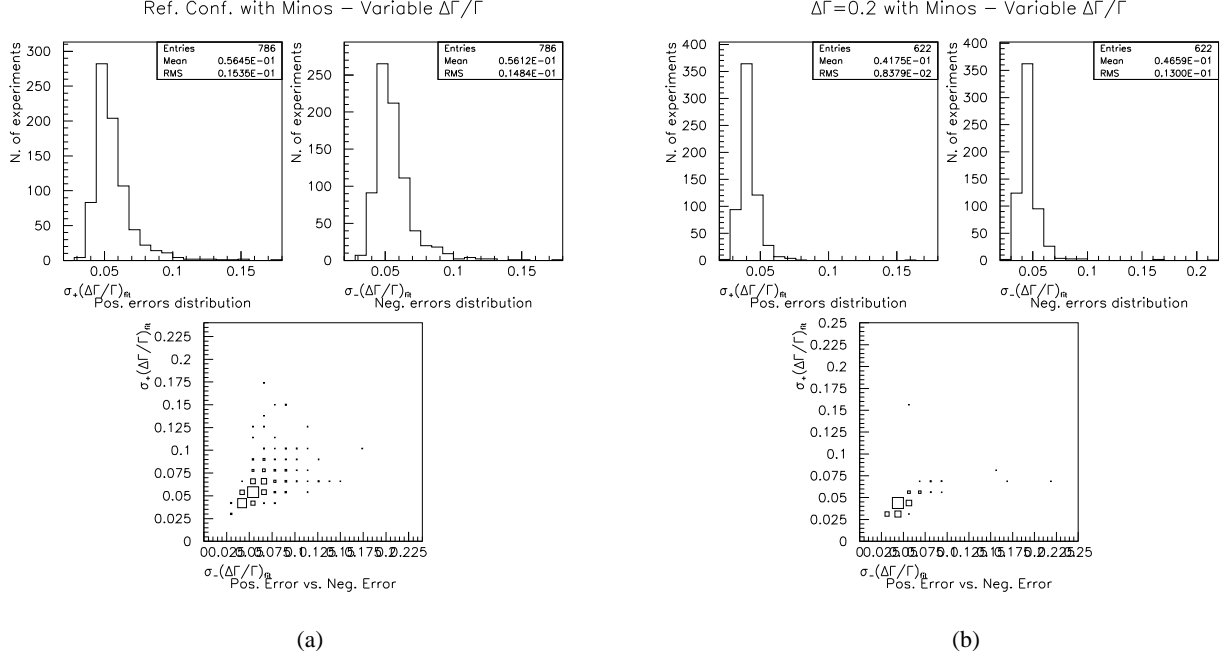
Figure 35: Positive and negative asymmetric errors and their correlation for $\Delta\Gamma/\Gamma$ from signal only fits (*GExp* resolution model, ≈ 60 fb^{-1}). The generated values correspond to the reference configuration (a) and reference with $\Delta\Gamma/\Gamma$=0.2 (b).

	Reference configuration, *GExp* model					
	$\frac{1-|\epsilon|^2}{1+|\epsilon|^2}\frac{Re\delta}{1+|\epsilon|^2}$	$\frac{Im\delta}{1+|\epsilon|^2}$	$\frac{Im\epsilon}{1+|\epsilon|^2}$	$\frac{Re\epsilon}{1+|\epsilon|^2}$	$\Delta\Gamma/\Gamma$	Δm
Mean residual	$(1.4\pm2.7)\cdot10^{-3}$	$(-0.9\pm0.6)\cdot10^{-3}$	$(3.1\pm1.4)\cdot10^{-3}$	$(-1.7\pm2.4)\cdot10^{-4}$	$(-1.2\pm2.2)\cdot10^{-3}$	$(-3.9\pm3.2)\cdot10^{-4}$
RMS residual	$(7.7\pm0.2)\cdot10^{-2}$	$(1.6\pm0.0)\cdot10^{-2}$	$(4.1\pm0.1)\cdot10^{-2}$	$(6.7\pm0.2)\cdot10^{-3}$	$(6.1\pm0.2)\cdot10^{-2}$	$(8.9\pm0.3)\cdot10^{-3}$
Av. error (Gauss)	$7.0\cdot10^{-2}$	$1.7\cdot10^{-2}$	$3.9\cdot10^{-2}$	$7.1\cdot10^{-3}$	$5.6\cdot10^{-2}$	$9.3\cdot10^{-3}$
Av. positive error	$7.1\cdot10^{-2}$	—	—	—	$5.6\cdot10^{-2}$	—
Av. negative error	$7.2\cdot10^{-2}$	—	—	—	$5.6\cdot10^{-2}$	—
Gauss. error cov.	$(61.1\pm3.5)\%$	$(68.5\pm3.8)\%$	$(67.6\pm3.8)\%$	$(69.3\pm3.9)\%$	$(61.5\pm3.6)\%$	$(71.4\pm3.9)\%$
Non-Gaussian err. cov.	$(62.9\pm3.6)\%$	—	—	—	$(63.7\pm3.6)\%$	—

Table 19: Summary of results for the reference configuration from signal only fits (*GExp* resolution model, ≈ 60 fb^{-1}) with asymmetric errors calculation. This set of experiments is independent from the one used for Table 15.

4.1.5 Correlations

Disclaimer: After running some of the toy Monte Carlo experiments documented so far, also used in this section, it was found a wrong sign in the fitting code which affected $\Delta\Gamma/\Gamma$ for CP events. This does not change the conclusions of our studies, but we should take this into account when looking at the correlations of $\Delta\Gamma/\Gamma$ with the other parameters, since they will have the opposite sign to that shown in the figures. The affected figures will be explicitly marked with a comment in the caption. The numbers quoted in the text have already the correct sign.

The analysis of the set of experiments in the reference configuration confirms the absence of significant
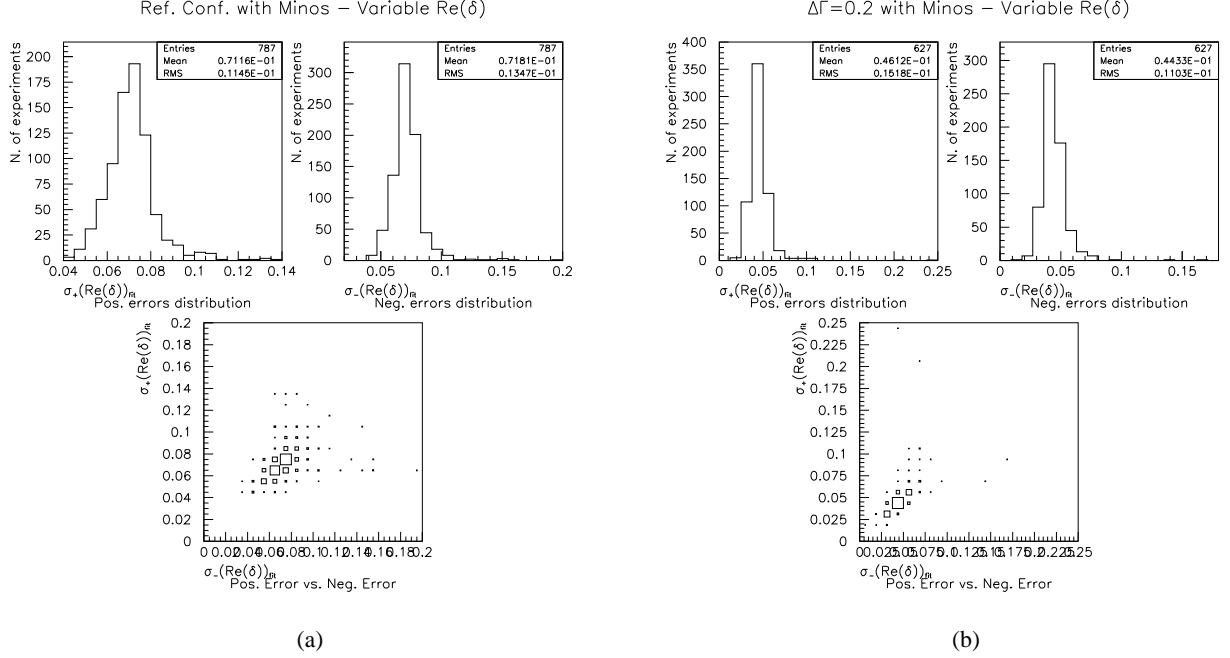
Figure 36: Positive and negative asymmetric errors and their correlation for $\frac{1-|\varepsilon|^2}{1+|\varepsilon|^2}\frac{\text{Re}\varepsilon}{1+|\varepsilon|^2}$ from signal only fits (*GExp* resolution model, ≈ 60 fb^{-1}). The generated values correspond to the reference configuration (a) and reference with $\Delta\Gamma/\Gamma$=0.2 (b).

	$\Delta\Gamma/\Gamma$=0.2 configuration, *GExp* model					
	$\frac{1-\|\varepsilon\|^2}{1+\|\varepsilon\|^2}\frac{\text{Re}\delta}{1+\|\varepsilon\|^2}$	$\frac{\text{Im}\delta}{1+\|\varepsilon\|^2}$	$\frac{\text{Im}\varepsilon}{1+\|\varepsilon\|^2}$	$\frac{\text{Re}\varepsilon}{1+\|\varepsilon\|^2}$	$\Delta\Gamma/\Gamma$	Δm
Mean residual	$(2.2\pm1.7)\cdot10^{-3}$	$(1.3\pm0.7)\cdot10^{-3}$	$(-2.1\pm1.6)\cdot10^{-3}$	$(-1.7\pm2.8)\cdot10^{-4}$	$(-1.1\pm1.7)\cdot10^{-3}$	$(-4.5\pm3.8)\cdot10^{-4}$
RMS residual	$(4.3\pm0.1)\cdot10^{-2}$	$(1.9\pm0.1)\cdot10^{-2}$	$(4.0\pm0.1)\cdot10^{-2}$	$(7.2\pm0.2)\cdot10^{-3}$	$(4.2\pm0.1)\cdot10^{-2}$	$(9.7\pm0.3)\cdot10^{-3}$
Av. error (Gauss)	$4.4\cdot10^{-2}$	$1.9\cdot10^{-2}$	$3.9\cdot10^{-2}$	$7.0\cdot10^{-3}$	$4.3\cdot10^{-2}$	$9.7\cdot10^{-3}$
Av. positive error	$4.6\cdot10^{-2}$	—	—	—	$4.2\cdot10^{-2}$	—
Av. negative error	$4.4\cdot10^{-2}$	—	—	—	$4.7\cdot10^{-2}$	—
Gauss. error cov.	$(65.7\pm4.1)\%$	$(70.0\pm4.3)\%$	$(66.8\pm4.1)\%$	$(66.6\pm4.1)\%$	$(69.7\pm4.2)\%$	$(68.3\pm4.2)\%$
Non-Gaussian err. cov.	$(61.2\pm3.9)\%$	—	—	—	$(67.6\pm4.2)\%$	—

Table 20: Summary of results for the $\Delta\Gamma/\Gamma$=0.2 configuration from signal only fits (*GExp* resolution model, ≈ 60 fb^{-1}) with asymmetric errors calculation. This set of experiments is independent from the one used for Table 17.

correlations among different physics parameters at the order of few percent, as it can be seen in figures 37 and 38, where we show the scatter plot and the correlation coefficients, respectively, among all possible combinations of the 6 physics parameters. The largest observed correlation is between $\Delta\Gamma/\Gamma$ and $\frac{\text{Re}\varepsilon}{1+|\varepsilon|^2}$ (-11%). The largest correlation between $\frac{\text{Re}\delta}{1+|\varepsilon|^2}$ and any other physics parameter is, as expected, with $\Delta\Gamma/\Gamma$ (+6%). See disclaimer at the begining of this section.

The larger identified correlation between a physics parameter and any other parameter entering in the fit procedure is between $\frac{\text{Re}\varepsilon}{1+|\varepsilon|^2}$ and the difference of the mistag fractions for B^0 and $\overline{B}^0$, Δw^α. The average correlations are 23%, 32%, 15% and 10%, for the Lepton, Kaon, NT1, NT2 tagging categories, re-

63
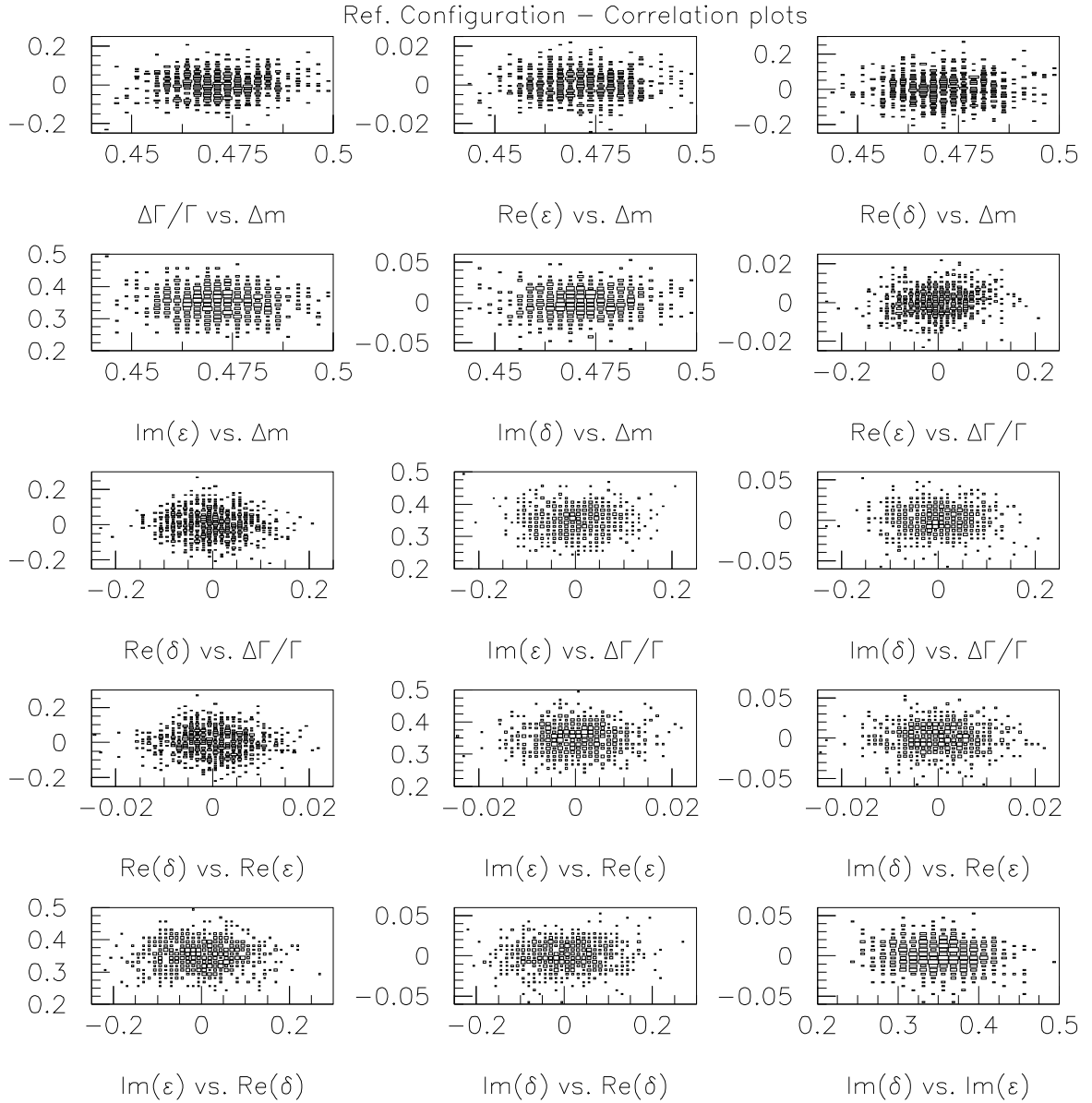
Figure 37: Scatter distributions among all combinations of the physics parameters, for the reference config-uration (*GExp* model, ≈ 60 fb^{-1}). See disclaimer at the begining of section 4.1.5.
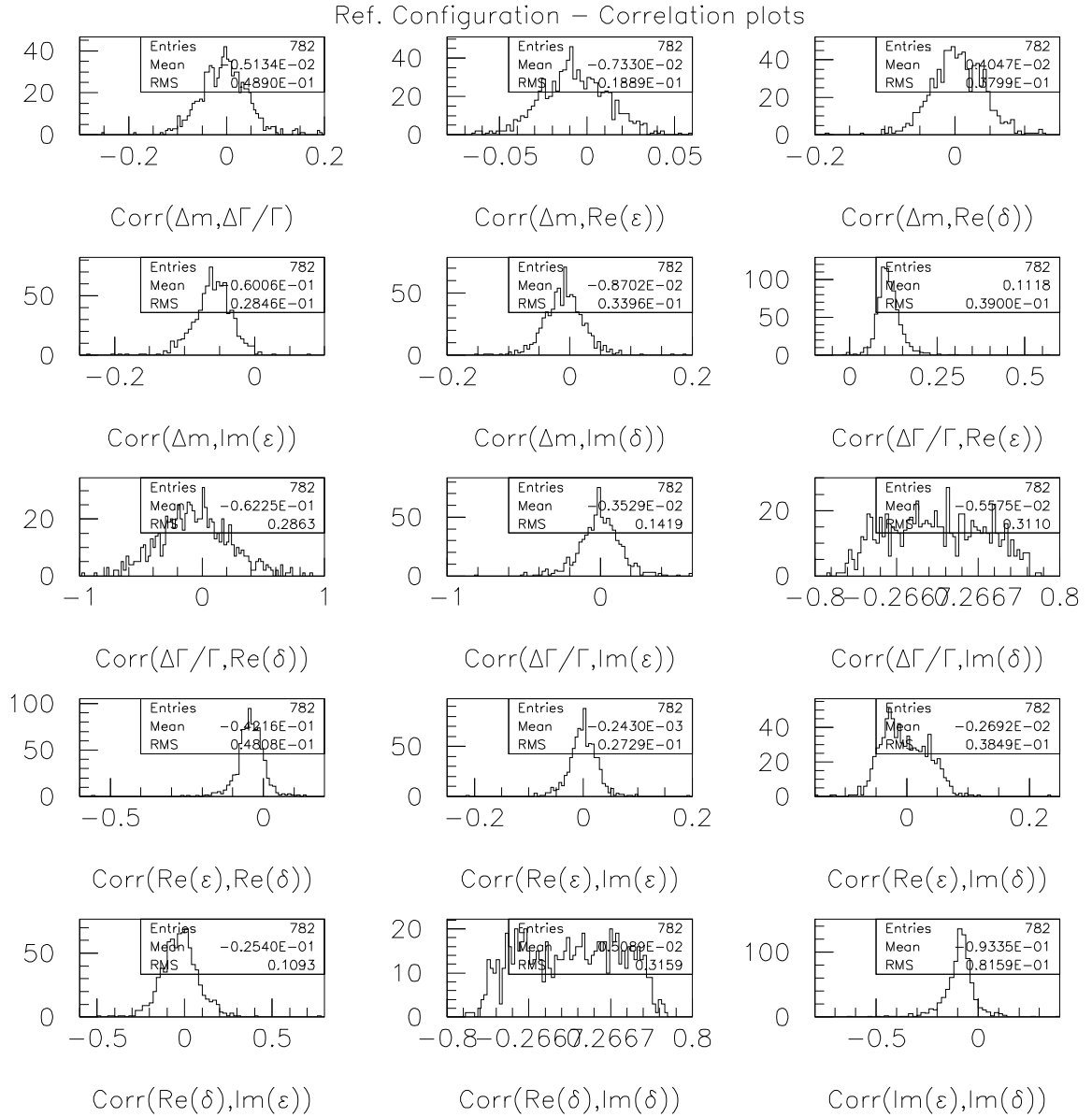
Figure 38: Correlation coefficients among all combinations of the physics parameters, for the reference configuration (*GExp* model, ≈ 60 fb^{-1}). See disclaimer at the begining of section 4.1.5.

spectively. The correlation between Δm and the mistag fractions, w_0^α, are, repectively, -22%, -10%, -13% and -8%. The only significant correlation with a resolution function parameter is between Δm and the scale of the central Gaussian (S), 25%, for the *GExp* model, and between Δm and the fraction and the bias of the tail component (f_{tail} and δ_{tail}), 20% and 10% respectively, for the *GG* model. All the other correlations are within few per cent. It is worth noting that the CPT parameter, $\frac{1-|\varepsilon|^2}{1+|\varepsilon|^2}\frac{\mathrm{Re}\delta}{1+|\varepsilon|^2}$, is largely uncorrelated with the resolution function and mistag parameters, as shown in figure 39.

A strong correlation is however observed between the w_0^α and w_{slope}^α for the Kaon category, as expected from the linear parameterization of the tagging/vertexing correlations, equation (84). Finally, several of the resolution function parameters are internally correlated. In the *GExp* model, the correlation among the effective lifetime, τ_r^α, and the fraction of the exponential part, f_{Exp}^α, is at the -80% level, for all tagging categories. The averaged correlation of these parameters with the scale S of the central Gaussian is small, below 10%. In the *GG* model the correlation pattern is much more complex. The most correlated resolution parameter with any other is S_{core} with the Gaussian tail parameters, f_{tail} (-65%), δ_{tail} (-42%) and S_{tail} (28%), as well as f_{tail} with δ_{tail} and δ_{tail}, 65% and -44% respectively. The cross correlations among all δ_{core}^α and with f_{tail} and S_{tail} are at the $\pm 10\%$ level. Finally, the correlation between S_{core} and δ_{core}^α is below 10% averaged over tagging categories.

For large values of $\Delta\Gamma/\Gamma$, the correlation pattern is different. If we take as example $\Delta\Gamma/\Gamma$=0.2, the correlation among the physics parameters is shown in figure 40. Correlations which become now significant and were negligible or small in the reference configuration are: $\Delta m - \Delta\Gamma/\Gamma$ (+10%), $\Delta\Gamma/\Gamma - \frac{\mathrm{Im}\varepsilon}{1+|\varepsilon|^2}$ (−20%) and $\frac{1-|\varepsilon|^2}{1+|\varepsilon|^2}\frac{\mathrm{Re}\delta}{1+|\varepsilon|^2} - \frac{\mathrm{Im}\delta}{1+|\varepsilon|^2}$ (+60%). The correlation between $\Delta\Gamma/\Gamma$ and the fraction of outliers, $f_{outlier}$, becomes now also large, about -45%, while is was negligible for $\Delta\Gamma/\Gamma$=0. This effect is not surprising since the contribution of $\Delta\Gamma/\Gamma$ to the time distributions appears at relatively large Δt, just the region where the ouliers have their larger relative contribution. This however, does not introduce any noticeable bias in the determination of $\Delta\Gamma/\Gamma$ (as shown in section 4.1.3), provided that the PDF normalization is performed properly, as discussed in section 4.1.8.

The small correlations among the physics parameters in the reference configuration can easily be understood. The sensitivity to $\frac{1-|\varepsilon|^2}{1+|\varepsilon|^2}\frac{\mathrm{Re}\delta}{1+|\varepsilon|^2}$ and $\frac{\mathrm{Im}\varepsilon}{1+|\varepsilon|^2}$ is largely provided by the B_{CP} events (see table 18), for which the Δt dependence is even for the former and odd for the latter. The B_{flav} sample contributes marginally because for these events there is no explicit dependence on $\frac{\mathrm{Im}\varepsilon}{1+|\varepsilon|^2}$, and the dependence with $\frac{\mathrm{Re}\delta}{1+|\varepsilon|^2}$ is scaled by the $\sin(\Delta\Gamma\Delta t/2)$ term, which neglects for small $\Delta\Gamma$. On the contrary, $\frac{\mathrm{Re}\varepsilon}{1+|\varepsilon|^2}$ and $\frac{\mathrm{Im}\delta}{1+|\varepsilon|^2}$ (and Δm) are completely dominated by the large statistics B_{flav} sample, for which the Δt dependence is even for the former and odd for the latter. As it was already discussed in section 4.1.3, the $\Delta\Gamma/\Gamma$ determination is dominated by the CP sample in this configuration. The physics parameters correlation pattern changes for large $\Delta\Gamma/\Gamma$ because in this regime since the flavor sample dominates its determination, and as a consequence: i) the correlation with Δm increases (same sample and both parameters have even Δt dependence), ii) the dependence with $\frac{\mathrm{Re}\delta}{1+|\varepsilon|^2}$ in the flavor sample is now significant, and it is odd in Δt (as for $\frac{\mathrm{Im}\delta}{1+|\varepsilon|^2}$), therefore inducing the large correlation among these two parameters.

4.1.6   Correlations with τ_B^0

The correlation of the average B^0 lifetime (assumed as fixed in the nominal fit) with all the physics parameters has been evaluated by fitting also it. The check has been done for the reference configuration and $\Delta\Gamma/\Gamma$=0.2. The results are shown in figure 41. In the reference, the only significant correlation is with Δm (−30%). For the $\Delta\Gamma/\Gamma$=0.2 configuration, τ_B^0 becomes additionally correlated with two parameters:
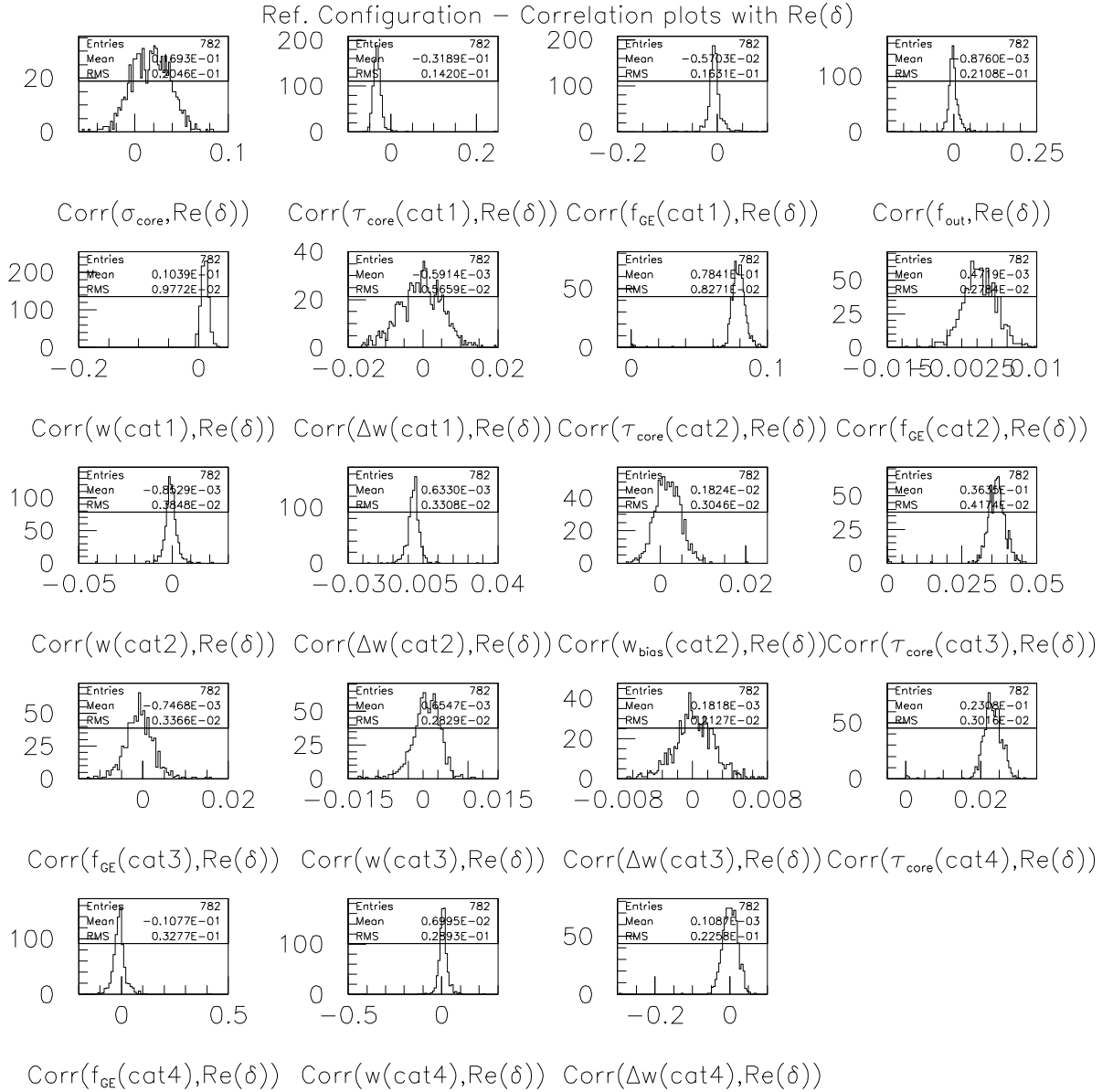
Figure 39: Correlation coefficients among $\frac{1-|\varepsilon|^2}{1+|\varepsilon|^2}\frac{\mathrm{Re}\delta}{1+|\varepsilon|^2}$ and the resolution function and mistag parameters, for the reference configuration (*GExp* model, ≈ 60 fb^{-1}).
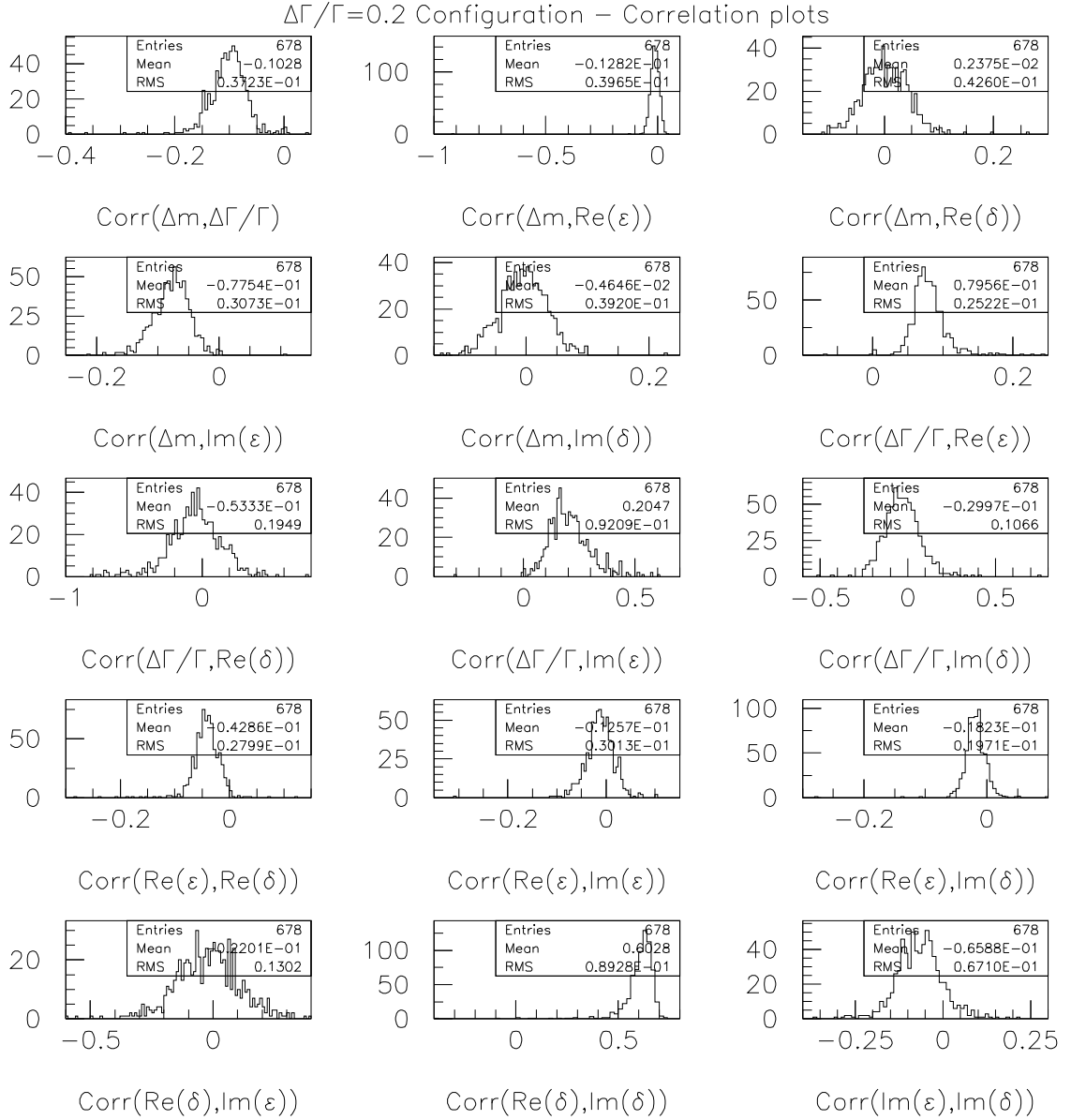
Figure 40: Correlation coefficients among all combinations of the physics parameters, for the $\Delta\Gamma/\Gamma = 0.2$ configuration (*GExp* model, ≈ 60 fb^{-1}). See disclaimer at the begining of section 4.1.5.

$\Delta\Gamma/\Gamma(-56\%)$ and $\frac{\text{Im}\varepsilon}{1+|\varepsilon|^2}$ (-19%).

4.1.7 Fit validation with backgrounds

The analysis has also been validated in toy Monte Carlo by including backgrounds (combinatorial and peaking) for the B_{flav} and $B_{CPK_S^0}$ samples in the generation and fitting procedure. Due to the very significant significant increase of CPU that the inclusion of background means for the fitting part, we performed this check rescaling yields to the equivalent of 30 fb^{-1}. The results for the reference configuration are summarized in table 21. The conclusions from this study do not differ from those we got with signal only fits.

	Reference configuration with backgrounds					
	$\frac{1-|\varepsilon|^2}{1+|\varepsilon|^2}\frac{\text{Re}\delta}{1+|\varepsilon|^2}$	$\frac{\text{Im}\delta}{1+|\varepsilon|^2}$	$\frac{\text{Im}\varepsilon}{1+|\varepsilon|^2}$	$\frac{\text{Re}\varepsilon}{1+|\varepsilon|^2}$	$\Delta\Gamma/\Gamma$	Δm
Mean residual	$(-4.2\pm4.7)\cdot10^{-3}$	$(-1.8\pm1.1)\cdot10^{-3}$	$(0.8\pm2.5)\cdot10^{-3}$	$(1.1\pm4.4)\cdot10^{-4}$	$(0.6\pm3.8)\cdot10^{-3}$	$(0.6\pm5.7)\cdot10^{-4}$
RMS residual	$(1.0\pm0.0)\cdot10^{-1}$	$(2.3\pm0.1)\cdot10^{-2}$	$(5.6\pm0.2)\cdot10^{-2}$	$(9.5\pm0.4)\cdot10^{-3}$	$(8.3\pm0.3)\cdot10^{-2}$	$(1.2\pm0.1)\cdot10^{-2}$
Av. error (Gauss)	$9.6\cdot10^{-2}$	$2.4\cdot10^{-2}$	$5.6\cdot10^{-2}$	$9.5\cdot10^{-3}$	$7.3\cdot10^{-2}$	$1.2\cdot10^{-2}$
Gauss. error cov.	$(62.7\pm4.6)\%$	$(69.7\pm5.0)\%$	$(65.7\pm4.8)\%$	$(67.8\pm4.9)\%$	$(57.9\pm4.4)\%$	$(67.8\pm4.9)\%$

Table 21: Summary of results for the reference configuration (table 13) from signal + background fits (*GG* resolution model, ≈ 30 fb^{-1}).

4.1.8 Asymptotic vs finite PDF normalization

In the nomalization of the PDF, equations (96), (97) and (93), asymptotic limits are used by default through these studies. This normalization has the advantage of reducing dramatically CPU usage, but it has the drawback that it does not take into account the event selection Δt cut, $|\Delta t| < 20$ ps. The effect of this simplification has been investigated in the extreme case of the $\Delta\Gamma/\Gamma=0.2$ configuration asuming a single (unbiassed) Gaussian together with an outlier component for the resolution ($|\Delta t| < 20$ cut applied and asymptotic normalization is used). The results are summarized in table 22. A bias at the 4σ level is observed on $\Delta\Gamma/\Gamma$, and about 2.5σ level on $\frac{\text{Re}\varepsilon}{1+|\varepsilon|^2}$, while all the other parameters are within one sigma. The bias in the estimation of $\Delta\Gamma/\Gamma$ can be understood due to the overestimation of the PDF normalization which originates from two different sources. First, the resolution function has an outlier component with width $\sigma = 8$ ps, so a cut on Δt at ±20 ps excludes a significant fraction of it, while it is not accounted for in the normalization. Second, large values of $|\Delta\Gamma/\Gamma|$ contribute at large $|\Delta t|$, so again, the Δt cut removes a non-negligible fraction of the area. The second reason explains that the size of the $\Delta\Gamma/\Gamma$ bias increases with $|\Delta\Gamma/\Gamma|$, and for very small values it is negligible. The apparent bias on $\frac{\text{Re}\varepsilon}{1+|\varepsilon|^2}$ is a consequence of the the $\Delta\Gamma/\Gamma$ bias.

Given that the value of $\Delta\Gamma/\Gamma$ is expected to be very small, and in order to reduce the CPU usage, the asymptotic normalization is used by default, and differences between it and the finite normalization can be evaluated as a contribution to the systematic uncertainty. However, to remove any possible bias contribution to $\Delta\Gamma/\Gamma$ in all our toy Monte Carlo studies, in particular for configurations with $\Delta\Gamma/\Gamma \neq 0$, the Δt cut was removed. All the tables shown so far have been produced using this asumption. In particular, results shown in figure 29 and table 17, corresponding to the same $\Delta\Gamma/\Gamma=0.2$ configuration used above but there using the *GExp* model, shows no bias neither on $\Delta\Gamma/\Gamma$ nor $\frac{\text{Re}\varepsilon}{1+|\varepsilon|^2}$. In the full Monte Carlo checks of section 4.2 the Δt cut was however applied.
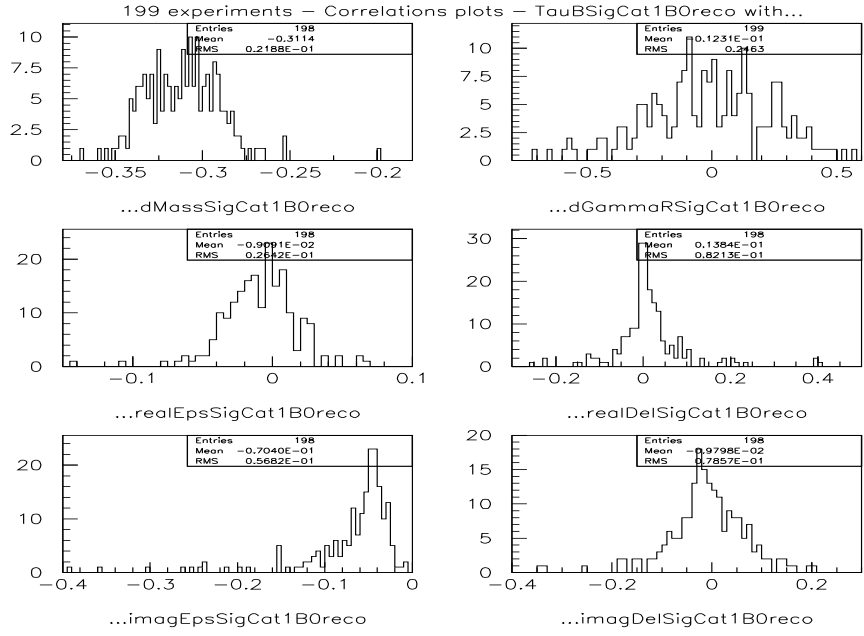
(a)
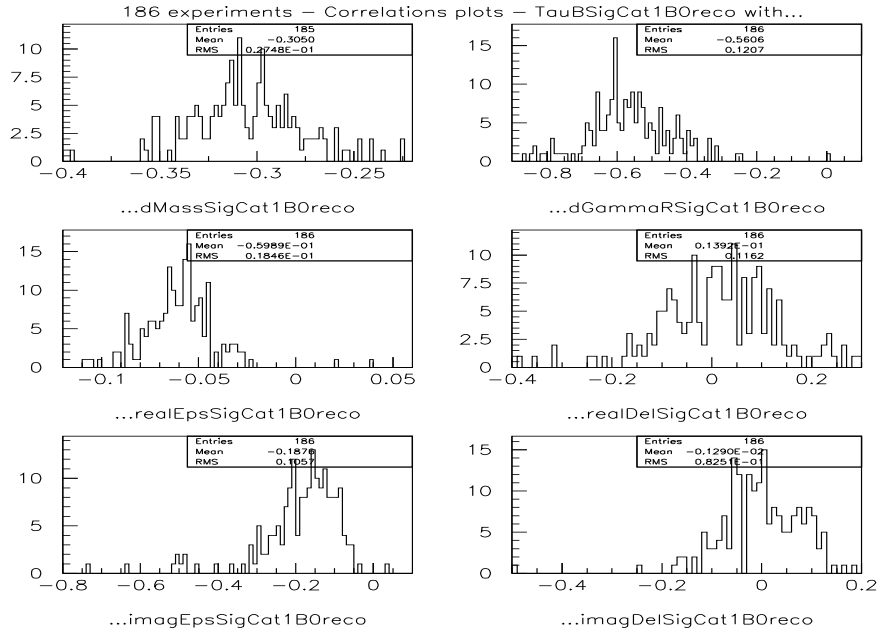
(b)

Figure 41: Correlation coefficients among τ_B^0 and all the 6 physics parameters for (a) the reference configuration and (b) $\Delta\Gamma/\Gamma$=0.2 (*GExp* model, ≈ 60 fb^{-1}).

	ΔΓ/Γ=0.2 configuration, Δt = ±20 ps cut, asymptotic normalization				
	$\frac{1-\|\varepsilon\|^2}{1+\|\varepsilon\|^2}\frac{\mathrm{Re}\delta}{1+\|\varepsilon\|^2}$	$\frac{\mathrm{Im}\varepsilon}{1+\|\varepsilon\|^2}$	$\frac{\mathrm{Re}\varepsilon}{1+\|\varepsilon\|^2}$	ΔΓ/Γ	Δm
Mean residual	$(0.3\pm0.7)\cdot10^{-3}$	$(-0.8\pm0.8)\cdot10^{-3}$	$(-3.7\pm1.5)\cdot10^{-4}$	$(3.5\pm0.8)\cdot10^{-3}$	$(-0.3\pm2.0)\cdot10^{-4}$
RMS residual	$(3.15\pm0.06)\cdot10^{-2}$	$(3.85\pm0.06)\cdot10^{-2}$	$(6.88\pm0.12)\cdot10^{-3}$	$(3.88\pm0.06)\cdot10^{-2}$	$(9.12\pm0.14)\cdot10^{-3}$
Average error (Gauss)	$3.2\cdot10^{-2}$	$3.7\cdot10^{-2}$	$6.9\cdot10^{-3}$	$4.3\cdot10^{-2}$	$9.1\cdot10^{-3}$

Table 22: Summary of results for the reference configuration with $\Delta\Gamma/\Gamma$=0.2 (≈ 60 fb^{-1}) for (top) $\Delta t = \pm20$ ps cut and asymptotic normalization, (middle) $\Delta t = \pm20$ ps cut and finite normalization and (bottom) no Δt cut with asymptotic normalization. The resolution model used for this study was a single unbiassed Gaussian.

4.1.9 Validation with the $(\mid q/p\mid,\lambda,z)$ formalism

The $(\mid q/p\mid,\lambda,z)$ formalism outlined in section 2.7 have been also used to check the feasibility of the analysis. From a comparison of tables 1 and 2 with tables 5 and 6, the correspondence between the physics parameters with the (ε,δ) formalism becomes apparent. It is then clear that all the studies performed so far apply here, and there is no need to redo all of them. We checked here explicitly the feasibility of the combined fit for the reference (table 23) and $\Delta\Gamma/\Gamma$=0.2 configurations, for an statistics of $\approx 60\,\mathrm{fb}^{-1}$. The average and RMS of the residual distributions as well as the average Gaussian error and its coverage are summarized in tables 24 and 25. The same remarks to those of the (ε,δ) formalism apply here. The distributions of the correlation coefficients among all possible combinations of the 6 physics parameters is shown in figure 42. Again, all cross correlations among the physics parameters are small, at the few per cent level, and they are the same as for (ε,δ).

Parameter	Generated value
$\frac{\mathrm{Re}\lambda}{\|\lambda\|}\mathrm{Re}z$	0.00
$\mathrm{Im}z$	0.00
$\frac{\mathrm{Im}\lambda}{\|\lambda\|}$	0.70
$\mid q/p\mid$	1.00
$\Delta\Gamma/\Gamma$	0.00
$\Delta m(\mathrm{ps}^{-1})$	0.472

Table 23: Generated physics parameter values for the reference configuration, $(\mid q/p\mid,\lambda,z)$ formalism.

	Reference configuration, GG model					
	$\frac{\mathrm{Re}\lambda}{\|\lambda\|}\mathrm{Re}z$	$\mathrm{Im}z$	$\frac{\mathrm{Im}\lambda}{\|\lambda\|}$	$\mid q/p\mid$	$\Delta\Gamma/\Gamma$	Δm
Mean residual	$(2.0\pm3.0)\cdot10^{-3}$	$(0.6\pm6.2)\cdot10^{-4}$	$(5.2\pm3.1)\cdot10^{-3}$	$(5.3\pm5.7)\cdot10^{-4}$	$(-0.8\pm2.6)\cdot10^{-3}$	$(0.3\pm3.8)\cdot10^{-4}$
RMS residual	$(7.3\pm0.2)\cdot10^{-2}$	$(1.5\pm0.1)\cdot10^{-2}$	$(7.5\pm0.2)\cdot10^{-2}$	$(1.4\pm0.1)\cdot10^{-2}$	$(6.2\pm0.2)\cdot10^{-2}$	$(9.1\pm0.3)\cdot10^{-3}$
Av. error (Gauss)	$7.3\cdot10^{-2}$	$1.6\cdot10^{-2}$	$7.9\cdot10^{-2}$	$1.4\cdot10^{-2}$	$5.8\cdot10^{-2}$	$9.5\cdot10^{-3}$
Gauss. error cov.	$(68.0\pm4.4)\%$	$(70.1\pm4.5)\%$	$(69.3\pm4.5)\%$	$(70.8\pm4.6)\%$	$(62.5\pm4.2)\%$	$(69.4\pm4.5)\%$

Table 24: Summary of results for the reference configuration with the $(\mid q/p\mid,\lambda,z)$ formalism, for ≈ 60 fb^{-1} (GG model).

4.1.10 Fitting for the $B^0\bar{B}^0$ reconstruction and tagging differences

The nominal fitting procedure adopted for all the studies in this note, as explained in section 3.5, assumes that the $B^0\bar{B}^0$ differences in reconstruction and tagging efficiencies, ν and μ^α, are fixed to the values extracted
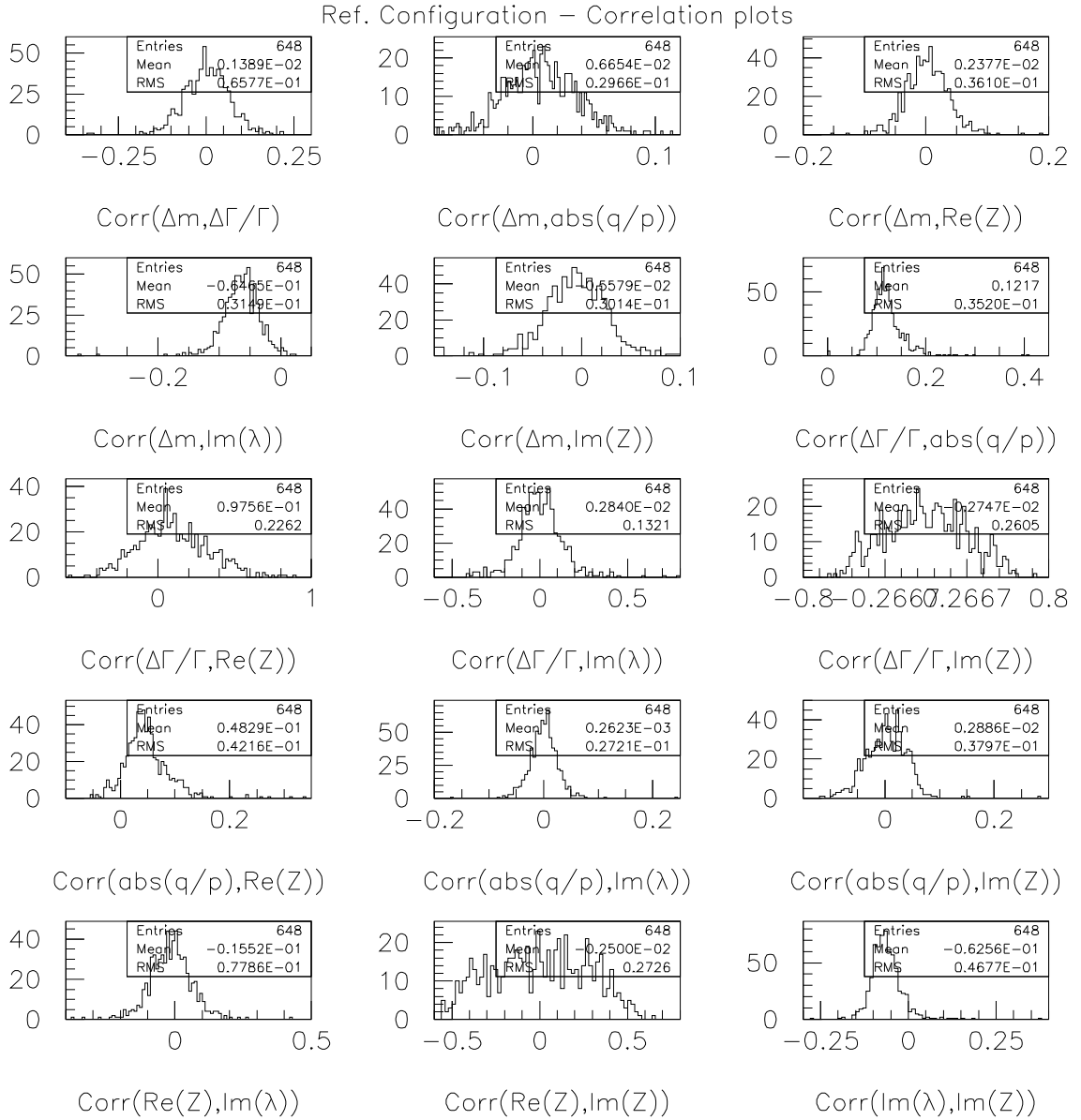
Figure 42: Correlation coefficients among all combinations of the physics parameters, for the reference configuration and $(\mid q/p \mid, \lambda, z)$ formalism (table 23).

	$\frac{\mathrm{Re}\lambda}{|\lambda|}\mathrm{Re}z$	$\mathrm{Im}z$	$\frac{\mathrm{Im}\lambda}{|\lambda|}$	$|q/p|$	$\Delta\Gamma/\Gamma$	Δm
	$\Delta\Gamma/\Gamma$=0.2 configuration, *GG* model					
Mean residual	$(0.0\pm2.2)\cdot10^{-3}$	$(6.4\pm8.7)\cdot10^{-4}$	$(2.1\pm3.4)\cdot10^{-3}$	$(-3.8\pm5.9)\cdot10^{-4}$	$(-1.7\pm2.0)\cdot10^{-3}$	$(4.0\pm4.1)\cdot10^{-4}$
RMS residual	$(5.2\pm0.2)\cdot10^{-2}$	$(2.0\pm0.1)\cdot10^{-2}$	$(8.0\pm0.3)\cdot10^{-2}$	$(1.4\pm0.1)\cdot10^{-2}$	$(4.6\pm0.2)\cdot10^{-2}$	$(9.7\pm0.3)\cdot10^{-3}$
Av. error (Gauss)	$5.4\cdot10^{-2}$	$1.9\cdot10^{-2}$	$7.8\cdot10^{-2}$	$1.4\cdot10^{-2}$	$4.6\cdot10^{-2}$	$9.9\cdot10^{-3}$
Gauss. error cov.	$(70.1\pm4.7)\%$	$(65.1\pm4.4)\%$	$(66.6\pm4.5)\%$	$(69.7\pm4.6)\%$	$(66.2\pm4.5)\%$	$(70.1\pm4.7)\%$

Table 25: Summary of results for the $\Delta\Gamma/\Gamma$=0.2 configuration with the $(|q/p|,\lambda,z)$ formalism, for ≈ 60 fb^{-1} (*GG* model).

from the B_{flav} sample (see section 3.1 and appendix B for details). This approach requires to make an initial guess about the actual values of Δm, $\Delta\Gamma$ and $\frac{\mathrm{Re}\varepsilon}{1+|\varepsilon|^2}$. As these are parameters to be extracted from the time dependent analysis, there appears a potential circularity problem. This effect is critical for the extraction of $\frac{\mathrm{Re}\varepsilon}{1+|\varepsilon|^2}$, since this parameter is fully anti-correlated with the detector asymmetries (evaluated to be -96%).

To overcome this problem, the following approach has been investigated. The parameters ν and μ^α can be included as free parameters in the time dependent fit, applying the additional constraint provided by the time integrated relationship between them and Δm, $\Delta\Gamma$ and $\frac{\mathrm{Re}\varepsilon}{1+|\varepsilon|^2}$, -equations (115) and (116) of the appendix B-. To properly account for the Poisson statistics from the counting of $B^0,\bar{B}^0$ tagged and untagged events, we can construct an Extended Likelihood,

$$\ln\mathcal{L}_{Extended} \;\;=\;\; \ln\mathcal{L}+\sum_\alpha\Delta\ln\mathcal{L}_\alpha \tag{100}$$

where $\ln\mathcal{L}$ was defined in equation (99) and

$$
\begin{aligned}
\Delta\ln\mathcal{L}_\alpha \;\;=\;\; & -\ln N_{B_r^0,tag\;\alpha}! + N_{B_r^0,tag\;\alpha}\ln\eta_{B_r^0,tag\;\alpha} - \eta_{B_r^0,tag\;\alpha}\\
& -\ln N_{\bar{B}_r^0,tag\;\alpha}! + N_{\bar{B}_r^0,tag\;\alpha}\ln\eta_{\bar{B}_r^0,tag\;\alpha} - \eta_{\bar{B}_r^0,tag\;\alpha}\\
& -\ln N_{B_r^0,notag\;\alpha}! + N_{B_r^0,notag\;\alpha}\ln\eta_{B_r^0,notag\;\alpha} - \eta_{B_r^0,notag\;\alpha}\\
& -\ln N_{\bar{B}_r^0,notag\;\alpha}! + N_{\bar{B}_r^0,notag\;\alpha}\ln\eta_{\bar{B}_r^0,notag\;\alpha} - \eta_{\bar{B}_r^0,notag\;\alpha}
\end{aligned}
\tag{101}
$$

$N_{B_r^0(\bar{B}_r^0),tag\;\alpha}$ is the number of events reconstructed as $B^0(\bar{B}^0)$ and tagged in tagging category α, and $N_{B_r^0(\bar{B}_r^0),notag\;\alpha}$ is the number of events reconstructed as $B^0(\bar{B}^0)$ excluding those tagged in tagging category α. $\eta_{B_r^0(\bar{B}_r^0),tag\;\alpha/notag\;\alpha}$ denote the corresponding expected number of events. This method can be applied using only signal region events. For background components, where we assume Δm=0, $\Delta\Gamma/\Gamma$=0 and $\frac{\mathrm{Re}\varepsilon}{1+|\varepsilon|^2}$=0, the parameters ν and μ^α can be fixed to the estimates using side band events.

Two toy Monte Carlo studies, using the *GG* resolution model, were dedicated to check this approach. The first one was the usual set of more than 600 experiments with an equivalent luminosity of ≈ 60 fb^{-1}and the reference configuration for the physics parameters and the default $B^0\bar{B}^0$ reco and tagging asymmetries, as given in section 3.1. Table 26 shows the summary of the results of this test, which should be compared to the results coming from the standard likelihood method, summarized in table 14. The only parameter affected is $\frac{\mathrm{Re}\varepsilon}{1+|\varepsilon|^2}$, whose error increased by about 30%, as expected due to the correlation between $\frac{\mathrm{Re}\varepsilon}{1+|\varepsilon|^2}$ and the detector asymmetries. At the end of the fitting procedure, the values of ν and μ^α are consistent with those generated. The second check was devoted to verify that this procedure is able to disentangle

the physics ($\frac{\text{Re}\varepsilon}{1+|\varepsilon|^2} \neq 0$) and detector asymmetries. Here, we generated 200 toy Monte Carlo experiments with a large detector asymmetry ($\nu = 10\%$ and μ^α is 5%, 10%, 5% and 5% for the `lepton`, `kaon`, `NT1`, `NT2` tagging categories, respectively), as well as a large value of $\frac{\text{Re}\varepsilon}{1+|\varepsilon|^2}$, 0.05. The samples were then fitted using two different sets of starting values for ν, μ^α, $\frac{\text{Re}\varepsilon}{1+|\varepsilon|^2}$ and $\Delta\Gamma/\Gamma$: i) the generated values, ii) all zero and $\Delta\Gamma/\Gamma$=0.1. Figure 43 shows the sample-by-sample comparison of the results of the fit for $\Delta\Gamma/\Gamma$ and $\frac{\text{Re}\varepsilon}{1+|\varepsilon|^2}$ (the correlation and the differences). From this check we conclude that with this procedure the fit is stable and we are able to disentangle the physics and detector asymmetries which would result in an asymmetry in the number of $B^0\overline{B}^0$ events, at the cost of a reasonable increase in the statistical error on $\frac{\text{Re}\varepsilon}{1+|\varepsilon|^2}$.

	Reference configuration with extendend likelihood					
	$\frac{1-|\varepsilon|^2}{1+|\varepsilon|^2}\frac{\text{Re}\delta}{1+|\varepsilon|^2}$	$\frac{\text{Im}\delta}{1+|\varepsilon|^2}$	$\frac{\text{Im}\varepsilon}{1+|\varepsilon|^2}$	$\frac{\text{Re}\varepsilon}{1+|\varepsilon|^2}$	$\Delta\Gamma/\Gamma$	Δm
Mean residual	$(0.2\pm2.9)\cdot10^{-3}$	$(-1.0\pm0.6)\cdot10^{-3}$	$(-0.2\pm1.4)\cdot10^{-3}$	$(-1.1\pm3.4)\cdot10^{-4}$	$(0.2\pm2.3)\cdot10^{-3}$	$(1.2\pm3.5)\cdot10^{-4}$
RMS residual	$(8.0\pm0.2)\cdot10^{-2}$	$(1.7\pm0.1)\cdot10^{-2}$	$(3.8\pm0.1)\cdot10^{-2}$	$(9.5\pm0.3)\cdot10^{-3}$	$(6.4\pm0.2)\cdot10^{-2}$	$(9.7\pm0.3)\cdot10^{-3}$
Av. error (Gauss)	$7.1\cdot10^{-2}$	$1.7\cdot10^{-2}$	$4.0\cdot10^{-2}$	$9.4\cdot10^{-3}$	$5.6\cdot10^{-2}$	$9.5\cdot10^{-3}$
Gauss. error cov.	$(57.4\pm3.4)\%$	$(68.2\pm3.8)\%$	$(68.6\pm3.9)\%$	$(66.8\pm3.8)\%$	$(59.7\pm3.5)\%$	$(66.4\pm3.8)\%$

Table 26: Summary of results for the reference configuration (table 13) from signal fits (*GG* resolution model, ≈ 60 fb^{-1}) using the extended likelihood approach.

4.2 Standard full Monte Carlo

High statistics full Monte Carlo fits (signal+background), with reference values (table 13) were also performed to validate the fitting procedure, for both the *GG* and *GExp* resolution models. We used the set `anal10h` of ASCII files (B^0 and B^+ cocktails for the B_{flav} sample). The total statistics of reconstructed events (after vertexing cuts: tag vertex convergence, $|\Delta t| < 20$ ps, $\sigma(\Delta t) < 2.4$ ps) for each sample is given in table 27. It should be noted that the relative statistics among the samples as we have in the data was not kept here, since our goal in this case was to validate the fit with maximum available statistics. Roughly, the relative weight of the B_{CP} sample with respect to the B_{flav} one in this check is about 2.5 times larger than what we have in our current data.

Sample	Statistics (after vertexing cuts)
B_{flav}	160900
$B_{CPK_S^0}$	30600
$B_{CPK_L^0}$	8700
B^+	112800

Table 27: Full Monte Carlo statistics (`anal10h` ASCII files) for each sample used in the fit procedure validation. The generated values correspond to our reference configuration given in table 13.

The results of different fit configurations are given in tables 28 and 29 for the signal parameters, *GG* and *GExp* resolution models respectively. The corresponding tables for the parameters describing the background are 30 and 31. Table 32 gives the physics parameters from a similar fit (*GG* model) using the $(|q/p|, \lambda, z)$ formalism. The peaking background in these fits was assumed to be 0. Asymmetric errors, extremely CPU consuming, were not switched on in these fits. Figures 44 and 45 show the projections on the Δt axis of the nominal CPT/CP/T fits for the B_{flav}, $B_{CPK_S^0}$ and $B_{CPK_L^0}$ samples, for the *GExp* resolution model. The corresponding normalized residuals (defined as the difference between data and the fit projection divided by the error) are shown in figures 46 and 47.

74

Parameter	B_{flav} lifetime	B^+ mixing	B_{flav} mixing	$B_{flav}+B_{CPK_S^0}$	$B_{flav}+B_{CP}$	$\sin 2\beta$
$\frac{1-|\varepsilon|^2}{1+|\varepsilon|^2}\frac{\mathrm{Re}\delta}{1+|\varepsilon|^2}$	–	–	–	-0.003 ± 0.019	0.004 ± 0.016	–
$\frac{\mathrm{Im}\delta}{1+|\varepsilon|^2}$	–	–	0.004 ± 0.006	0.002 ± 0.005	0.002 ± 0.005	–
$\frac{\mathrm{Im}\varepsilon}{1+|\varepsilon|^2}$	–	–	–	0.350 ± 0.010	0.353 ± 0.009	0.354 ± 0.009
$\frac{\mathrm{Re}\varepsilon}{1+|\varepsilon|^2}$	–	–	-0.0009 ± 0.0027	-0.0008 ± 0.0026	-0.0005 ± 0.0025	–
$\Delta\Gamma/\Gamma$	–	–	0.000 ± 0.043	-0.020 ± 0.015	-0.008 ± 0.013	–
Δm	–	0	0.4778 ± 0.0034	0.4767 ± 0.0033	0.4774 ± 0.0033	0.4774 ± 0.0033
τ	1.528 ± 0.009	1.643 ± 0.011	1.548	1.548	1.548	1.548
S_{core}	1.163 ± 0.023	1.09 ± 0.04	1.164 ± 0.020	1.155 ± 0.019	1.155 ± 0.018	1.154 ± 0.018
δ_{core}^{lepton}	-0.078 ± 0.03	-0.10 ± 0.04	-0.064 ± 0.024	-0.071 ± 0.022	-0.070 ± 0.022	-0.071 ± 0.022
δ_{core}^{kaon}	-0.244 ± 0.016	-0.238 ± 0.023	-0.249 ± 0.015	-0.243 ± 0.014	-0.244 ± 0.014	-0.245 ± 0.014
δ_{core}^{NT1}	-0.153 ± 0.03	-0.137 ± 0.04	-0.14 ± 0.03	-0.13 ± 0.03	-0.13 ± 0.03	-0.13 ± 0.03
δ_{core}^{NT2}	-0.200 ± 0.022	-0.22 ± 0.03	-0.196 ± 0.022	-0.200 ± 0.020	-0.205 ± 0.020	-0.206 ± 0.019
f_{tail}	0.058 ± 0.010	0.07 ± 0.03	0.047 ± 0.008	0.047 ± 0.008	0.047 ± 0.007	0.047 ± 0.007
S_{tail}	4.0 ± 0.3	3.4 ± 0.5	3.83 ± 0.24	3.78 ± 0.22	3.79 ± 0.21	3.78 ± 0.21
δ_{tail}	-1.6 ± 0.3	-0.8 ± 0.3	-1.8 ± 0.3	-1.9 ± 0.3	-1.9 ± 0.3	-1.9 ± 0.3
$f_{outlier}$	0.0024 ± 0.0007	0.0001 ± 0.0006	0.0021 ± 0.0006	0.0022 ± 0.0005	0.0023 ± 0.0005	0.0023 ± 0.0005
w_0^{lepton}	–	0.0370 ± 0.0016	0.070 ± 0.003	0.070 ± 0.003	0.069 ± 0.003	0.069 ± 0.003
w_0^{kaon}	–	0.1087 ± 0.0016	0.058 ± 0.006	0.059 ± 0.006	0.060 ± 0.006	0.060 ± 0.006
w_0^{NT1}	–	0.165 ± 0.004	0.185 ± 0.005	0.185 ± 0.005	0.185 ± 0.005	0.185 ± 0.005
w_0^{NT2}	–	0.351 ± 0.004	0.348 ± 0.004	0.349 ± 0.004	0.349 ± 0.004	0.349 ± 0.004
w_{slope}^{lepton}	–	0	0	0	0	0
w_{slope}^{kaon}	–	0	0.139 ± 0.009	0.138 ± 0.009	0.138 ± 0.009	0.138 ± 0.009
w_{slope}^{NT1}	–	0	0	0	0	0
w_{slope}^{NT2}	–	0	0	0	0	0
Δw^{lepton}	–	-0.003 ± 0.003	-0.007 ± 0.005	-0.005 ± 0.005	-0.006 ± 0.005	-0.006 ± 0.005
Δw^{kaon}	–	-0.009 ± 0.003	-0.016 ± 0.004	-0.013 ± 0.004	-0.014 ± 0.004	-0.014 ± 0.003
Δw^{NT1}	–	0.021 ± 0.008	0.019 ± 0.008	0.019 ± 0.007	0.023 ± 0.007	0.023 ± 0.007
Δw^{NT2}	–	0.028 ± 0.008	-0.031 ± 0.007	-0.033 ± 0.006	-0.030 ± 0.006	-0.030 ± 0.006

Table 28: Full Monte Carlo validation signal parameter results (*GG* resolution model).

Parameter	B_{flav} lifetime	B^+ mixing	B_{flav} mixing	$B_{flav}+B_{CPK_S^0}$	$B_{flav}+B_{CP}$	$\sin 2\beta$
$\frac{1-|\varepsilon|^2}{1+|\varepsilon|^2}\frac{\text{Re}\delta}{1+|\varepsilon|^2}$	−	−	−	-0.006 ± 0.019	0.0017 ± 0.016	−
$\frac{\text{Im}\delta}{1+|\varepsilon|^2}$	−	−	0.003 ± 0.006	0.002 ± 0.005	0.001 ± 0.005	−
$\frac{\text{Im}\varepsilon}{1+|\varepsilon|^2}$	−	−	−	0.350 ± 0.010	0.353 ± 0.009	0.354 ± 0.009
$\frac{\text{Re}\varepsilon}{1+|\varepsilon|^2}$	−	−	-0.0009 ± 0.0027	-0.0011 ± 0.0026	-0.0007 ± 0.0026	−
$\Delta\Gamma/\Gamma$	−	−	-0.00 ± 0.10	-0.019 ± 0.016	-0.007 ± 0.013	−
Δm	−	0	0.4751 ± 0.0034	0.4744 ± 0.0033	0.4750 ± 0.0032	0.4750 ± 0.0032
τ	1.546 ± 0.009	1.662 ± 0.010	1.548	1.548	1.548	1.548
S	1.092 ± 0.021	1.06 ± 0.03	1.099 ± 0.017	1.089 ± 0.015	1.087 ± 0.015	1.087 ± 0.015
τ_r^{lepton}	2.1 ± 0.4	1.4 ± 0.5	2.1 ± 0.4	2.1 ± 0.3	2.2 ± 0.3	2.2 ± 0.3
τ_r^{kaon}	1.26 ± 0.012	0.97 ± 0.14	1.28 ± 0.10	1.33 ± 0.09	1.32 ± 0.09	1.32 ± 0.09
τ_r^{NT1}	1.2 ± 0.4	1.9 ± 0.6	1.6 ± 0.3	1.8 ± 0.3	1.8 ± 0.3	1.8 ± 0.3
τ_r^{NT2}	1.70 ± 0.15	1.01 ± 0.21	1.69 ± 0.15	1.65 ± 0.14	1.67 ± 0.14	1.67 ± 0.13
f_{Exp}^{lepton}	0.083 ± 0.020	0.10 ± 0.05	0.071 ± 0.017	0.071 ± 0.016	0.071 ± 0.016	0.071 ± 0.016
f_{Exp}^{kaon}	0.25 ± 0.03	0.29 ± 0.04	0.249 ± 0.023	0.241 ± 0.019	0.243 ± 0.018	0.244 ± 0.018
f_{Exp}^{NT1}	0.18 ± 0.07	0.11 ± 0.04	0.12 ± 0.03	0.10 ± 0.03	0.106 ± 0.024	0.107 ± 0.024
f_{Exp}^{NT2}	0.177 ± 0.021	0.27 ± 0.06	0.172 ± 0.021	0.177 ± 0.020	0.179 ± 0.019	0.180 ± 0.019
$f_{outlier}$	0.0035 ± 0.0007	0.0038 ± 0.0006	0.0032 ± 0.0006	0.0032 ± 0.0005	0.0033 ± 0.0005	0.0033 ± 0.0005
w_0^{lepton}	−	0.0370 ± 0.0016	0.072 ± 0.003	0.071 ± 0.003	0.071 ± 0.003	0.071 ± 0.003
w_0^{kaon}	−	0.1087 ± 0.0016	0.059 ± 0.006	0.060 ± 0.006	0.060 ± 0.006	0.060 ± 0.006
w_0^{NT1}	−	0.165 ± 0.004	0.187 ± 0.005	0.186 ± 0.005	0.186 ± 0.005	0.186 ± 0.005
w_0^{NT2}	−	0.351 ± 0.004	0.349 ± 0.004	0.349 ± 0.004	0.349 ± 0.004	0.349 ± 0.004
w_{slope}^{lepton}	−	0	0	0	0	0
w_{slope}^{kaon}	−	0	0.139 ± 0.009	0.138 ± 0.009	0.138 ± 0.009	0.138 ± 0.009
w_{slope}^{NT1}	−	0	0	0	0	0
w_{slope}^{NT2}	−	0	0	0	0	0
Δw^{lepton}	−	-0.003 ± 0.003	-0.006 ± 0.005	-0.006 ± 0.005	-0.006 ± 0.005	-0.006 ± 0.005
Δw^{kaon}	−	-0.009 ± 0.003	-0.016 ± 0.004	-0.014 ± 0.004	-0.014 ± 0.004	-0.014 ± 0.003
Δw^{NT1}	−	0.021 ± 0.008	0.020 ± 0.008	0.019 ± 0.007	0.023 ± 0.007	0.023 ± 0.007
Δw^{NT2}	−	-0.028 ± 0.008	-0.031 ± 0.007	-0.034 ± 0.006	-0.030 ± 0.006	-0.030 ± 0.006

Table 29: Full Monte Carlo validation signal parameter results (*GExp* resolution model).

Parameter	B_{flav} lifetime	B^+ mixing	B_{flav} mixing	$B_{flav}+B_{CPK_S^0}$	$B_{flav}+B_{CP}$	$\sin 2\beta$
$f_{prompt,B_{flav}}^{lepton}$	0.0000 ± 0.0013	0.43 ± 0.12	0.31 ± 0.05	0.31 ± 0.05	0.31 ± 0.05	0.31 ± 0.05
$f_{prompt,B_{flav}}^{kaon}$	0.12 ± 0.04	0.25 ± 0.09	0.35 ± 0.03	0.36 ± 0.03	0.36 ± 0.03	0.36 ± 0.03
$f_{prompt,B_{flav}}^{NT1}$	0.09 ± 0.06	0.27 ± 0.13	0.33 ± 0.05	0.33 ± 0.05	0.33 ± 0.05	0.33 ± 0.05
$f_{prompt,B_{flav}}^{NT2}$	0.19 ± 0.05	0.32 ± 0.10	0.42 ± 0.05	0.43 ± 0.05	0.43 ± 0.05	0.43 ± 0.05
S_{back}	1.41 ± 0.07	1.76 ± 0.12	1.76 ± 0.06	1.78 ± 0.06	1.78 ± 0.06	1.78 ± 0.06
δ_{back}	-0.24 ± 0.03	-0.32 ± 0.07	-0.25 ± 0.03	-0.24 ± 0.03	-0.24 ± 0.03	-0.24 ± 0.03
$f_{back,outlier}$	0.013 ± 0.004	0.011 ± 0.009	0.006 ± 0.003	0.007 ± 0.003	0.007 ± 0.003	0.007 ± 0.003
$w_{0,prompt}^{lepton}$	$-$	0.11 ± 0.06	0.0000 ± 0.0002	0.0000 ± 0.0002	0.0000 ± 0.0002	0.0000 ± 0.0002
$w_{0,prompt}^{kaon}$	$-$	0.22 ± 0.08	0.0000 ± 0.0003	0.0000 ± 0.0003	0.0000 ± 0.0003	0.0000 ± 0.0003
$w_{0,prompt}^{NT1}$	$-$	0.30 ± 0.18	0.0000 ± 0.0003	0.0000 ± 0.0003	0.0000 ± 0.0003	0.0000 ± 0.0003
$w_{0,prompt}^{NT2}$	$-$	0.51 ± 0.12	0.25 ± 0.05	0.24 ± 0.05	0.24 ± 0.05	0.24 ± 0.05
$w_{0,non-prompt}^{lepton}$	$-$	0.07 ± 0.05	0.31 ± 0.03	0.31 ± 0.03	0.31 ± 0.03	0.31 ± 0.03
$w_{0,non-prompt}^{kaon}$	$-$	0.16 ± 0.03	0.458 ± 0.023	0.460 ± 0.022	0.460 ± 0.022	0.460 ± 0.022
$w_{0,non-prompt}^{NT1}$	$-$	0.19 ± 0.07	0.52 ± 0.04	0.52 ± 0.04	0.52 ± 0.04	0.52 ± 0.04
$w_{0,non-prompt}^{NT2}$	$-$	0.40 ± 0.06	0.51 ± 0.04	0.51 ± 0.04	0.51 ± 0.04	0.51 ± 0.04
$\tau_{non-prompt}$	1.41 ± 0.04	1.57 ± 0.14	1.61 ± 0.05	1.59 ± 0.05	1.59 ± 0.05	1.59 ± 0.05
$f_{prompt,B_{CPK_S^0}}$	$-$	$-$	$-$	0.37 ± 0.09	0.37 ± 0.09	0.37 ± 0.09

Table 30: Full Monte Carlo validation background parameter results (*GG* resolution model).

Parameter	B_{flav} lifetime	B^+ mixing	B_{flav} mixing	$B_{flav}+B_{CPK_S^0}$	$B_{flav}+B_{CP}$	$\sin 2\beta$
$f^{lepton}_{prompt,B_{flav}}$	0.0000 ± 0.0006	0.42 ± 0.13	0.30 ± 0.05	0.30 ± 0.05	0.30 ± 0.05	0.30 ± 0.05
$f^{kaon}_{prompt,B_{flav}}$	0.12 ± 0.04	0.22 ± 0.10	0.37 ± 0.03	0.37 ± 0.03	0.37 ± 0.03	0.37 ± 0.03
$f^{NT1}_{prompt,B_{flav}}$	0.07 ± 0.06	0.30 ± 0.15	0.33 ± 0.05	0.33 ± 0.05	0.34 ± 0.05	0.34 ± 0.05
$f^{NT2}_{prompt,B_{flav}}$	0.18 ± 0.05	0.30 ± 0.11	0.44 ± 0.05	0.44 ± 0.05	0.44 ± 0.05	0.44 ± 0.05
S_{back}	1.28 ± 0.08	1.71 ± 0.13	1.64 ± 0.06	1.66 ± 0.06	1.66 ± 0.06	1.66 ± 0.06
$\tau_{r,back}$	1.8 ± 0.3	3.6 ± 0.7	1.5 ± 0.3	1.5 ± 0.3	1.5 ± 0.3	1.5 ± 0.3
$f_{back,outlier}$	0.012 ± 0.003	0.0000 ± 0.0001	0.005 ± 0.003	0.006 ± 0.003	0.006 ± 0.003	0.006 ± 0.003
$w^{lepton}_{0,prompt}$	–	0.11 ± 0.07	0.0000 ± 0.0002	0.0000 ± 0.0002	0.0000 ± 0.0002	0.0000 ± 0.0002
$w^{kaon}_{0,prompt}$	–	0.23 ± 0.10	0.0000 ± 0.0003	0.0000 ± 0.0003	0.0000 ± 0.0003	0.0000 ± 0.0003
$w^{NT1}_{0,prompt}$	–	0.34 ± 0.20	0.0000 ± 0.0003	0.0000 ± 0.0003	0.0000 ± 0.0003	0.0000 ± 0.0003
$w^{NT2}_{0,prompt}$	–	0.54 ± 0.14	0.24 ± 0.05	0.24 ± 0.05	0.24 ± 0.05	0.24 ± 0.05
$w^{lepton}_{0,non-prompt}$	–	0.06 ± 0.05	0.31 ± 0.03	0.31 ± 0.03	0.31 ± 0.03	0.31 ± 0.03
$w^{kaon}_{0,non-prompt}$	–	0.16 ± 0.03	0.466 ± 0.024	0.469 ± 0.024	0.469 ± 0.024	0.469 ± 0.024
$w^{NT1}_{0,non-prompt}$	–	0.17 ± 0.08	0.52 ± 0.04	0.52 ± 0.04	0.52 ± 0.04	0.52 ± 0.04
$w^{NT2}_{0,non-prompt}$	–	0.39 ± 0.07	0.52 ± 0.04	0.53 ± 0.04	0.53 ± 0.04	0.53 ± 0.04
$\tau_{non-prompt}$	1.35 ± 0.04	1.40 ± 0.11	1.58 ± 0.05	1.57 ± 0.05	1.57 ± 0.05	1.57 ± 0.05
$f_{prompt,B_{CPK_S^0}}$	–	–	–	0.37 ± 0.09	0.37 ± 0.09	0.37 ± 0.09

Table 31: Full Monte Carlo validation background parameter results (*GExp* resolution model).
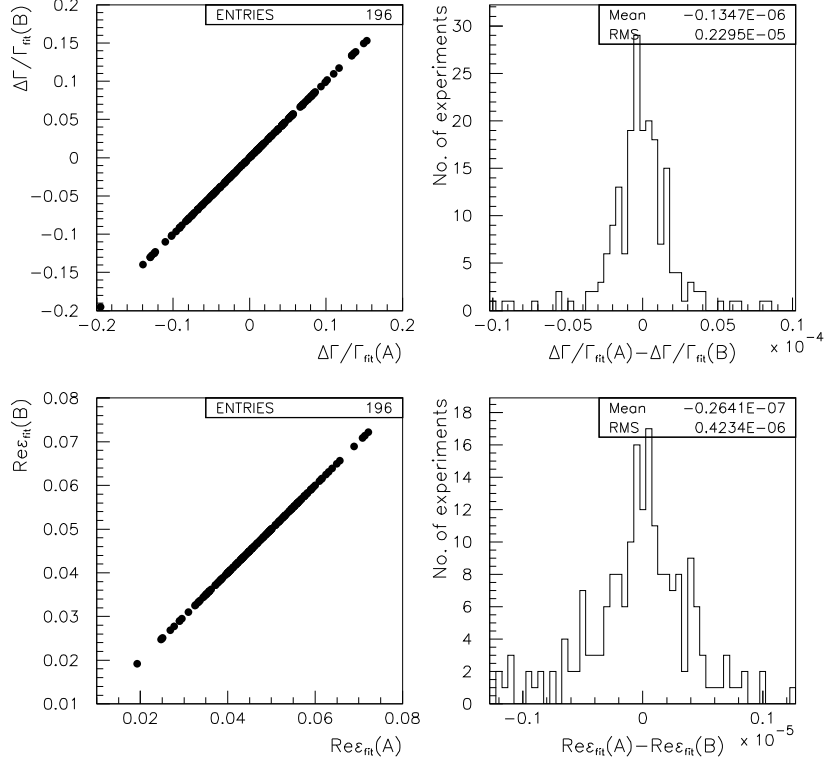
Figure 43: Comparison between the results obtained fitting the same 60 fb^{-1} samples generated with large $B^0\bar{B}^0$ differences in reconstruction and tagging efficiencies and large $\frac{\text{Re}\varepsilon}{1+|\varepsilon|^2}$, using different starting points for the corresponding parameters (see text for details). The upper left plot shows the correlation among the fitted values of $\Delta\Gamma/\Gamma$ from the two sets of starting points, while the upper right shows the distribution of the differnce between the two fitted parameters. The lower plots show the analogous for the $\frac{\text{Re}\varepsilon}{1+|\varepsilon|^2}$ parameter.

The cross correlation coefficients among all 6 fitted physics parameters in the (ε, δ) formalism for the *GG* and *GExp* models can be found in tables 33 and 34, respectively. For the $(|q/p|, \lambda, z)$ formalism the corresponding correlations are similar, and compatible with those predicted by toy Monte Carlo exercises (sections 4.1.5 and 4.1.9).

4.3 Non-standard full Monte Carlo

The general CPT/CP, CP/T models (including $\Delta\Gamma$ effects) in mixing and CP events have been implemented and validated in `EvtGen` [40]. They are briefly described below:

- `VSS_BMIXCPT`: **BrFr B1 B2 VSS_BMIX dm dgog absqop argqop absAf argAf absAbarf argAbarf absAfbar argAfbar absAbarfbar argAbarfbar rez imz** This model is an extension of the standard `VSS_BMIX` model [40], the difference being only the CPT effects in mixing as well as possible double Cabbido supressed contributions and CPT violation in the decay. The sign convention
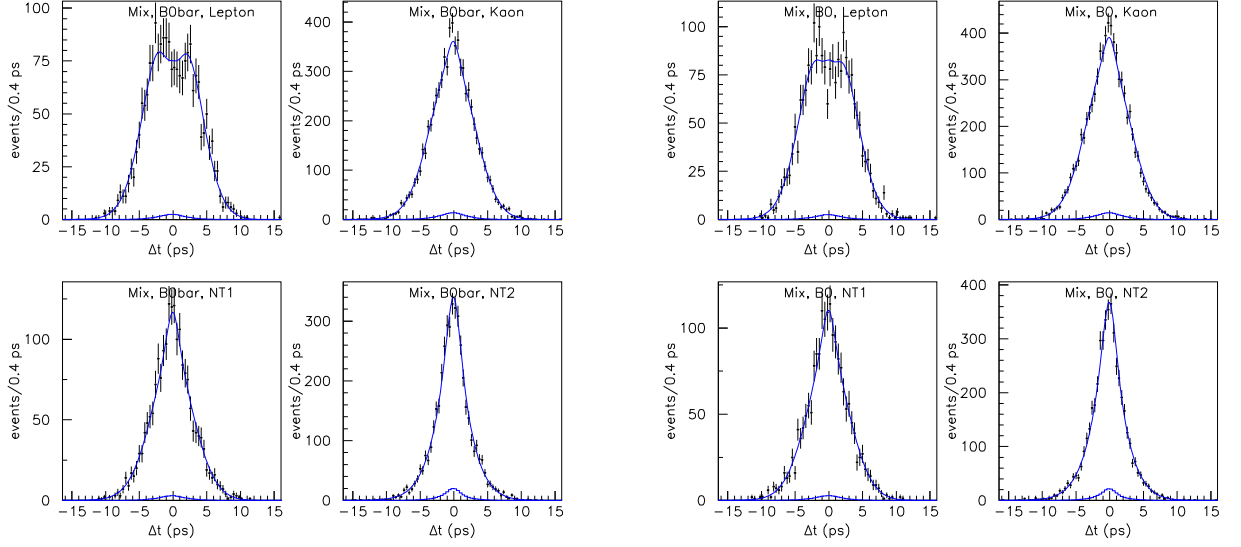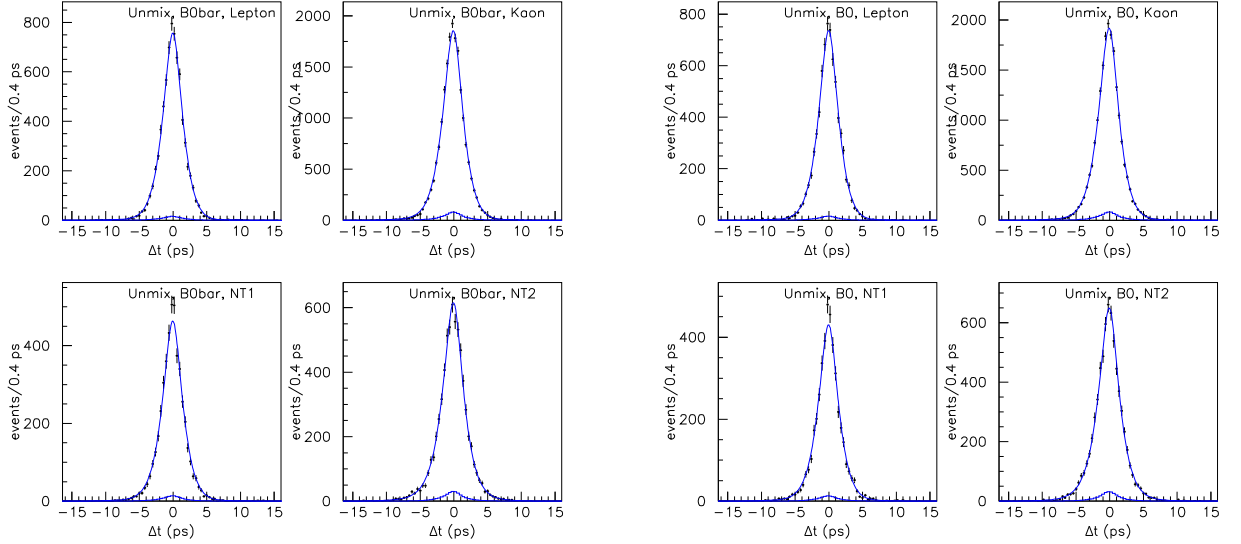
79
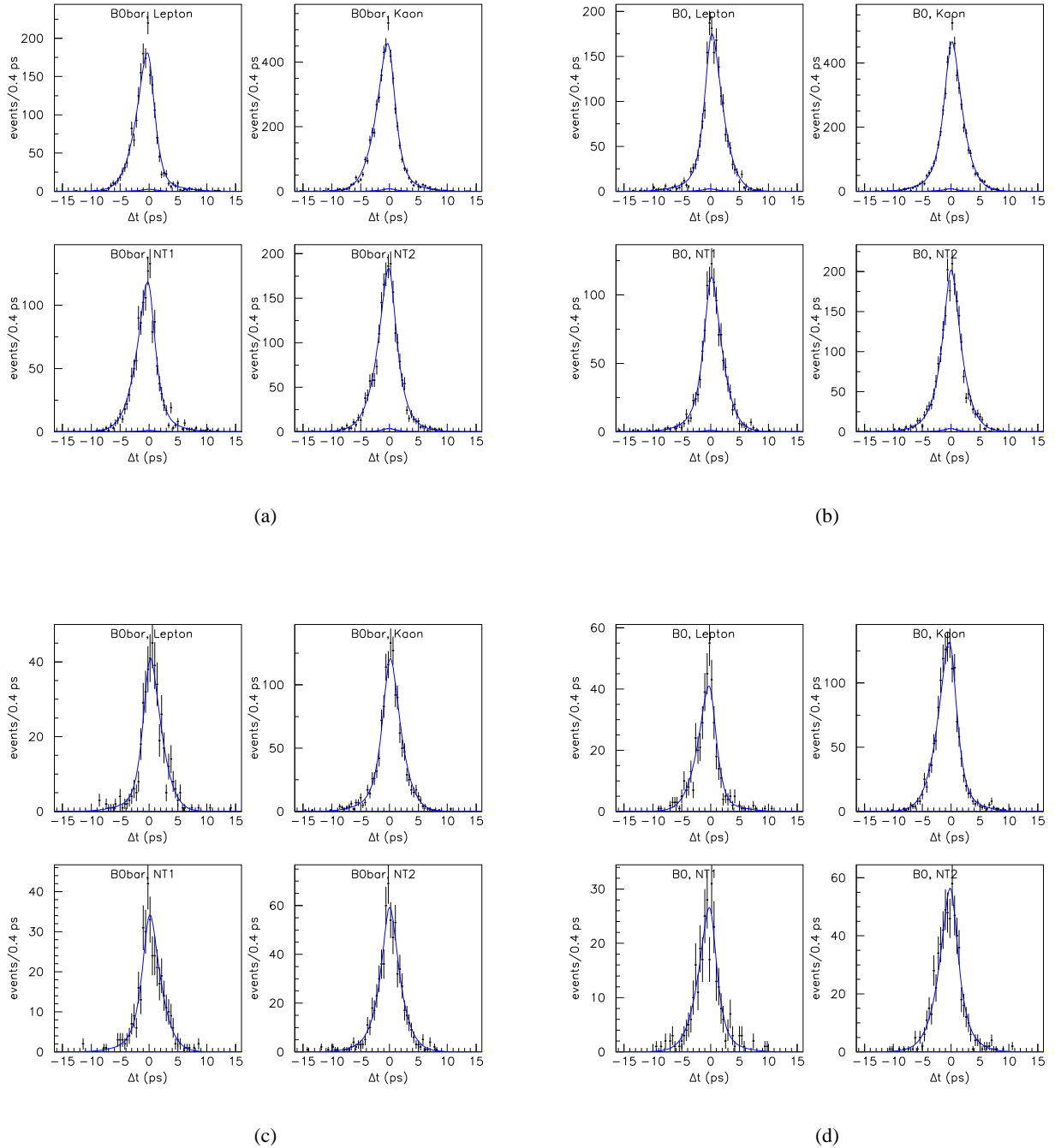
Figure 44: Δt projections of the nominal CPT/CP/T fit for (a) mixed $\overline{B}^0$, (b) mixed B^0, (c) unmixed $\overline{B}^0$ and (d) ubmixed B^0 events, for the different tagging categories (*GExp* model).

Figure 45: Δt projections of the nominal CPT/CP/T fit for (a) $B_{CPK_S^0}\,\overline{B}^0$, (b) $B_{CPK_S^0}\,B^0$, (c) $B_{CPK_L^0}\,\overline{B}^0$ and (d) $B_{CPK_L^0}B^0$ events, for the different tagging categories (*GExp* model).

(a)

(b)

(c)

(d)
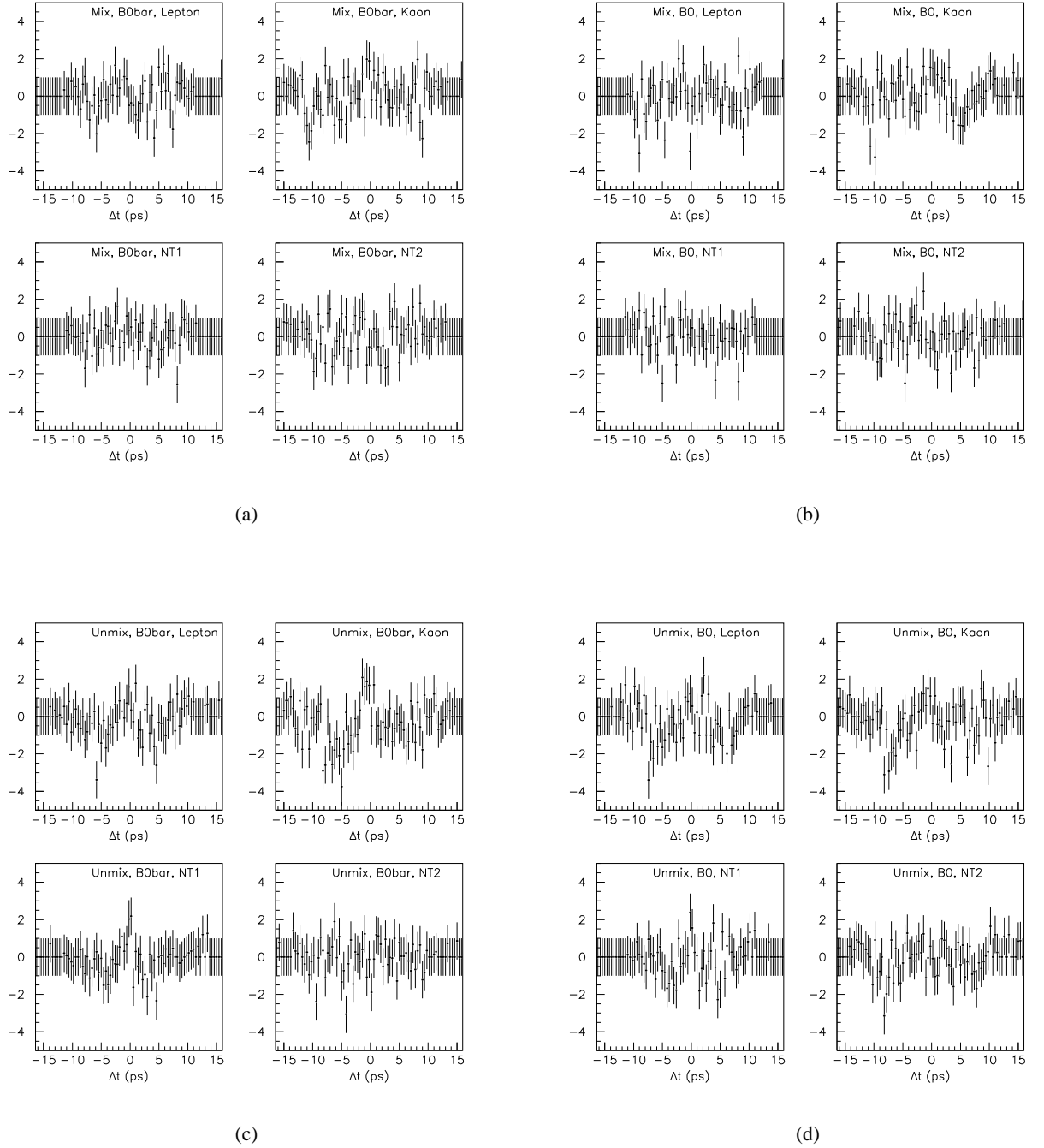
Figure 46: Normalized residuals of the Δt projections of the nominal CPT/CP/T fit for (a) mixed $\bar{B}^0$, (b) mixed B^0, (c) unmixed $\bar{B}^0$ and (d) ubmixed B^0 events, for the different tagging categories (*GExp* model).
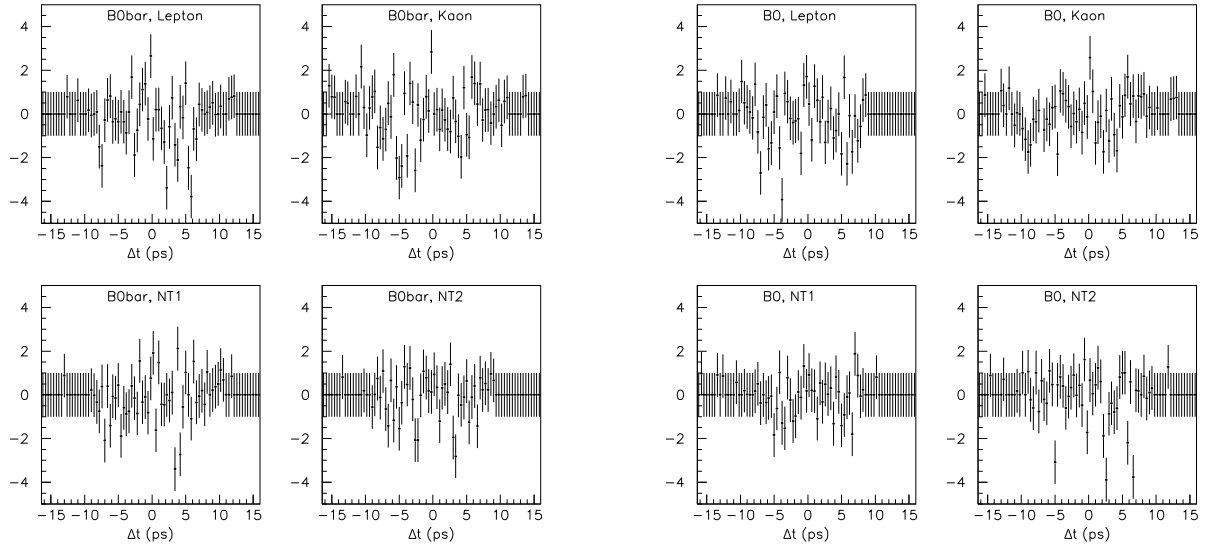
(a)
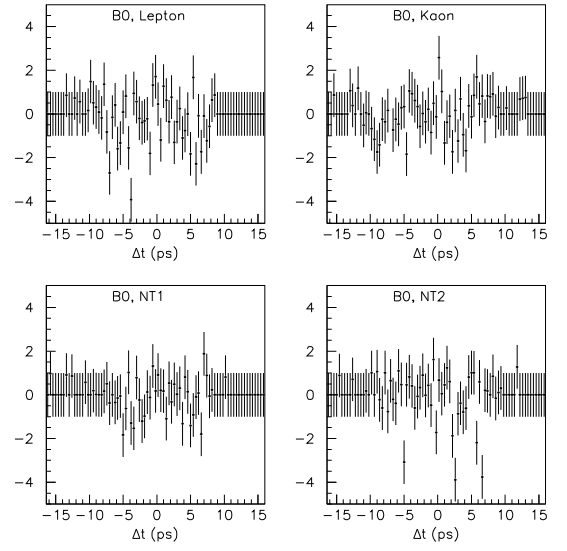
(b)
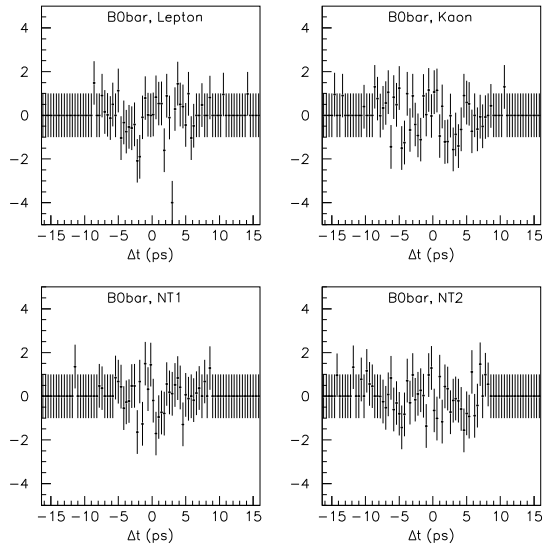
(c)
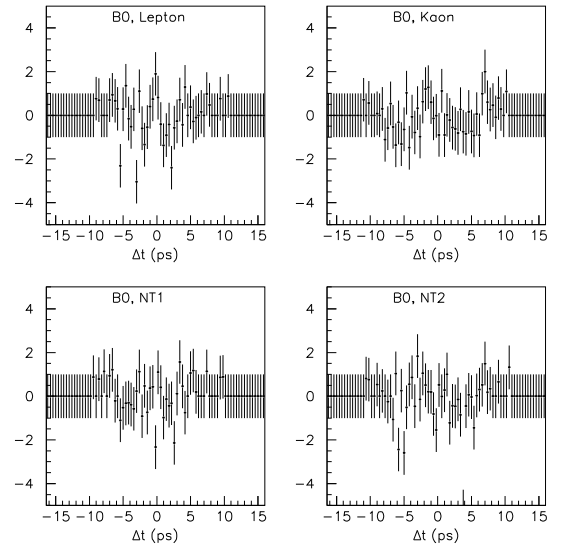
(d)

Figure 47: Normalized residuals of the Δt projections of the nominal CPT/CP/T fit for (a) $B_{CPK_S^0} \overline{B}^0$, (b) $B_{CPK_S^0} B^0$, (c) $B_{CPK_L^0} \overline{B}^0$ and (d) $B_{CPK_L^0} B^0$ events, for the different tagging categories (*GExp* model).

Parameter	B_{flav} mixing	$B_{flav}+B_{CP}$
$\frac{\mathrm{Re}\lambda}{|\lambda|}\mathrm{Re}z$	–	0.003 ± 0.016
$\mathrm{Im}z$	-0.0041 ± 0.006	-0.010 ± 0.005
$\frac{\mathrm{Im}\lambda}{|\lambda|}$	–	0.703 ± 0.018
$|q/p|$	1.002 ± 0.005	1.001 ± 0.005
$\Delta\Gamma/\Gamma$	0.000 ± 0.043	-0.011 ± 0.013
Δm	0.4778 ± 0.0034	0.4771 ± 0.0033
τ	1.548	1.548

Table 32: Full Monte Carlo validation physics parameter results for the $(|q/p|,\lambda,z)$ formalism (*GG* resolution model).

	$\frac{1-|\varepsilon|^2}{1+|\varepsilon|^2}\frac{\mathrm{Re}\delta}{1+|\varepsilon|^2}$	$\frac{\mathrm{Im}\delta}{1+|\varepsilon|^2}$	$\frac{\mathrm{Im}\varepsilon}{1+|\varepsilon|^2}$	$\frac{\mathrm{Re}\varepsilon}{1+|\varepsilon|^2}$	$\Delta\Gamma/\Gamma$	Δm
$\frac{1-|\varepsilon|^2}{1+|\varepsilon|^2}\frac{\mathrm{Re}\delta}{1+|\varepsilon|^2}$	1.000	0.031	-0.004	-0.099	0.197	0.014
$\frac{\mathrm{Im}\delta}{1+|\varepsilon|^2}$		1.000	-0.125	0.000	-0.011	-0.022
$\frac{\mathrm{Im}\varepsilon}{1+|\varepsilon|^2}$			1.000	-0.003	-0.011	-0.085
$\frac{\mathrm{Re}\varepsilon}{1+|\varepsilon|^2}$				1.000	-0.192	-0.006
$\Delta\Gamma/\Gamma$					1.000	0.011
Δm						1.000

Table 33: Correlations among the 6 physics parameters for the reference configuration with the *GG* resolution function model.

for $\Delta\Gamma/\Gamma$ is $\Gamma_L - \Gamma_H$. Four combinations of parameters can be provided to the model (3,8,12,14).

- SSDCP: **BrFr V S SVS_CP dm dgog absqop argqop absAf argAf absAbarf argAbarf absAfbar argAfbar absAbarfbar argAbarfbar rez imz** This is un upgraded version of an already existing model [40] (but not yet used in production), the difference again being the CPT effects. As above, the sign convention for $\Delta\Gamma/\Gamma$ is $\Gamma_L - \Gamma_H$. The q/p convention used here uses the light state, which is opposite to the convention used in this document. This introduces a relative π phase in **argqop**. Three combinations of parameters can be provided to the model (8,12,14).

The implementation of the models (based on the amplitude) was cross-validated with the calculations of the time dependent intensities and their implementation by producing standard ASCII files when running testEvtGen and then fitting them to truth information. About 150k B_{flav}, $B_{CPK_S^0}$ and $B_{CPK_L^0}$ each were generated for several sets of parameters. The samples were fitted separately and all together, using the two formalisms. In all cases the fit results reproduced the input values. As an example, table 35 reports the results of the combined fit for a configuration with non-zero values for all the parameters. Figure 48 shows the corresponding generated and fitted time distributions and their residuals.
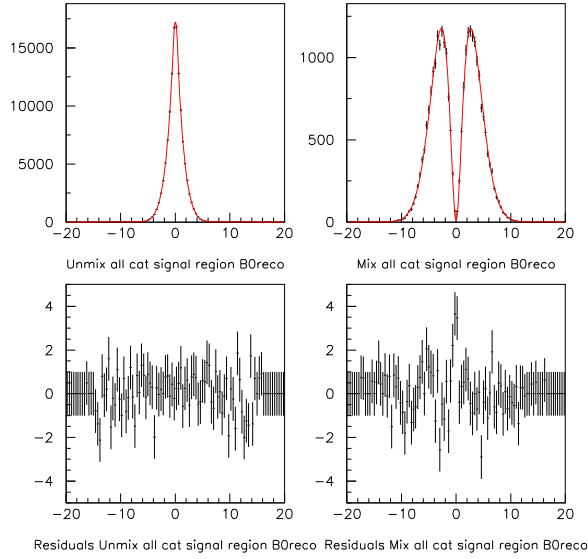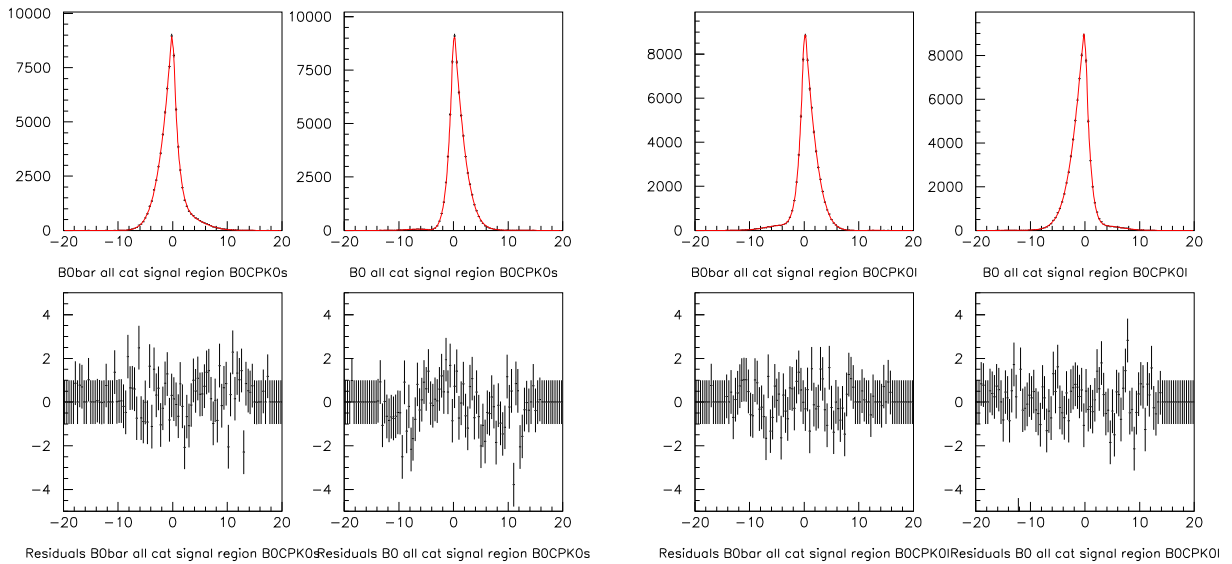
Figure 48: Generated and fitted time distributions and their residuals used for the validation of the VSS_BMIXCPT and SSDCP models. Each generated sample (B_{flav}, $B_{CPK_S^0}$ and $B_{CPK_L^0}$) had about 150k events.

	$\frac{1-\|\varepsilon\|^2}{1+\|\varepsilon\|^2}\frac{\mathrm{Re}\delta}{1+\|\varepsilon\|^2}$	$\frac{\mathrm{Im}\delta}{1+\|\varepsilon\|^2}$	$\frac{\mathrm{Im}\varepsilon}{1+\|\varepsilon\|^2}$	$\frac{\mathrm{Re}\varepsilon}{1+\|\varepsilon\|^2}$	$\Delta\Gamma/\Gamma$	Δm
$\frac{1-\|\varepsilon\|^2}{1+\|\varepsilon\|^2}\frac{\mathrm{Re}\delta}{1+\|\varepsilon\|^2}$	1.000	0.029	-0.011	-0.103	0.205	0.017
$\frac{\mathrm{Im}\delta}{1+\|\varepsilon\|^2}$		1.000	-0.123	-0.008	-0.003	-0.019
$\frac{\mathrm{Im}\varepsilon}{1+\|\varepsilon\|^2}$			1.000	-0.002	-0.008	-0.084
$\frac{\mathrm{Re}\varepsilon}{1+\|\varepsilon\|^2}$				1.000	-0.198	-0.006
$\Delta\Gamma/\Gamma$					1.000	0.016
Δm						1.000

Table 34: Correlations among the 6 physics parameters for the reference configuration with the *GExp* resolution function model.

Parameter	Generated value	Fit result
τ_B (ps)	1.54774	1.5497 ± 0.0024
$\Delta m(\mathrm{ps}^{-1})$	0.472	0.4715 ± 0.0011
$\Delta\Gamma/\Gamma$	0.20	0.1979 ± 0.0029
$\| q/p \|$	1.05	1.0517 ± 0.0022
$\frac{\mathrm{Re}\lambda}{\|\lambda\|}\mathrm{Re}z$	0.1428	0.1393 ± 0.0024
$\frac{\mathrm{Im}\lambda}{\|\lambda\|}$	0.70	0.7030 ± 0.0026
$\mathrm{Im}z$	0.05	0.0488 ± 0.0025

Table 35: Results from the combined fit to `EvtGen` generated events. The input values provided to the models are Δm=0.472 ps^{-1}, $\Delta\Gamma/\Gamma$=0.20, $\| q/p \|$=1.05, $arg(q/p) = -0.776565$, Rez=0.20 and Imz=0.05.

5 CPT, CP and T reach and sensitivity

5.1 Projections and sensitivity at low luminosity

In addition to the physics parameters configurations described in section 4.1, which results were summarized in tables 14, 15, 16 and 17 and figure 30, we considered here the following:

- reference with $\frac{1-\|\varepsilon\|^2}{1+\|\varepsilon\|^2}\frac{\mathrm{Re}\delta}{1+\|\varepsilon\|^2}$= 0.20;

- reference with $\frac{\mathrm{Im}\delta}{1+\|\varepsilon\|^2}$= 0.05;

- reference with $\frac{\mathrm{Re}\varepsilon}{1+\|\varepsilon\|^2}$= 0.05.

The average and RMS of the residual distribution as well as the average Gaussian error and its coverage are summarized in tables 36, 37 and 38.

5.2 High luminosity projections

Different values of integrated luminosity experiments have been considered in order to evaluate the error behaviour and scaling as a function of the data sample size. We considered for the reference configuration two additional data sample integrated luminosity:

	$\frac{1-|\varepsilon|^2}{1+|\varepsilon|^2}\frac{\mathrm{Re}\delta}{1+|\varepsilon|^2}=0.2$ configuration, *GG* model				
	$\frac{1-|\varepsilon|^2}{1+|\varepsilon|^2}\frac{\mathrm{Re}\delta}{1+|\varepsilon|^2}$	$\frac{\mathrm{Im}\varepsilon}{1+|\varepsilon|^2}$	$\frac{\mathrm{Re}\varepsilon}{1+|\varepsilon|^2}$	$\Delta\Gamma/\Gamma$	Δm
Mean residual	$(-2.8\pm2.3)\cdot10^{-3}$	$(1.7\pm1.3)\cdot10^{-3}$	$(-2.3\pm2.3)\cdot10^{-4}$	$(1.4\pm1.1)\cdot10^{-3}$	$(-1.8\pm2.9)\cdot10^{-4}$
RMS residual	$(6.7\pm0.2)\cdot10^{-2}$	$(3.8\pm0.1)\cdot10^{-2}$	$(6.9\pm0.2)\cdot10^{-3}$	$(3.4\pm0.1)\cdot10^{-2}$	$(8.8\pm0.2)\cdot10^{-3}$
Average error (Gauss)	$7.1\cdot10^{-2}$	$3.9\cdot10^{-2}$	$7.1\cdot10^{-3}$	$3.4\cdot10^{-2}$	$9.5\cdot10^{-3}$
Gaussian error coverage	$(71.5\pm3.7)\%$	$(67.8\pm3.6)\%$	$(69.0\pm3.6)\%$	$(67.4\pm3.6)\%$	$(71.4\pm3.7)\%$

Table 36: Summary of results for the $\frac{1-|\varepsilon|^2}{1+|\varepsilon|^2}\frac{\mathrm{Re}\delta}{1+|\varepsilon|^2}=0.2$ configuration from signal only fits (*GG* resolution model, ≈ 60 fb^{-1}).

	$\frac{\mathrm{Im}\delta}{1+|\varepsilon|^2}=0.05$ configuration, *GG* model					
	$\frac{1-|\varepsilon|^2}{1+|\varepsilon|^2}\frac{\mathrm{Re}\delta}{1+|\varepsilon|^2}$	$\frac{\mathrm{Im}\delta}{1+|\varepsilon|^2}$	$\frac{\mathrm{Im}\varepsilon}{1+|\varepsilon|^2}$	$\frac{\mathrm{Re}\varepsilon}{1+|\varepsilon|^2}$	$\Delta\Gamma/\Gamma$	Δm
Mean residual	$(4.2\pm2.6)\cdot10^{-3}$	$(0.2\pm6.0)\cdot10^{-4}$	$(-1.1\pm1.4)\cdot10^{-3}$	$(-1.7\pm2.5)\cdot10^{-4}$	$(0.0\pm2.2)\cdot10^{-3}$	$(2.3\pm3.3)\cdot10^{-4}$
RMS residual	$(7.2\pm0.2)\cdot10^{-2}$	$(1.6\pm0.0)\cdot10^{-2}$	$(4.0\pm0.1)\cdot10^{-2}$	$(6.9\pm0.2)\cdot10^{-3}$	$(6.1\pm0.2)\cdot10^{-2}$	$(9.1\pm0.3)\cdot10^{-3}$
Av. error (Gauss)	$6.9\cdot10^{-2}$	$1.7\cdot10^{-2}$	$4.0\cdot10^{-2}$	$7.1\cdot10^{-3}$	$5.6\cdot10^{-2}$	$9.5\cdot10^{-3}$
Gauss. error cov.	$(65.7\pm3.8)\%$	$(67.6\pm3.9)\%$	$(67.1\pm3.8)\%$	$(70.6\pm4.0)\%$	$(62.5\pm3.7)\%$	$(69.8\pm4.0)\%$

Table 37: Summary of results for the $\frac{\mathrm{Im}\delta}{1+|\varepsilon|^2}=0.05$ configuration from signal only fits (*GG* resolution model, ≈ 60 fb^{-1}).

	$\frac{\mathrm{Re}\varepsilon}{1+|\varepsilon|^2}=0.05$ configuration, *GG* model				
	$\frac{1-|\varepsilon|^2}{1+|\varepsilon|^2}\frac{\mathrm{Re}\delta}{1+|\varepsilon|^2}$	$\frac{\mathrm{Im}\varepsilon}{1+|\varepsilon|^2}$	$\frac{\mathrm{Re}\varepsilon}{1+|\varepsilon|^2}$	$\Delta\Gamma/\Gamma$	Δm
Mean residual	$(1.6\pm2.5)\cdot10^{-3}$	$(-0.4\pm1.3)\cdot10^{-3}$	$(0.5\pm2.4)\cdot10^{-4}$	$(-1.8\pm2.1)\cdot10^{-3}$	$(1.3\pm3.2)\cdot10^{-4}$
RMS residual	$(7.5\pm0.2)\cdot10^{-2}$	$(4.0\pm0.1)\cdot10^{-2}$	$(7.0\pm0.2)\cdot10^{-3}$	$(6.2\pm0.2)\cdot10^{-2}$	$(9.4\pm0.2)\cdot10^{-3}$
Average error (Gauss)	$6.8\cdot10^{-2}$	$3.9\cdot10^{-2}$	$7.0\cdot10^{-3}$	$5.4\cdot10^{-2}$	$9.5\cdot10^{-3}$
Gaussian error coverage	$(61.0\pm3.4)\%$	$(68.6\pm3.6)\%$	$(68.3\pm3.6)\%$	$(59.1\pm3.3)\%$	$(67.8\pm3.6)\%$

Table 38: Summary of results for the $\frac{\mathrm{Re}\varepsilon}{1+|\varepsilon|^2}=0.05$ configuration from signal only fits (*GG* resolution model, ≈ 60 fb^{-1}). $\frac{\mathrm{Im}\delta}{1+|\varepsilon|^2}$ was fixed in these fits.

- 200 fb^{-1} (100 experiments);
- 400 fb^{-1} (100 experiments).

Table 39 shows the RMS of the residual distribution and the average estimated (Gaussian) error on all the physics parameters, comparing them to the low luminosity (60 fb^{-1}) projections. It can be seen that the scaling of the error with $1/\sqrt{N}$ applies well. Let us note the 2% statistical precision could be reach with 400 fb^{-1} for $\Delta\Gamma/\Gamma$.

5.3 Impact from an eventual improved Δt resolution

Here we plan to estimate the improvement in the statistical error due to an eventual improved Δt resolution (better Δz algorithms, beam pipe reduction, additional and closer SVT layers).

	Scaling of the error on physical parameters					
	$\frac{1-|\varepsilon|^2}{1+|\varepsilon|^2}\frac{\mathrm{Re}\delta}{1+|\varepsilon|^2}$	$\frac{\mathrm{Im}\delta}{1+|\varepsilon|^2}$	$\frac{\mathrm{Im}\varepsilon}{1+|\varepsilon|^2}$	$\frac{\mathrm{Re}\varepsilon}{1+|\varepsilon|^2}$	$\Delta\Gamma/\Gamma$	Δm
RMS residual						
60 fb^{-1}	$(7.6\pm0.2)\cdot10^{-2}$	$(1.80\pm0.05)\cdot10^{-2}$	$(4.0\pm0.1)\cdot10^{-2}$	$(7.0\pm0.2)\cdot10^{-3}$	$(6.4\pm0.2)\cdot10^{-2}$	$(9.2\pm0.2)\cdot10^{-3}$
200 fb^{-1}	$(4.1\pm0.4)\cdot10^{-2}$	$(7.7\pm1.0)\cdot10^{-3}$	$(2.0\pm0.2)\cdot10^{-2}$	$(4.3\pm0.5)\cdot10^{-3}$	$(3.2\pm0.5)\cdot10^{-2}$	$(6.5\pm0.6)\cdot10^{-3}$
400 fb^{-1}	$(2.4\pm0.3)\cdot10^{-2}$	$(6.6\pm0.9)\cdot10^{-3}$	$(1.6\pm0.2)\cdot10^{-2}$	$(2.5\pm0.3)\cdot10^{-3}$	$(2.4\pm0.3)\cdot10^{-2}$	$(2.8\pm0.3)\cdot10^{-3}$
Average error						
60 fb^{-1}	$6.8\cdot10^{-2}$	$1.9\cdot10^{-2}$	$4.0\cdot10^{-2}$	$7.0\cdot10^{-3}$	$5.3\cdot10^{-2}$	$9.5\cdot10^{-3}$
200 fb^{-1}	$4.0\cdot10^{-2}$	$8.5\cdot10^{-3}$	$2.1\cdot10^{-2}$	$4.0\cdot10^{-3}$	$3.2\cdot10^{-2}$	$5.2\cdot10^{-3}$
400 fb^{-1}	$2.8\cdot10^{-2}$	$6.0\cdot10^{-3}$	$1.5\cdot10^{-2}$	$2.7\cdot10^{-3}$	$2.3\cdot10^{-2}$	$3.6\cdot10^{-3}$

Table 39: Summary of results for the error scaling with the reference configuration, for 60-200-400 fb^{-1}.

6 Summary and conclusions

We have shown in this note that with the already available statistics accumulated by the *BABAR* experiment, an analysis probing simultaneous and consistenly the CPT/CP and CP/T discrete symmetries of the effective Hamiltonian of evolution for the B_d^0 system is feasible, and all that with independence of the vanishingly small expected value of $\Delta\Gamma$. The analysis, which exploits the complete flavor-tag and Δt structure of the B_d^0-$\overline{B}_d^0$ meson system, will help to disentangle whether the CP violation is due to T or CPT violation. The number of theoretical inputs required are mininum if we restrict to samples free of direct CP violation (both flavor and CP specific). Nevertheless, the possible competing contributions from direct CP violation and double-Cabbibo supressed decays can be parameterized and included as systematic uncertainties. Effects from non-vanishing values of $\Delta\Gamma$, the main competing source which can contribute producing fake effects on the asymmetries, are parameterized and extracted simultenously from the data, providing a robust and precise measurement of $\Delta\Gamma/\Gamma$.

The study has been performed using two phase-convention independent formalisms: the (ε,δ), similar to that used in kaon system phenomenology, and the $(|q/p|,\lambda,z)$. As expected, the conclusions of the study are the same whatever approach is adopted. The physics parameters to which the analysis is sensitive are, for the former, $\frac{1-|\varepsilon|^2}{1+|\varepsilon|^2}\frac{\mathrm{Re}\delta}{1+|\varepsilon|^2}$, $\frac{\mathrm{Im}\delta}{1+|\varepsilon|^2}$, $\frac{\mathrm{Re}\varepsilon}{1+|\varepsilon|^2}$, $\frac{\mathrm{Im}\varepsilon}{1+|\varepsilon|^2}$, $sign\left(\frac{1-|\varepsilon|^2}{1+|\varepsilon|^2}\right)\Delta\Gamma/\Gamma$ and Δm, and for the latter, $\frac{\mathrm{Re}\lambda}{|\lambda|}$, $\mathrm{Im}z$, $|q/p|$, $\frac{\mathrm{Im}\lambda}{|\lambda|}$, $sign(\mathrm{Re}\lambda)\Delta\Gamma/\Gamma$ and Δm. The average B_d^0 lifetime is kept fixed. The determination of all these parameters is unbiased and largely uncorrelated (few per cent). The statistical reach for all the physics parameters for an integrated luminosity of $\approx 60\,\mathrm{fb}^{-1}$ is:

scaling well according to the $1/\sqrt{N}$ rule.

Physics Parameter	Estimated statistical error, $\approx 60\,\text{fb}^{-1}$
(ε, δ) formalism	
$\frac{1-|\varepsilon|^2}{1+|\varepsilon|^2}\frac{\text{Re}\delta}{1+|\varepsilon|^2}$	7.6×10^{-2}
$\frac{\text{Im}\delta}{1+|\varepsilon|^2}$	1.6×10^{-2}
$\frac{\text{Im}\varepsilon}{1+|\varepsilon|^2}$	4.0×10^{-2}
$\frac{\text{Re}\varepsilon}{1+|\varepsilon|^2}$	6.7×10^{-3}
$(|q/p|, \lambda, z)$ formalism	
$\frac{\text{Re}\lambda}{|\lambda|}\text{Re}z$	7.6×10^{-2}
$\text{Im}z$	1.6×10^{-2}
$\frac{\text{Im}\lambda}{|\lambda|}$	8.0×10^{-2}
$|q/p|$	1.3×10^{-2}
Common	
$\Delta\Gamma/\Gamma$	6.2×10^{-2}
Δm	9.3×10^{-3}

A Parameterization of direct CP effects in the (ε, δ) formalism

Possible direct CP violation in B_{CP} processes implies that the final states $B_{r\pm}$ have contributions from both CP eigenstates, $|B_{\pm}(t)\rangle$, as given in equation (27) (the one with the same CP eigenvalue and a small contribution from the opposite one):

$$
\begin{aligned}
|B_{r+}(t)\rangle &= \frac{1}{\sqrt{1+|\xi|^2}}[|B_+(t)\rangle + \xi |B_-(t)]\rangle \\
|B_{r-}(t)\rangle &= \frac{1}{\sqrt{1+|\xi|^2}}[|B_-(t)\rangle + \xi |B_+(t)]\rangle \ .
\end{aligned}
\tag{102}
$$

ξ is the complex valued parameter which parameterizes the degree of CP violation in the decay.

Equations (102) can be worked out in the same way as it was done in section 2.5 to obtain the coefficients of the time dependent decay rate:

- CP tag, $X = B_{r-}, Y = B_t^0(\bar{B}_t^0)$:

$$
\begin{aligned}
\eta_+ &= |1-\xi\varepsilon_2|^2 + |\varepsilon_1 - \xi\varepsilon_1\varepsilon_2|^2 + s_t 2\text{Re}\left[(\varepsilon_1 - \xi\varepsilon_1\varepsilon_2)(1-\xi^*\varepsilon_2^*)\right] \\
\eta_- &= |\xi\varepsilon_2 - \varepsilon_1\varepsilon_2|^2 + |\xi - \varepsilon_1|^2 + s_t 2\text{Re}\left[(\xi - \varepsilon_1)(\xi^*\varepsilon_2^* - \varepsilon_1^*\varepsilon_2^*)\right] \\
\eta_{re} &= 2\text{Re}\left\{(\xi\varepsilon_2 - \varepsilon_1\varepsilon_2)(1-\xi^*\varepsilon_2^*) + (\xi - \varepsilon_1)(\varepsilon_1^* - \xi^*\varepsilon_1^*\varepsilon_2^*)\right\} + \\
&\quad s_t 2\text{Re}\left\{(\xi\varepsilon_2 - \varepsilon_1\varepsilon_2)(\varepsilon_1^* - \xi^*\varepsilon_1^*\varepsilon_2^*) + (\xi - \varepsilon_1)(1-\xi^*\varepsilon_2^*)\right\} \\
\eta_{im} &= -2\text{Im}\left\{(\xi\varepsilon_2 - \varepsilon_1\varepsilon_2)(1-\xi^*\varepsilon_2^*) + (\xi - \varepsilon_1)(\varepsilon_1^* - \xi^*\varepsilon_1^*\varepsilon_2^*)\right\} - \\
&\quad s_t 2\text{Im}\left\{(\xi\varepsilon_2 - \varepsilon_1\varepsilon_2)(\varepsilon_1^* - \xi^*\varepsilon_1^*\varepsilon_2^*) + (\xi - \varepsilon_1)(1-\xi^*\varepsilon_2^*)\right\}
\end{aligned}
\tag{103}
$$

- CP tag, $X = B_{r+}, Y = B_t^0(\bar{B}_t^0)$:

$$
\begin{aligned}
\eta_+ &= |\xi\varepsilon_1 - \varepsilon_1\varepsilon_2|^2 + |\xi - \varepsilon_2|^2 + s_t 2\text{Re}\left[(\xi - \varepsilon_2)(\xi^*\varepsilon_1^* - \varepsilon_1^*\varepsilon_2^*)\right] \\
\eta_- &= |1-\xi\varepsilon_1|^2 + |\varepsilon_2 - \xi\varepsilon_1\varepsilon_2|^2 + s_t 2\text{Re}\left[(\varepsilon_2 - \xi\varepsilon_1\varepsilon_2)(1-\xi^*\varepsilon_1^*)\right] \\
\eta_{re} &= 2\text{Re}\left\{(1-\xi\varepsilon_1)(\xi^*\varepsilon_1^* - \varepsilon_1^*\varepsilon_2^*) + (\varepsilon_2 - \xi\varepsilon_1\varepsilon_2)(\xi^* - \varepsilon_2^*)\right\} + \\
&\quad s_t 2\text{Re}\left\{(1-\xi\varepsilon_1)(\xi^* - \varepsilon_2^*) + (\varepsilon_2 - \xi\varepsilon_1\varepsilon_2)(\xi^*\varepsilon_1^* - \varepsilon_1^*\varepsilon_2^*)\right\} \\
\eta_{im} &= -2\text{Im}\left\{(1-\xi\varepsilon_1)(\xi^*\varepsilon_1^* - \varepsilon_1^*\varepsilon_2^*) + (\varepsilon_2 - \xi\varepsilon_1\varepsilon_2)(\xi^* - \varepsilon_2^*)\right\} - \\
&\quad s_t 2\text{Im}\left\{(1-\xi\varepsilon_1)(\xi^* - \varepsilon_2^*) + (\varepsilon_2 - \xi\varepsilon_1\varepsilon_2)(\xi^*\varepsilon_1^* - \varepsilon_1^*\varepsilon_2^*)\right\} \ .
\end{aligned}
\tag{104}
$$

It is verified that in the limit $\xi = 0$ we recover equations (36) and (37).

B $B^0\bar{B}^0$ reconstruction and tagging efficiency differences from time-integrated data in presence of $\Delta\Gamma$ and T/CP violation

As it was originally proposed in [32], the differences in tagging and reconstruction efficiencies can be determined using time-integrated data. The method proposed counts the numbers of events with the various tagging categories and the events that are untagged in the high statistics B_{flav} sample, and then they are extrapolated to the B_{CP} samples. This method does not spoil the statistical precision while the associated systematic uncertainties will be under control.

Integrating over $-\infty < \Delta t < +\infty$ equation (82) for the different (X,Y) configurations for flavor-to-flavor transitions, we obtain:

$$
\begin{aligned}
F^\alpha(B_r^0, B_t^0) &= (1+\nu)\left\{(1+\mu^\alpha)T^\alpha(1-w^\alpha-\Delta w^\alpha/2)F(B_r^0,B_t^0)+\right.\\
&\quad \left. (1-\mu^\alpha)T^\alpha(w^\alpha-\Delta w^\alpha/2)F(B_r^0,\bar{B}_t^0)\right\}\\
F^\alpha(\bar{B}_r^0, B_t^0) &= (1-\nu)\left\{(1+\mu^\alpha)T^\alpha(1-w^\alpha-\Delta w^\alpha/2)F(\bar{B}_r^0,B_t^0)+\right.\\
&\quad \left. (1-\mu^\alpha)T^\alpha(w^\alpha-\Delta w^\alpha/2)F(\bar{B}_r^0,\bar{B}_t^0)\right\}\\
F^\alpha(B_r^0, \bar{B}_t^0) &= (1+\nu)\left\{(1-\mu^\alpha)T^\alpha(1-w^\alpha+\Delta w^\alpha/2)F(B_r^0,\bar{B}_t^0)+\right.\\
&\quad \left. (1+\mu^\alpha)T^\alpha(w^\alpha+\Delta w^\alpha/2)F(B_r^0,B_t^0)\right\}\\
F^\alpha(\bar{B}_r^0, \bar{B}_t^0) &= (1-\nu)\left\{(1-\mu^\alpha)T^\alpha(1-w^\alpha+\Delta w^\alpha/2)F(\bar{B}_r^0,\bar{B}_t^0)+\right.\\
&\quad \left. (1+\mu^\alpha)T^\alpha(w^\alpha+\Delta w^\alpha/2)F(\bar{B}_r^0,B_t^0)\right\}\\
F^\alpha(B_r^0, no\ tag) &= (1+\nu)\left\{[1-T^\alpha(1+\mu^\alpha)]F(B_r^0,B_t^0)+\right.\\
&\quad \left. [1-T^\alpha(1-\mu^\alpha)]F(B_r^0,\bar{B}_t^0)\right\}\\
F^\alpha(\bar{B}_r^0, no\ tag) &= (1-\nu)\left\{[1-T^\alpha(1+\mu^\alpha)]F(\bar{B}_r^0,B_t^0)+\right.\\
&\quad \left. [1-T^\alpha(1-\mu^\alpha)]F(\bar{B}_r^0,\bar{B}_t^0)\right\}
\end{aligned}
\tag{105}
$$

where ν, μ^α and T^α where defined in equations (78), (79), (80) and (81); and $F(X,Y) = \int_{-\infty}^{+\infty} f(X,Y;\Delta t)d\Delta t$, where $f(X,Y;\Delta t)$ was given in equation (42). Only the Δt odd terms of (42) are relevant (the even terms cancel out), therefore $F(X,Y)$ dependends only on Δm, $\Delta\Gamma$ and $\frac{\mathrm{Re}\varepsilon}{1+|\varepsilon|^2}$. The above expressions have been normalized for a reconstruction efficiency $R=1$.

We form now combinations of the above quantities:

$$
\begin{aligned}
F^\alpha(B_r^0, any\ tag) &= F^\alpha(B_r^0,B_t^0)+F^\alpha(B_r^0,\bar{B}_t^0) =\\
&\quad (1+\nu)T^\alpha\left[(1+\mu^\alpha)F(B_r^0,B_t^0)+(1-\mu^\alpha)F(B_r^0,\bar{B}_t^0)\right]
\end{aligned}
\tag{106}
$$

$$
\begin{aligned}
F^\alpha(\bar{B}_r^0, any\ tag) &= F^\alpha(\bar{B}_r^0,B_t^0)+F^\alpha(\bar{B}_r^0,\bar{B}_t^0) =\\
&\quad (1-\nu)T^\alpha\left[(1+\mu^\alpha)F(\bar{B}_r^0,B_t^0)+(1-\mu^\alpha)F(\bar{B}_r^0,\bar{B}_t^0)\right]
\end{aligned}
\tag{107}
$$

$$
\begin{aligned}
F^\alpha(B_r^0) &= F^\alpha(B_r^0,no\ tag)+F^\alpha(B_r^0,any\ tag) =\\
&\quad (1+\nu)\left[F(B_r^0,B_t^0)+F(B_r^0,\bar{B}_t^0)\right]
\end{aligned}
\tag{108}
$$

$$F^{\alpha}(\bar{B}_r^0) \;=\; F^{\alpha}(\bar{B}_r^0, no\ tag) + F^{\alpha}(\bar{B}_r^0, any\ tag) =$$
$$(1-\nu)\left[F(\bar{B}_r^0, B_t^0) + F(\bar{B}_r^0, \bar{B}_t^0)\right] \tag{109}$$

or equivalently,

$$x \;=\; (1+\nu)T^{\alpha}\left[(1+\mu^{\alpha})a + (1-\mu^{\alpha})b\right] \tag{110}$$

$$y \;=\; (1-\nu)T^{\alpha}\left[(1+\mu^{\alpha})c + (1-\mu^{\alpha})d\right] \tag{111}$$

$$z \;=\; (1+\nu)(a+b) \tag{112}$$

$$w \;=\; (1-\nu)(c+d) \tag{113}$$

where

$$a = F(B_r^0, B_t^0)\ , \quad b = F(B_r^0, \bar{B}_t^0)\ , \quad c = F(\bar{B}_r^0, B_t^0)\ , \quad d = F(\bar{B}_r^0, \bar{B}_t^0)$$

$$x = F^{\alpha}(B_r^0, any\ tag)\ , \quad y = F^{\alpha}(\bar{B}_r^0, any\ tag)\ , \quad z = F^{\alpha}(B_r^0)\ , \quad w = F^{\alpha}(\bar{B}_r^0)$$

Equations (110), (111), (112) and (113) can be worked out to obtain T^{α}, μ^{α} and ν:

$$T^{\alpha} \;=\; \frac{1}{1-\nu^2}\frac{x(c-d)(1-\nu) - y(a-b)(1+\nu)}{2b(c-d)} \tag{114}$$

$$\mu^{\alpha} \;=\; \frac{1}{T^{\alpha}(a-b)}\left[\frac{x}{1+\nu} - (a+b)\right] \tag{115}$$

$$\nu \;=\; \frac{z-w-(a+b-c-d)}{a+b+c+d} \tag{116}$$

These expressions are also valid when the Δt resolution is considered.

C   The CPT/CP/T/Mixing Toy Monte Carlo generator

Toy Monte Carlo events are extensively used in this work to validate the fitting strategy, to study the behaviour of the different parameters (physics, resolution function, mistags and background parameters) and to estimate the physics reach and sensitivity. The generated events are used as input to the fitter in the same way as when using full Monte Carlo events and in a future, real data events. The generation and fitting procedures can be done in a single step or separately via the production of ASCII files in standard format. The generator has been extensively tests. Among many other validation checks, we generated very high statistics samples and then we compared to the truth values (for both, time integrated and time dependent quantities).

C.1   General description

Each generated event is characterized by the following items:

1. error on Δt, $\sigma(\Delta t)$;

2. tagging category;

3. reconstructed beam-energy-substituted mass (m_{ES}) for B_{flav} and $B_{CPK_S^0}$ samples, and ΔE for the $B_{CPK_L^0}$ sample;

4. reco (B_{flav} samples only) and tagging side B^0-$\bar{B}^0$ flavors;

5. Δt.

The generation of the previous quantities considers the following effects:

- signal or background (prompt, non-prompt, peaking,...) event;

- mistag rates, $B^0\bar{B}^0$ differences in the mistags and linear correlation between the average mistag fractions and $\sigma(\Delta t)$;

- $B^0\bar{B}^0$ differences in the reconstruction (B_{flav} samples only) and tagging efficiencies;

- Δt dependence according to the theoretical time distribution;

- Δt smearing using a *GG* or *GExp* resolution model.

The generation of the $\sigma(\Delta t)$ distribution is performed using the FUNLUX subroutine of the CERN library, which generates random numbers according to a given normalized distribution $f(x)$. This distribution is taken as a Crystal Ball shape, and the parameters are tuned from an unbinned likelihood fit to the $\sigma(\Delta t)$ distributions of the full B_{flav}, $B_{CPK_S^0}$ and $B_{CPK_L^0}$ Monte Carlo samples (figure 11). The soubroutine FUNLUX finds the desired random number by calling RANLUX(V115) and uses a 4-point interpolation algorithm to transform the uniform random number to the distribution specified. RANLUX generates pseudorandom numbers uniformily in the interval $(0,1)$ with a period of the sequence greater than 10^{165}. A 32-bit integer provides initialization of the sequence, which guarantees statistical independence and reproducibility of the different experiments.

C.2 Generation of time-integrated rates

The generation of 2, 3 and 4 is the most delicate part of the procedure. The complication arises due to the interplay between the time integrated theoretical rates (mixing, CPT/CP/T violation and $\Delta\Gamma$) and detector effects (reconstruction and tagging efficiencies, $B^0\bar{B}^0$ differences in reconstruction and tagging efficiencies, mistag fractions and $B^0\bar{B}^0$ differences in the mistags, background levels, tagging innefficiencies,...). All these effects together determine the rates of events falling in the various event categories (tagging categories, $B^0\bar{B}^0$ tagged, mixed/unmixed, right/wrong tag, untagged) and the $m_{ES}/\Delta E$ value. This implies that 2,3 and 4 have to be generated in a single shot, as described below.

Candidate m_{ES} (ΔE) values for all tagging categories, according to the tagging category dependent m_{ES} (ΔE) distributions, are first generated using an acceptance/rejection method based on the RANLUX subroutine. The candidate m_{ES} (ΔE), for each tagging category, is then used to calculate the signal probability, $p_{sig}^\alpha(m_{ES})$. The calculated signal probability together with the background fractions, f_β^α and f_{peak}^α -see equation (94)-, are then used to generate the signal/background component candidate, for each tagging category separately. Let us note here that

$$(1 - f_{peak}^\alpha)p_{sig}^\alpha(m_{ES}) + f_{peak}p_{sig}^\alpha(m_{ES}) + \sum_\beta (1 - p_{sig}^\alpha(m_{ES}))f_\beta^\alpha = 1 \qquad (117)$$

The tagging category in wich the event will fall in will be decided later.

Time-integrated rates for each tagging category are then calculated for all signal/background components using equations (105) for B_{flav} samples. In the case of CP events, the corresponding time-integrated expressions read

$$
\begin{aligned}
F^\alpha(B_t^0) &= (1 + \mu^\alpha)T^\alpha(1 - w^\alpha - \Delta w^\alpha/2)F(B_t^0) + (1 - \mu^\alpha)T^\alpha(w^\alpha - \Delta w^\alpha/2)\bar{B}_t^0) \\
F^\alpha(\bar{B}_t^0) &= (1 - \mu^\alpha)T^\alpha(1 - w^\alpha + \Delta w^\alpha/2)F(\bar{B}_t^0) + (1 + \mu^\alpha)T^\alpha(w^\alpha + \Delta w^\alpha/2)F(B_t^0) \\
F^\alpha(no\ tag) &= [1 - T^\alpha(1 + \mu^\alpha)]F(B_t^0) + [1 - T^\alpha(1 - \mu^\alpha)]F(\bar{B}_t^0)
\end{aligned}
\qquad (118)
$$

All rates together verify

$$
\sum_\alpha \{F^\alpha(B_r^0, B_t^0) + F^\alpha(B_r^0, \bar{B}_t^0) + F^\alpha(\bar{B}_r^0, B_t^0) + F^\alpha(\bar{B}_r^0, \bar{B}_t^0) +
$$

$$
F^\alpha(B_r^0, no\ tag) + F^\alpha(\bar{B}_r^0, no\ tag)\} = 1 \qquad (119)
$$

and

$$
\sum_\alpha \{F^\alpha(B_t^0) + F^\alpha(\bar{B}_t^0) + F^\alpha(no\ tag)\} = 1 \qquad (120)
$$

Let us stress the fact that these rates account for tagging efficiencies, $B^0\bar{B}^0$ differences in reconstruction and tagging efficiencies and $B^0\bar{B}^0$ differences in the mistag fractions. Is here were the mixing/$\Delta\Gamma$ and CPT/CP/T violating effects in time integrated rates enter in. Splitting each equation in (105) and (118) into the two parts on the right hand side, we can also calculate the time-integrated rates of right and wrongly tagged events, for each tagging category and signal/background component.

To define the final boundaries of the event categories, rates (105) and (118) are multiplied by the component (signal/background) probabilities: $(1 - f_{peak}^\alpha)p_{sig}^\alpha(m_{ES})F^\alpha(X,Y)$ for signal, $f_{peak}p_{sig}^\alpha(m_{ES})F^\alpha(X,Y)$ for

peaking background and $(1 - p^{\alpha}_{sig}(m_{ES}))f^{\alpha}_{\beta}F^{\alpha}(X,Y)$ for combinatorial background components. Summed over all components and tagging categories, it can be verified that the total rate is consistently normalized to 1.

In this way, we have defined a total of $N_T \times N_C \times N_E$ event categories, where $N_T = 4$ is the number of tagging categories, N_C the number of components (signal+background) and N_E is 10 for B_{flav} samples (mixed B^0_t right tag, unmixed B^0_t right tag, mixed $\overline{B}^0_t$ right tag, unmixed $\overline{B}^0_t$ right tag, mixed B^0_t wrong tag, unmixed B^0_t wrong tag, mixed $\overline{B}^0_t$ wrong tag, unmixed $\overline{B}^0_t$ wrong tag, untagged B^0_r, untagged $\overline{B}^0_r$) and 5 for B_{CP} samples (B^0_t right tag, $\overline{B}^0_t$ right tag, B^0_t wrong tag, $\overline{B}^0_t$ wrong tag, untagged). Summation over all the $N_T \times N_C \times N_E$ event categories is again 1, and with their boundaries the generator decides the event class for the current event.

C.3 Time-dependence generation and smearing

Once it has been decided the event category, the time dependence can be generated unambiguously. To do so, the theoretical dependence is generated first, using the PDF (42). Again, an acceptance/rejection method based on RANLUX is used here. When deciding the Δt limits, special attention has to be put to insure that the limits are well beyond the region with non-negligible contribution from the theoretical distribution and resolution function, otherwise the generated distribution would be truncated, causing undesirable effects in the fitting procedure. The value used through this study has been ± 40 ps. The Δt smearing is performed in a similar way, using as PDF the equations (85) and (87), for the *GG* and *GExp* resolution models, respectively. Present Δt smearing limits are also ± 40 ps.

Acknowledgments

References

[1] R.F. Streater and A.S. Wightman, *PCT, Spin and Statistics, and All That*, Benjamin, New York, 1964.

[2] M.B. Gavela et al., *Mod. Phys. Lett.* **A9** (1994) 795.

[3] I.I. Bigi, A.I. Sanda, *CP Violation*, Cambridge University Press, 2000.

[4] L. Wolfenstein, *Nucl. Phys* **B246** (1984) 45; M. B. Gavela et al., *Phys. Lett.* **B162** (1985) 197; Z. Xing, *Phys. Rev.* **D53** (1996) 204.

[5] M. Kobayashi and A. I. Sanda, *Phys. Rev. Lett.* **69** (1992) 3139; Z. Xing, *Phys. Rev.* **D50** (1994) 2957; V. A. Kostelecký and R. Van Kooten, *Phys. Rev.* **D54** (1996) 5585; P. Colangello and G. Corcella, *Eur. Phys. J.* **C1** (1998) 515.

[6] S.W. Hawking, *Phys. Rev.* **D14** (1975) 2460; *Commun. Math. Phys.* **87** 395 (1982); V.V. Barmin et al., *Nucl. Phys.* **B247** (1985) 293.

[7] P. K. Kabir, The CP Puzzle, *Academic Press* (1968), p. 99

[8] J.H. Christenson, J.W. Cronin, V.L. Fitch and R. Turlay, *Phys. Rev. Lett.* **13** 138 (1964).

[9] A. Apostolakis et al., *Phys. Lett.* **B456** (1999) 297.

[10] *BABAR* Analysis Document # 199, Study of CP, T and CPT violations in the mixing with Inclusive Dilepton Events.

[11] V. Khoze et al., *Yad. Fiz.* **46** (1987) 181; A. Acuto and D. Cocolicchio, *Phys. Rev.* **D47** (1993) 3945.

[12] M. C. Bañuls, J. Bernabéu, *Phys. Lett.* **B423** (1998) 151; *Phys. Lett.* **B464** (1999) 117; *Nucl. Phys.* **B590** (2000) 19.

[13] D. Colladay and V. A. Kostelecký, *Phys. Lett.* **B344** (1995) 259; V. A. Kostelecký, *Phys. Rev.* **D64** 076001 (2001).

[14] B. Aubert et al., The BaBar Collaboration, Observation of CP Violation in the B^0 meson system, accepted by *Phys. Rev. Lett.*, preprint hep-ex/0107013.

[15] M. C. Bañuls, J. Bernabéu, *JHEP* **9906:032** (1999).

[16] M. Kobayashi and T. Maskawa, *Prog. Theor. Phys.* **49** (1973) 652; L. Wolfenstein, *Phys. Rev. Lett.* **51** (1983) 1945.

[17] D. Colladay and V. A. Kostelecký, *Phys. Lett.* **B344** (1995) 259; A. Mohapatra, M. Satpathy, K. Abe and Y. Sakai, *Phys. Rev.* **D58** (1998) 036003; Z. Z. Xing, *Phys. Lett.* **B450** (1999) 202.

[18] *BABAR* Analysis Document # 188, A general model for Neutral B decay time distributions.

[19] *BABAR* Analysis Document # 115, Supporting document for the Run1 $\sin 2\beta$ analysis.

[20] *BABAR* Analysis Document # 205, Supporting document for the summer 2001 $\sin 2\beta$ analysis.

[21] *BABAR* Analysis Document # 99, Measurement of the CP asymmetry $\sin 2\beta$ using the decay mode $B^0 \to J/\psi K_L^0$.

[22] *BABAR* Analysis Document # 206, Aspects of the summery 2001 $\sin 2\beta$ measurement specific to the decay mode $B^0 \rightarrow J/\psi K_L^0$.

[23] *BABAR* Analysis Document # 102, The BaBar Vertexing.

[24] *BABAR* Analysis Document # 125, Measurement of $B^0 \bar{B}^0$ mixing with fully reconstructed hadronic B decays.

[25] *BABAR* Analysis Document # 144, Measurements of the charged and neutral B meson lifetimes using fully reconstructed B decays.

[26] *BABAR* Analysis Document # 119, B Tagging in BaBar: Status for the 2001 $\sin 2\beta$ Publications.

[27] *BABAR* Analysis Document # 130, Vertexing performances and systematic checks with fully reconstructed B events.

[28] *BABAR* Analysis Document # 254, Vertexing supporting document for Summer 2001 Conferences.

[29] *BABAR* Analysis Document # 18, A User's Guide to the RootFitTools Package for Unbinned Maximum Likelihood Fitting.

[30] F. Martinez-Vidal, A note on tagging/vertexing correlations and their impact on mixing and $\sin 2\beta$, `http://babar-hn.slac.stanford.edu:5090/HyperNews/get/VertexTools/214.html`.

[31] Chih-hsiang Cheng, Summary of vertexing investigations, Talk at the Joint $\sin 2\beta / \sin 2\alpha$/tagging/vertexing Workshop, October 16th 2001, `http://www.slac.stanford.edu/BFROOT/www/Physics/CP/beta/Meetings/16Oct01/JointSin2b+a.html`

[32] R. Cahn, Determining efficiency differences from time-integrated data, $\sin 2\beta$ HNs #183, or `http://www.slac.stanford.edu/~cahn/internal/differing_efficiencies.ps`

[33] NAG software, `http://wwwinfo.cern.ch/asd/nag/`

[34] F. James, MINUIT reference manual, CERN program library. `http://wwwinfo.cern.ch/asdoc/Welcome.html`

[35] `http://wwwinfo.cern.ch/asd/lhc++/SHORT-WRITEUPS/html/shortindex.html`

[36] Sections 4.4, 4.5.1 and 4.5.2 of Gill P.E., Murray W. and Wright M.H. (1981), *Practical Optimization*, Academic Press.

[37] Thomas Kittelmann, Measuring $\Delta\Gamma$ with CP events, Talk given at the $B^0 \bar{B}^0$mixing, lifetime, CP, T and CPT violation Workshop, December 4-5, 2001. `http://www.slac.stanford.edu/BFROOT/www/Physics/Analysis/AWG/BBMixingHadr/Workshop/agenda.html`

[38] R. Cahn, Some Things about $\Delta\Gamma$, `http://www.slac.stanford.edu/ cahn/internal/delta_Gamma.ps`

[39] Soeren Prell, $\Delta\Gamma$ studies with hadronic events, Talk given at the $B^0 \bar{B}^0$mixing, lifetime, CP, T and CPT violation Workshop, December 4-5, 2001.

[40] EvtGen, A Monte Carlo Generator for B-Physics.